ABSTRACT

Title of Document: ONLINE APPROXIMATION ASSISTED MULTIOBJECTIVE OPTIMIZATION WITH HEAT EXCHANGER DESIGN APPLICATIONS

Khaled Hassan Mohamed Saleh, Doctor of Philosophy, 2012

Directed By: Shapour Azarm, Professor, Department of Mechanical Engineering

Computer simulations can be intensive as is the case in Computational Fluid Dynamics (CFD) and Finite Element Analysis (FEA). The computational cost can become prohibitive when using these simulations with multiobjective design optimization. One way to address this issue is to replace a computationally intensive simulation by an approximation which allows for a quick evaluation of a large number of design alternatives as needed by an optimizer.

This dissertation proposes an approach for multiobjective design optimization when combined with computationally expensive simulations for heat exchanger design problems. The research is performed along four research directions. These are: (1) a new Online Approximation Assisted Multiobjective Optimization (OAAMO) approach with a focus on the expected optimum region, (2) a new approximation assisted multiobjective optimization with global and local metamodeling that always

produces feasible solutions, (3) a framework that integrates OAAMO with multiscale simulations (OAAMOMS) for design of heat exchangers at the segment and heat exchanger levels, and (4) applications of OAAMO combined with CFD for shape design of a header for a new generation of heat exchangers using Non-Uniform Rational B-Splines (NURBS). The approaches developed in this thesis are also applied to optimize a coldplate used in electronic cooling devices and different types of plate heat exchangers. In addition many numerical test problems are solved by the proposed methods. The results of these studies show that the proposed online approximation assisted multiobjective optimization is an efficient approach that can be used to predict optimum solutions for a wide class of problems including heat exchanger design problems while reducing significantly the computational cost when compared with existing methods.

ONLINE APPROXIMATION ASSISTED MULTIOBJECTIVE OPTIMIZATION WITH HEAT EXCHANGER DESIGN APPLICATIONS

By

Khaled Hassan Mohamed Saleh

Dissertation submitted to the Faculty of the Graduate School of the
University of Maryland, College Park, in partial fulfillment
of the requirements for the degree of
Doctor of Philosophy
2012

Advisory Committee:
Professor Shapour Azarm, Chair and Advisor
Professor Reinhard Radermacher
Professor Amr Baz
Professor Inderjit Chopra (Dean's Representative)
Assistant Professor Amir Riaz

Dedication

To my father
Hassan Mohamed Saleh
Who passed away few days before my PhD defense

To everyone who believed in me, intellectually challenged,
advised and encouraged me:
My family, teachers, friends and colleagues

Acknowledgements

My sincere appreciation goes to my advisor, Prof. Shapour Azarm, for his guidance, continued advice, constant encouragement and for providing me with the opportunity to work at the Design Decision Support Laboratory (DDSL). I also express my sincere gratitude for my co-advisor, Prof. Reinhard Radermacher, for his support, guidance, and for offering me the opportunity to work at the Center for Environmental and Energy Engineering (CEEE). Working with Prof. Azarm and Prof. Radermacher was really a unique experience where I gained a lot of experience in both optimization and heat exchanger design disciplines. I am fortunate to have this opportunity. I would also like to thank my committee members, Prof. Amr Baz, Prof. Amir Riaz, and Prof. Inderjit Chopra (Dean's Reprehensive) for their time, efforts, and generous comments and suggestions for improving my thesis.

I would also like to thank my current and former lab partners at DDSL and CEEE, namely, Dr. Mian Li, Zhichao Wang, Amir Mortazavi, Ali Alalili, Abdullah AlAbdulkarem , Hongtao Qiao, Long Huang, Moon Soo Lee, Hoseong Lee, Weizhe Han, Jyothi Vinjumur, Dr. Jonathan Winkler, and Dr. Varun Singh. I am also especially thankful to Dr. Omar Abdelaziz for his help, support, and guidance during my first year in my PhD journey. I really learned many things from him in programming, CFD, and optimization. Special thanks go to Dr. Vikrant Aute for introducing me to the area of approximation assisted optimization and for helping me in programming and optimization at the early stages. Also, I would like to thank my closest friend at University of Maryland, Mr. Weiwei Hu, for sharing various research ideas and having other interesting discussions. Also, I would like to thank Mr. Gary

Mosier from Systems Engineering and Advanced Concepts Branch, NASA Goddard Space Flight Center, Greenbelt, MD, for his inputs and advices.

I am most grateful to my family for their help and support throughout the years. To my parents, I can never repay your debt. To my brother, Sherief, my sincere appreciation to you for taking care of our parents. I would also like to thank my lovely wife, Esraa Ali, and my beloved son, Omar, for their support and understanding during my PhD study. My gratitude to my family cannot be expressed in words; they deserve the credit for all my achievements.

The work presented in this dissertation was supported in part through a grant from the U.S. Office of Naval Research, Grant # N000140710468, and a GRA support as a result of a NASA IRAD research collaboration. Such support does not constitute an endorsement by the funding agency of the opinions expressed in the dissertation. This support is gratefully acknowledged.

Table of Contents

Nomenclature

Acronyms

AAO	Approximation Assisted Optimization
AAMO	Offline Approximation Assisted Multiobjective Optimization
AHTC	Air Heat Transfer Coefficient (W/m^2 K)
ADP	Air Pressure Drop (Pa)
CFD	Computational Fluid Dynamics
DOE	Design of Experiment
EGO	Efficient Global Optimization
Error	The difference between the actual response using simulation the predicted value using the metamodel
FEA	Finite Element Analysis
GA	Genetic Algorithm
HD	Hyperarea Difference
HX	Heat Exchanger
IPE	Inexact Pre-Evaluation
LHS	Latin Hypercube Sampling
LMTD	Logarithmic Mean Temperature Difference
MAE	Maximum Absolute Error
MED	Maximum Entropy Design
MFR	Mass Flow Rate
MOGA	Multi Objective Genetic Algorithm
MSFCVT	Multiresponse Space Filling Cross Validation Tradeoff
NSGA	Non-dominated Sorting Genetic Algorithm
NTU	Number of Transfer Units
NURBS	Non-Uniform Rational Basis Splines
OAAMO	Online Approximation Assisted Multiobjective Optimization
OAAMOMS	OAAMO for problems with Multiscale Simulation
OS	Overall Pareto Spread
PPCFD	Parallel Parameterized CFD

RError	Relative Error
RMSE	Root Mean Square Error
RRMSE	Relative Root Mean Square Error
SFCVT	Space Filling Cross Validation Tradeoff

English Symbols

C_2	Pressure-jump coefficient
d	Number of design variables
D	Current design
d_{crit}	Cluster threshold
det	Determinant of a matrix
Din	Inner diameter of tube, normalized, [mm]
D_{out}	Tube outer diameter, [mm]
ds	Scaled distance
H_{ch}	Channel height of microchannel [mm]
Hs	Horizontal spacing[mm]
H_o	Baseline height of channel[mm]
L	Tube length, [mm]
$L_{H,i}$	Header inlet height, [m]
$L_{H,o}$	Header outlet height, [m]
N_{init}	Number of points in initial design
n	Total number of samples
q	Heat flux on the top surface of the channel [W/cm²]
Re	Reynolds number $\mathrm{Re} = \frac{\rho v D}{\mu}$
s	Square root of Mean square prediction error
S	Space-filling metric based on maximin distance
v	Velocity, [m/s]
Vs	Vertical Spacing
W_{ch}	Channel width [mm]
w	Depth of heat exchanger[mm]

x	Design variable, input variable
x^+	Dimensionless tube length $x^+ = \dfrac{L/D}{\mathrm{Re}}$
$\hat{y}$	Predicted response
y	True response
Z	Model of the random process in Kriging

Greek Symbols

α	Permeability of the porous medium
σ	Control point height ratio in header optimization
σ^2	Variance in Kriging metamodel
σ_{MFR}	Mass flow rate relative standard deviation
μ	Laminar fluid viscosity, Pa-s
ρ	Density, kg/m^3
ε	Heat Exchanger Effectiveness

Chapter 1: Introduction

In this chapter, first, the motivation behind this dissertation, the research objectives, and the underlying assumptions are introduced. Afterwards, a brief description of the research thrusts is presented, followed by the organization of the dissertation.

1.1 Motivation

Coupling a CFD simulation of a new heat exchanger (HX) with an optimizer makes the design of an optimum HX considerably challenging from the computational cost point of view. Figure 1.1 shows a few examples (from left to right: A-Coil air-cooled HX, new generation of air-cooled HX, coldplate used in electronic cooling, and Chevron type plate HX) that require CFD simulations during the process of finding optimum design solutions. This problem with computational cost can be addressed by the use of approximation combined with optimization, also called as Approximation Assisted Optimization (AAO). Approximation involves three main phases: (i) design of experiments (DOE) or a sampling phase, (ii) metamodel development phase, and (iii) metamodel verification phase. The DOE phase involves systematic probing of the design space to generate a set of sample points for which the response from the computer simulation is evaluated. The results are then used to build a metamodel. A metamodel can be evaluated much more (often orders of magnitude) faster than an actual (high fidelity) simulation. Finally, there is a verification phase in which a set of points is chosen to evaluate the goodness of the metamodel in terms of its accuracy.

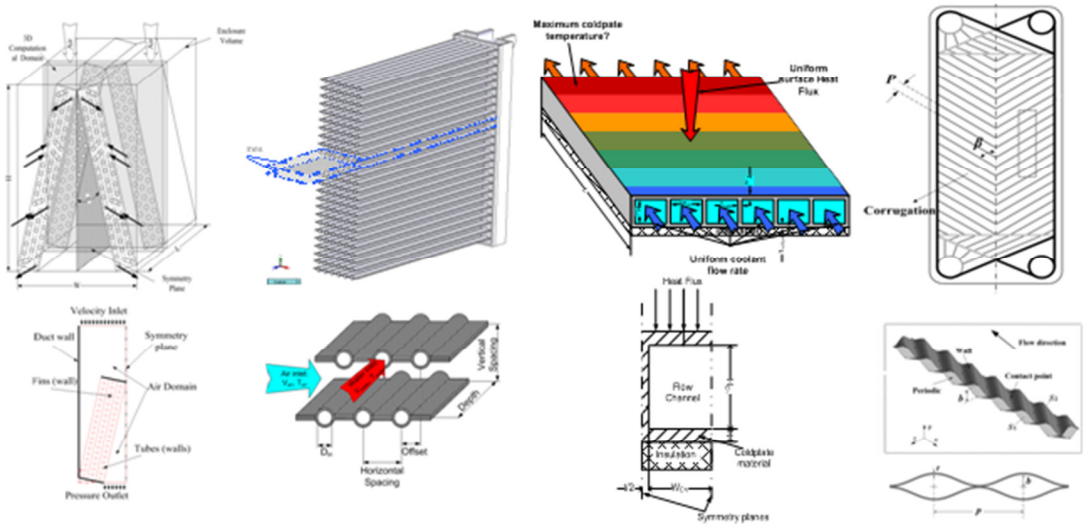

Figure 1.1 Heat exchanger examples

AAO can be carried out online or offline. In online AAO, the metamodels for objective and constraint functions (or optimization model) are adaptively updated in concert with optimization (Nair and Keane, 1998; Farina 2001, 2002; Jin et al., 2001, 2002; Hong et al., 2003; Nain and Deb, 2003). Online metamodeling can gradually improve the metamodel accuracy (Jin, 2005) while optimization is ongoing. In offline AAO, optimization is performed after the metamodels are constructed (Papadrakakis et al., 1999; Wilson et al., 2001; Koch et al., 2002; Lian and Liou, 2004; Fang et al., 2004).

1.2 Dissertation Objective

The overall objective of this dissertation is (a) to develop and verify a new online approximation assisted multiobjective optimization approach that updates the metamodels based on an estimate of optimum solutions including improving

closeness to target solutions and diversity of solutions, (b) to develop a new approximation assisted multiobjective optimization approach with global and local metamodeling by producing optimum solutions based on the samples observed using the actual simulation which provide always feasible solutions and eliminate the verification step of the obtained optimum solutions, (c) to develop an online approximation assisted multiobjective optimization framework for problems with multiscale simulation such as heat exchanger design optimization, (d) to use the developed AAO method for optimization of header design for novel air-cooled heat exchangers using Non-Uniform Rational Basis Splines (NURBS) in order to reduce the header volume while reducing the pressure drop inside the headers, and (e) to apply the online approximation assisted multiobjective optimization approaches developed in this dissertation to optimize the design of different types of heat exchangers such as coldplate and plate heat exchangers and many numerical test problems.

1.3 Assumptions

The following main assumptions are made in the development of the methods and models of this dissertation:

(a) The simulation models are deterministic. No matter how many times the simulation is invoked for the same input, the same simulation output is produced.

(b) The simulation responses are continuous and the corresponding simulation models are considered as z black-box.

(c) All design variables while building metamodels are continuous.

(d) The computational resources available to execute the simulation for numerous design alternatives, as required by the optimizer, are limited. Therefore, the number of available simulation calls is fixed and used as a stopping criterion.

(e) The computational time for performing a single simulation is much higher than that required for building a metamodel (which is an approximation to the simulation model).

1.4 Research Thrusts

A brief overview of the main research thrusts is presented in the following subsections.

1.4.1 Research Thrust-1: Online Approximation Assisted Multiobjective Optimization (OAAMO)

The focus of this research thrust is on developing a new online approximation assisted multiobjective optimization. In addition to reducing the computational cost, several issues are considered as part of this research thrust. These include: (1) improving iteratively the metamodels' performance in the expected optimum region by adding samples with high predicted Kriging variance which helps to improve the metamodels' accuracy in the expected optimum region, (2) improving the accuracy of the predicted optimum solutions by adding iteratively samples with high accuracy (low Kriging uncertainty) in the expected Pareto frontier, (3) handling multiobjective optimization problems with constraints while improving the accuracy of constraints' metamodels iteratively, (4) improving the quality of the optimum solutions by adding samplers that can improve both the closeness to target optimum solutions and the diversity of the solution points. The current literature in the area of online

approximation assisted multiobjective optimization reports progress in some but not all of the above mentioned aspects. The proposed approach uses multiobjective genetic algorithm as the optimization algorithm combined with a Kriging metamodeling technique (Cressie, 1993; Armstrong, 1998; Bakker, 2000). Several numerical test problems are used to investigate the new approach in addition to an engineering test problem and compare to previous methods.

1.4.2 Research Thrust-2: Approximation Assisted Optimization with Combined Global and Local Metamodeling

This research thrust proposes a new and novel online approximation assisted multiobjective optimization approach. The approach iteratively uses and updates both global and local metamodels for the objective and constraint functions in its pursuit for Pareto optimum solutions. The global metamodels allow the approach to explore the entire design space while a number of local metamodels with a higher accuracy focus on promising regions of the design space. These promising regions are determined based on a number of clusters using a newly developed clustering scheme. This scheme is adaptive and dynamically determines the number of clusters, their size and location in the design space. The proposed approach considers both objective and constraint functions as being computationally expensive and as such it can be used in a wide range of engineering design optimization applications. Compared to OAAMO of Research Thrust 1, all optimum solutions in the approach of this thrust are observed which ensure the feasibility of all optimum solutions and reduce the computational cost by eliminating the verification step of final solutions. A

numerical and an engineering test problem are used to demonstrate the new approach developed of this research thrust.

1.4.3 Research Thrust-3: Online Approximation Assisted Multiobjective Optimization for Problems with Multiscale Simulation

In the third research thrust, a new framework is proposed for optimizing new generations of heat exchangers. In these heat exchangers, the CFD simulations are used to predict thermal and hydraulic performance of the enhanced surfaces including the heat transfer coefficient and pressure drop values at the segment level. The segment level performance model is coupled with segmented ε-NTU solver to simulate the entire heat exchanger performance. By coupling the OAAMO developed in Research Thrust-1 with the multiscale simulation, the computational time required to find optimum heat exchanger design solutions can be reduced significantly compared to offline based approximation assisted multiobjective mulstiscale simulation approach.

1.4.4 Research Thrust-4: Header Optimization of New Generation of Air-Cooled Heat Exchangers using NURBS

With reducing the tubes and channels diameters (using mini and micro channels) in heat exchangers, it is necessary to design larger heat exchangers inlet and outlet distribution manifolds (headers) with the purpose of reducing the pressure drop. Consequently, there is a tradeoff between increasing the header size to reduce the refrigerant pressure drop and adding volume that obstructs the airside free flow area. In this part of the proposed dissertation, the OAAMO approach is used to find optimum header design solutions for a new generation of air cooled heat exchangers.

A three-dimensional CFD model is developed using NURBS to represent and optimize the outer shape of a header for a new generation of air-cooled heat exchangers.

1.4.5 Applications: Coldplate, Chevron Plate Heat Exchanger, and Rollbond Plate Heat Exchanger

Additional applications for using online approximation assisted optimization for the design of different heat exchangers and thermal devices are presented. These include: a coldplate used for electronic cooling, and two different types of plate heat exchangers. A summary of the lessons learned from applying online and offline approximation assisted multiobjective optimization approaches to these types of heat exchangers is briefly discussed.

1.5 Organization of The Dissertation

The dissertation is organized as shown in Figure 1.2. The background and terminology used in this dissertation are provided in Chapter 2, followed by the four research thrusts in Chapter 3 to 6, and examples for using the developed approaches for different heat exchangers applications in Chapter 7. The conclusions, contributions and recommendations for future directions are presented in Chapter 8.

In the next Chapter, the main definitions and terminologies used in this dissertation are briefly discussed.

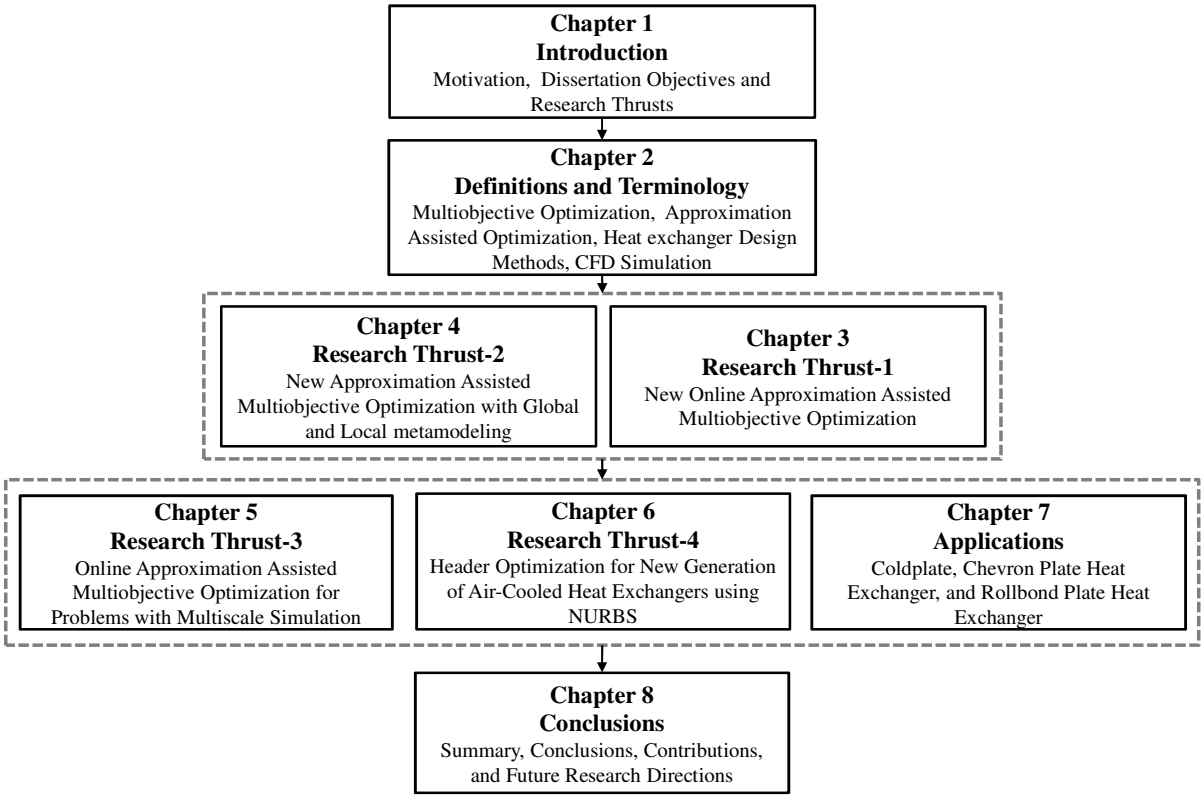

Figure 1.2 Organization of Dissertation

Chapter 2: Definitions and Terminology

2.1 Introduction

The concept of a deterministic computer simulation is explained first, followed by the definition of a multiobjective optimization problem. Then, the multi-objective genetic algorithm is described. Afterwards, approximation assisted optimization is elaborated with its different steps such as design of experiment, metamodeling, and verification. Three types of approximation assisted optimization techniques from the previous work are briefly discussed (ParEGO, PSP, and Forrester's) since they are the state-of-the-art and are used for comparison with the AAO methods developed in this dissertation. Finally, principles of heat exchanger design and CFD simulations are briefly discussed.

2.2 Deterministic Computer Simulation

A deterministic computer simulation can be schematically represented by Figure 2.1. The simulation takes the value from a vector of design variables x and produces the corresponding value for a vector of outputs or responses for f and g (objectives and constraints, respectively) as shown in Figure 2.1. The term function call denotes the process of invoking the simulation with a given value of input x. In this dissertation, CFD models for different types of heat exchanger are treated as a black-box simulation.

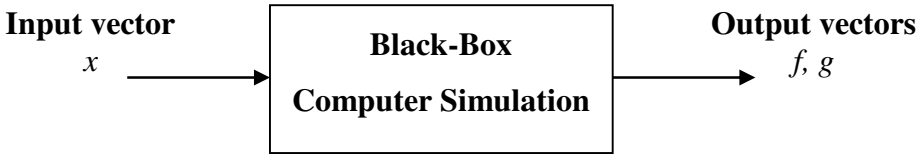

Figure 2.1 Schematic of a deterministic simulation

2.3 Multiobjective Optimization

A Multiobjective optimization formulation is used for many engineering design problems. For such problems, design objectives are considered to be at least partly conflicting with each other. An optimization approach that is used to solve a multiobjective optimization problem obtains a set of solutions called Pareto optimum solutions (Deb, 2001). A multiobjective optimization problem can be presented mathematically as follows:

$$\begin{aligned} &\text{minimize} && f_m(x) && m = 1,...,M \\ &\text{subject to:} && g_j(x) \le 0 && j = 1,...,J \\ & && x^{lower} \le x \le x^{upper} \end{aligned} \tag{2.1}$$

where x is a vector of design variables, $f_m(x)$ is the m^{th} objective function to be minimized, $g_j(x)$ is the j^{th} constraint, and x^{lower} and x^{upper} are the lower and upper bounds of x.

2.3.1 Methods for Solving Multiobjective Optimization Problems

Generally speaking, two classes of methods are used to solve multiobjective optimization problems; (a) classical methods and (b) non-classical methods (Deb, 2001). Classical methods are generally gradient-based or direct search methods. Examples for classical methods include: weighted-sum method (Cohon, 1978), ε-constraint method (Haimes, 1971), value function method (Keeny and Raiffa, 1976),

Schaffler's stochastic method (Schaffler et al., 2002), normal boundary intersection method (Das and Dennis, 1998), goal programming (Charnes et al., 1955) and others. Gradient based methods are deterministic in nature and yield locally Pareto optimum solutions one point at a time.

Many of the non-classical methods are nature based. These methods are population based such as evolutionary algorithms (Goldberg, 1989; Deb, 2001), particle swarm optimizers (Coello et al., 2004), multiobjective simulated annealing (Serafini, 1992; Nam and Park, 2000) to name a few. Several variations of population based multiobjective optimization based evolutionary algorithms have been reported in the literature (Fonseca and Fleming, 1993; Srinivas and Deb, 1994; Horn et al., 1994; Zitzler and Thiele, 1998; Deb, 2001; Coello et al., 2007). These methods try to assign fitness to a design point based on its objective and constraint values. It is also important to note that population-based methods require numerous function calls, at times several thousand or more depending on the dimension of the optimization problem, to evaluate the objectives and constraints. However, these methods can obtain globally Pareto optimum solutions although there is no guarantee that they can converge to such solutions.

In this dissertation, Multi-Objective Genetic Algorithm (MOGA) (Deb, 2001) is used for solving multiobjective optimization problems. However, the approaches proposed in this dissertation are not limited to MOGA. Any other multiobjective optimization technique can be used as well.

2.3.2 Dominance and Pareto Set

Most multiobjective optimization methods use the concept of domination to arrive at solutions. In any multiobjective optimization problem, there are two or more conflicting objectives. For these problems, two solutions are compared on the basis of whether or not one solution dominates the other based on multiple objectives. In the next paragraph the concept of domination is described.

Considering Eq. (2.1), a solution "**A**" is said to dominate (Goldberg, 1989; Deb, 2001) a solutions "**B**", if both conditions 1 and 2 are satisfied:

1. Solution "**A**" is better than or equal to "**B**" in terms of all the objectives and
2. Solution "**A**" is strictly better than "**B**" in at least one of the objectives.

When comparing two solutions, when the first condition is not satisfied, the two solutions are said to be non-dominated with respect to each other. In other words, if a point is not dominated by any other point, it is said to be non-dominated.

As shown in Figure 2.2, amongst a set of solutions **P**, the non-dominated subset of solutions **P'** are those that are not dominated by any other point in **P**. When **P** is the entire search space, then the resulting non-dominated set **P'** is termed as the Pareto optimal set and the solutions are said to form a Pareto frontier in the objective space (i.e., *f*-space).

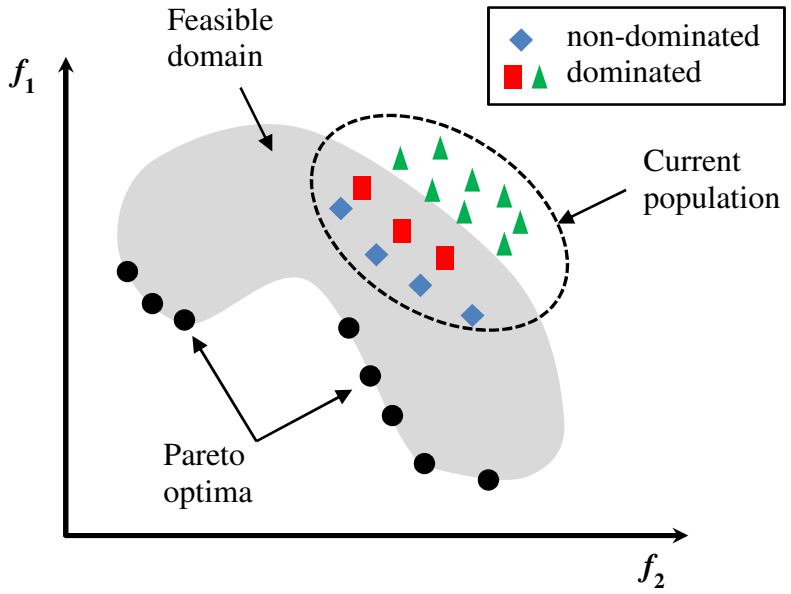

Figure 2.2 Feasible domain, dominated, non-dominated, and Pareto solutions in the objective space

2.3.3 Quality Metrics

After solving Eq. (2.1) a set of solutions is obtained. In order to evaluate the quality (goodness) of the solution set obtained, two quality metrics (Wu and Azarm, 2001) are used. These metrics are Hyperarea Difference (HD) and Overall Pareto Spread (OS).

Hyperarea Difference (HD): HD gives a measure of closeness of a set of points to a target (good) point. Geometrical interpretation for HD is presented in Figure 2.3. For a non-dominated set in the objective space P = {a,b,c,d,e} and P_{bad} and P_{good}, the "good" and "bad" points, respectively, HD is defined by the shaded area in Figure 3.2. This area is the difference between the rectangular area bounded between P_{bad} and P_{good} and the area between P_{bad} and the set P (formed by a staircase):

$$HD(P) = HA(P_{bad}, P_{good}) - HA(P_{bad}, a, b, c, d, e) \qquad (2.2)$$

where HA denotes the (hyper) area. For a minimization problem, a non-dominated set with a lower HD value is considered to be better than that with a higher value.

Overall Pareto Spread (OS): The overall Pareto spread is used to measure diversity of a set of solutions. OS, as shown in Figure 2.3, is defined as the ratio between the area bounded by the two extreme points, i.e., a and e, in P and the area bounded by P_{bad} and P_{good} as given in Eq. (2.3). When comparing two non-dominated sets based on OS, the set with a higher OS value is considered to be better.

$$OS = \frac{HA[extreme(P)]}{HA(P_{bad}, P_{good})} \tag{2.3}$$

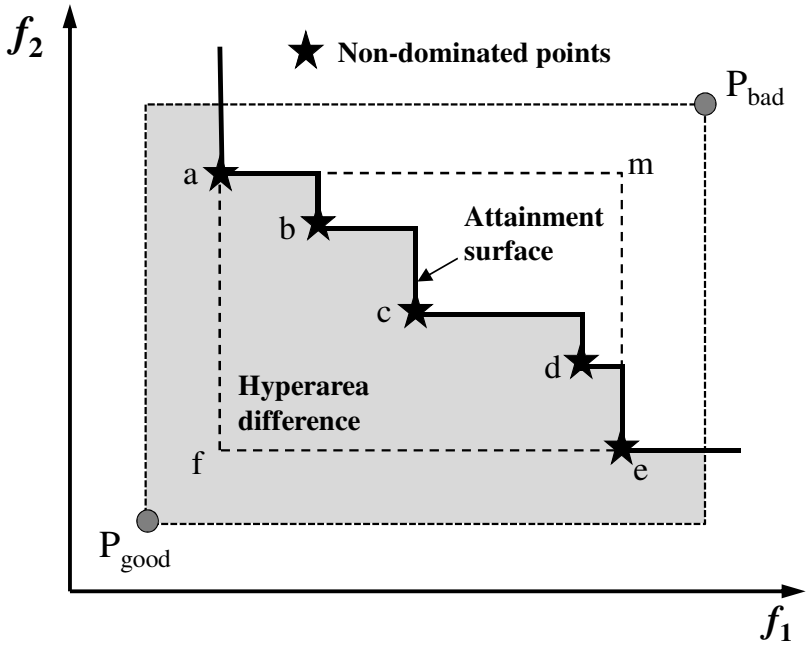

Figure 2.3 The attainment surface and quality metrics for a set of non- dominated points (Hu et al., 2012)

Attainment Surface: The attainment surface is a way to visualize a non-dominated set in the case of two objectives. It is constructed based on a union of the

non-dominated points (Voutchkov and Kean, 2010). The attainment surface can show how close a set of solutions is to another set or to a true Pareto set of solutions. The attainment surface can also represent the spread of non-dominated points.

2.4 Multi-Objective Genetic Algorithm (MOGA)

Genetic Algorithms (GAs) as defined by Goldberg (1989) are: "search algorithms based on natural selection and natural genetics". GA's maintain a pool of candidate points each of which is assigned a fitness based on its 'payoff'. Fitness is a scalar measure of how well a particular candidate point satisfies a given problem objective. At each iteration or generation of GA, candidate points are selected for reproduction based on their fitness to form new offspring points. The reproduction process is carried out by the use of genetic operators such as selection, crossover and mutation. A set of probabilistic rules determines how a candidate solution undergoes crossover or mutation. A powerful feature of GA is that it is a population based, searches along multiple directions simultaneously, does not require derivative information and can obtain a global optimum solution. This makes the GA an ideal tool for optimization of highly non-linear (or even discontinuous or black-box) functions involving a combination of continuous and discrete design variables.

GA is extended to solve multiobjective optimization problems, as in Multi-Objective Genetic Algorithm (MOGA). MOGA is based on using a non-dominated sorting GA proposed by Srinivas and Deb (1995). In this scheme, non-dominated sorting is performed and the solutions are ranked such that all the solutions in the same non-dominated set have the same fitness value which guarantees every non-dominated individual equal reproduction opportunity. Thus the points in the first non-

dominated set/front have the maximum fitness value. The flowchart of MOGA, which follows the NSGA approach (Srinivas and Deb, 1995) as implemented in this dissertation is shown in Figure 2.4 using MATLAB 2007a.

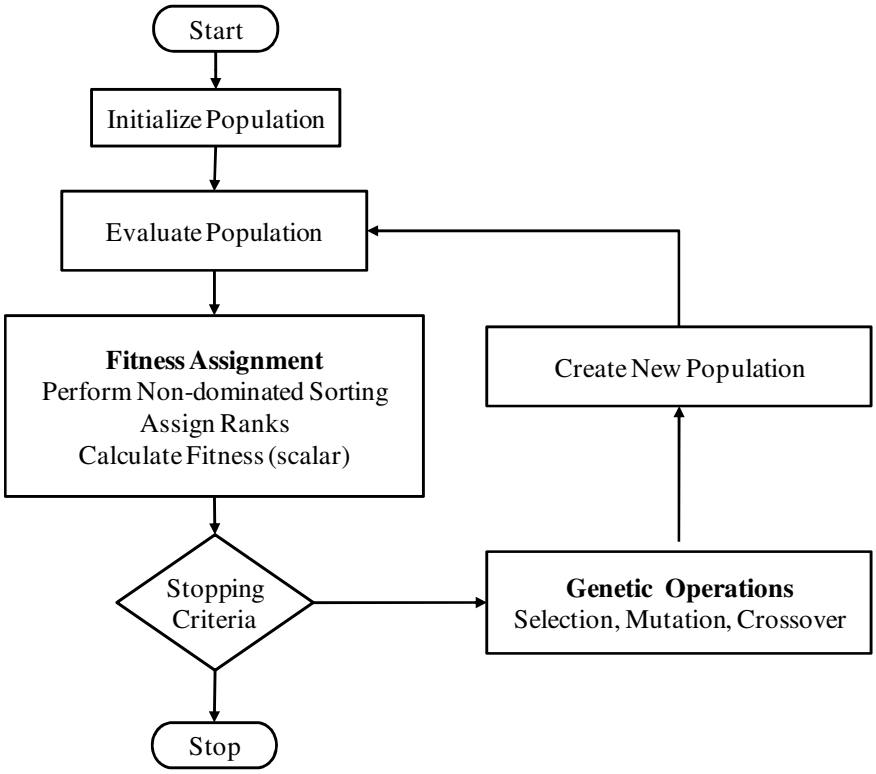

Figure 2.4 MOGA flowchart

2.5 Approximation Assisted Optimization

In this section, the main steps in approximation assisted optimization (AAO) are discussed in addition to a discussion for different types of AAO methods.

2.5.1 Overview

Computer simulations used for engineering design can be computationally intensive as in the case of Computational Fluid Dynamics (CFD) and aerodynamic shape design (e.g., Obayashi et al., 2005; Pineda et al., 2010; Sakata et al., 2011; Su

et al., 2011). The computational intensity can be exacerbated when such simulations are combined directly with an optimization approach for engineering design. This limitation can be overcome by the use of an Approximation Assisted Optimization (AAO) technique. Typically, AAO starts with Design of Experiments (DOE) or an initial set of sample points in the design space. These points are used to construct metamodels for the objective and constraint functions of an optimization problem. Some popular metamodeling methods in AAO include response surface techniques (Otto et al., 1996; Sobieski et al., 1998) such as quadratic polynomial (Ratle, 1998), multi-layer neural network (Hong et al., 2003), radial basis function (Karakasis et al., 2001), support vector machine (Nakayama et al., 2003), and Gaussian based methods (Buche et al., 2005) including Kriging (Jones et al., 1998). Adaptive use of various fidelity metamodels (Markine and Toropov, 2002) and aggregation of several metamodels have also been reported (Viana et al., 2009; Pilat and Neruda, 2012). Several comprehensive literature reviews of metamodeling approaches in engineering optimization have been reported as well (Simpson et al., 2001; Jin et al., 2002; Wang and Shah, 2007).

Most AAO approaches can be classified into two main groups: offline and online as shown in Figure 2.5. The main difference between these two groups is that offline metamodels are not updated during AAO while online metamodels are. In offline AAO, the metamodels are built, verified, and if they are not accurate enough then more samples are added to improve the accuracy. Afterwards, the optimization is performed with this global metamodel (Myers, 1995; Papadrakakis et al., 1999; Wilson et al., 2001; Koch et al., 2002; Lian and Liou; 2004; Fang et al., 2004; Fang et

al., 2005; Georgopolou and Giannakoglou, 2009; Abdelaziz et al., 2010). The offline approach can be computationally expensive as it may require many function evaluations to build a globally accurate metamodel. Moreover, additional and separate function evaluations are needed to verify the offline metamodel.

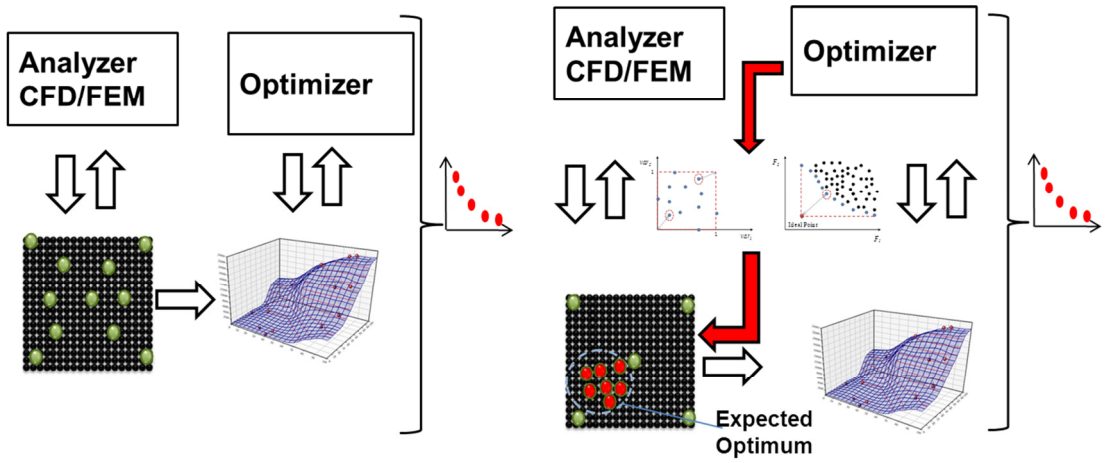

(a) (b)

Figure 2.5 Comparison between approximation assisted optimization approaches (a) offline and (b) online

On the other hand, in the online AAO there is a feedback loop from the optimizer for updating the metamodel using additional and carefully chosen sample points Farina, 2001; Farina, 2002; Hong et al., 2003; Jin et al., 2001; Jin et al., 2002; Nain and Deb, 2003; Nair and Kean, 1998; Pilat and Neruda, 2011; Hu et al., 2011; Hu et al., 2012). One significant advantage of the online AAO is that the predictive capabilities of the metamodel is progressively improved in the area where the optimum is expected to be, as more and more sample points are evaluated and added to the sample set. However, one limitation of online AAO is that in the initial stage a poorly estimated metamodel for objective and/or constraint functions can mislead the optimization process into sub-optimum or infeasible region of the design space.

Depending upon how frequent the metamodels (for objective and constraint functions) are updated, some online AAO approaches update the metamodels only after a certain number of iterations (Hacker, 2002; Li et al., 2008), while others update the metamodels at each optimization iteration (Grierso and Pak, 1993). One group of online AAO approaches, called Inexact Pre-Evaluation (IPE), uses metamodels to estimate a majority of intermediate design points, but only observe the best intermediate points (Nair et al., 1998; Karakasis et al., 2001; Praveen and Duvigneau, 2009).

In the next section, the DOE methods used in this thesis are briefly described.

2.5.2 Design of Experiment (DOE)

The DOE methods reported in the literature can be classified as classical, space filling, and sequential or adaptive methods (Simpson et al., 2001; Wang and Shah, 2007). In this thesis, the space filling sampling techniques, i.e., the Maximum Entropy Design (MED) and Latin Hypercube Sampling (LHS) methods are used to generate initial set of samples to represent the entire design space. In the next paragraph the MED method is described followed by LHS.

Maximum Entropy Design (MED): Entropy **H** is used as a measure of information (Shannon, 1948). Lindley (1956) interpreted Shannon's entropy as the amount of information retrieved from an experiment. The concept of entropy has been used to select the new sample point in order to maximize the retrieved information due to the new sample (Shewry and Wynn, 1987; Currin et al., 1988). In order to maximize the entropy **H** as a measure of information by adding a new sample x_{n+1} to a set of n current samples (x_1, x_2,…, x_n) the following equation is applied:

$$x_{n+1} = \text{argmax } \mathbf{H}\,(x_1, x_2, \ldots, x_{n;}\, x) \tag{2.4}$$

where "argmax" denotes the optimal solution of the maximum entropy optimization problems.

Further, under the assumption of normal priors (Shewry and Wynn, 1987; Koehler and Owen, 1996), it can be shown that the maximum of the entropy criterion is the same as maximizing the determinant of the prior covariance matrix R, i.e.,

$$x_{n+1} = \text{argmax det } (R) \tag{2.5}$$

where det indicates a determinant and R is an $((n+1) \times (n+1))$ covariance matrix of x. Each element of R is calculated using the augmented design $(x_1,x_2,\ldots,x_n,x_{n+1})$, where there are n existing designs and x_{n+1} is the new candidate design. The details of the covariance matrix based on the normal priors are given in Section 2.5.3.

Latin Hypercube Sampling (LHS): Latin hypercube was among the early DOE methods proposed specifically for computer experiments (McKay et al., 1979). A Latin hypercube is a matrix of n rows and k columns where n is the number of levels being examined and k is the number of design variables. Each of the k column contains the levels 1, 2,…, n, randomly permuted, and the k column are matched at random to form the Latin hypercube. Latin hypercube sampling offers flexible sample sizes while ensuring stratified sampling, i.e., each of the input variables is sampled at n levels (Sacks et al., 1989). Figure 2.6 shows a set of 20 samples generated in two design variables domain using MED and LHS methods. As it is shown in Figure 2.6, MED can give better spread near the boundaries. However, MED is computationally more expensive than LHS especially with an increase in the number of design variables.

After generating the initial samples using of the DOE methods described earlier, metamodels are built for all responses (objectives and constraints). In the next subsection, the metamodeling technique used in this dissertation is discussed in details.

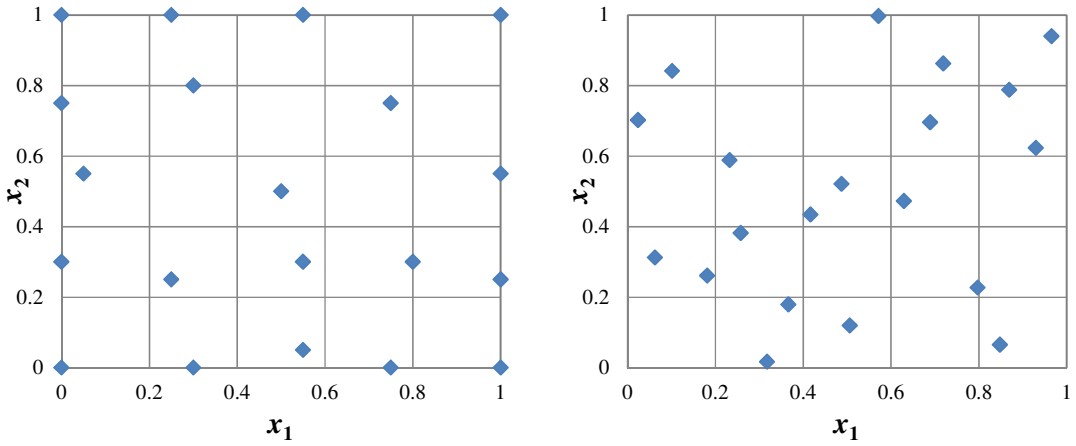

Figure 2.6 Design of experiment samples using (a) MED and (b) LHS

2.5.3 Kriging Metamodeling

Kriging is an interpolative metamodeling method for response approximation from a simulation (Sacks et al., 1989; Jones, 2001). It is widely used in the field of Geostatistics (Cressie, 1993; Armstrong, 1998) and is named after the South African mining engineer D. G. Krige. Kriging metamodeling can be viewed as a linear predictor that estimates an unknown value of a response for an input sample point based on the known values of the response and the distance of the sample from the known design points, as shown in Figure 2.7. Kriging treats the response from a deterministic simulation as a realization of a stochastic process as follows:

$$y(x) = f(x) + Y(x) \tag{2.6}$$

where $y(x)$ is the unknown function that is being modeled and $Y(x)$ is a normally distributed Gaussian process.

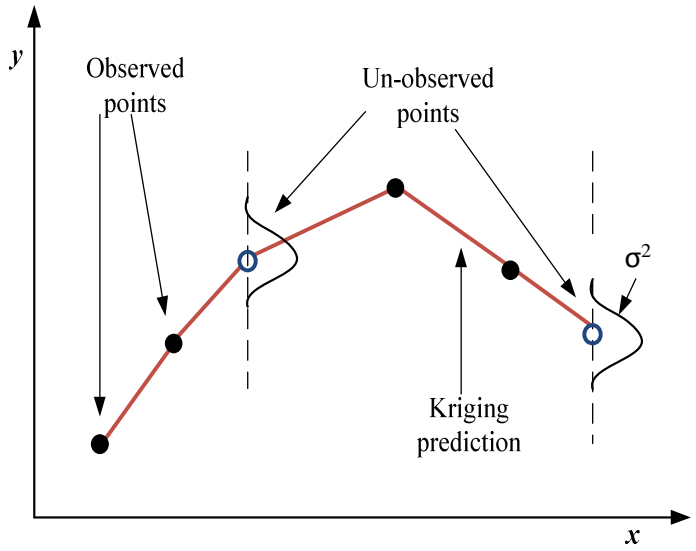

Figure 2.7 Kriging metamodeling technique

Several functional forms for $f(x)$ and $Y(x)$ are available in the literature (Jones, 2001; Martin and Simpson, 2005). The first term in Eq. (2.6), $f(x)$, represents a polynomial model in a response surface method and is equivalent to a global mean μ for the model. This global mean μ is the mean of all responses in the current design. However, $Y(x)$ term represents the local deviation from the global mean obtained by interpolating the available data based on distance between the available data based on distance between the unobserved point x_0 and the sampled points. The term $Y(x)$ is represented through the use of one of many correlation functions. One of the widely used correlation functions (Sacks et al., 1989; Jones, 2001) is:

$$Corr[Y(x_i), Y(x_j)] = \exp(-\sum_{i=1}^{d} \theta_l \left| x_{il} - x_{jl} \right|^{pl} \tag{2.7}$$

where d is the dimension of vector x, x_{il} and x_{jl} are the l^{th} components of the vectors x_i and x_j, θ_l is the degree of correlation between the responses in the l^{th} coordinate and is termed as the correlation parameter in the l^{th} direction, and p controls the smoothness of the function in the l^{th} direction. The terms θ_l and p_l provide a means for adjusting the relative importance in each dimension of the input space. For simplification, a single value of θ is used and the distance term is replaced by the Euclidean distance between x_i and x_j. When one value of θ is used, the model is termed as an isotropic model, which treats all dimensions equally. In Eq. (2.7) when p=1, the correlation is known as the exponential correlation. As for n responses in the current design, then let y represent the set of n observed true responses as given in Eq. (2.8):

$$y = \begin{bmatrix} y(x_1) \\ . \\ . \\ . \\ y(x_n) \end{bmatrix} \tag{2.8}$$

The uncertainty in the function values (local deviations) at the n points can be represented by a vector of random variables $Y(x)$ as:

$$Y(x) = \begin{bmatrix} Y(x_1) \\ . \\ . \\ . \\ Y(x_n) \end{bmatrix} \tag{2.9}$$

This vector has a covariance matrix Cov given by:

$$Cov(Y) = \sigma^2 R \tag{2.10}$$

where R is an $n \times n$ correlation matrix with the (i,j) element given by Eq. (2.7). The diagonal elements of R are always of the form $Corr[Y(x_i), Y(x_i)]$ and thus are always equal to 1. Let I denote an $n \times 1$ vector of ones and r denote the correlation of $Y(x_0)$, the unobserved point, with $Y(x_i)$, the current designs, as

$$r = \begin{bmatrix} Corr[Y(x_0), Y(x_1)] \\ . \\ . \\ . \\ Corr[Y(x_0), Y(x_n)] \end{bmatrix} \tag{2.11}$$

The values of the correlation parameters, such as μ, σ, θ and p_l need to be estimated. They are obtained by maximizing the likelihood function or in other words, to model the functions behavior so that it closely represents the observed data. Maximizing the likelihood function provides an estimate of the optimal values of μ, σ^2, as functions of R as follows

$$\hat{\mu} = \frac{I^T R^{-1} y}{I^T R^{-1} I} \tag{2.12}$$

$$\hat{\sigma}^2 = \frac{(y - I\hat{\mu})^T R^{-1} (y - I\hat{\mu})}{n} \tag{2.13}$$

Then the estimated response for an unobserved point x_0 is given using the Kriging predictor as:

$$\hat{y}(x_0) = \hat{\mu} + r^T R^{-1} (y - I\hat{\mu}) \tag{2.14}$$

In addition to the above predictor, the Kriging measure of uncertainty in the estimated response can be calculated as follows:

$$s^2(x_0) = \hat{\sigma}^2 \left[1 - r^T R^{-1} r + \frac{(1 - r^T R^{-1} r)^2}{I R^{-1} I} \right] \tag{2.15}$$

The derivation for this standard error is provided in Sacks et al. (1989) and Jones (2001). It can be seen that the variance s^2 is zero for an observed point. In utilizing Kriging predictor in approximation assisted optimization (Bakker, 2000; Jones, 2001), this standard error can serve as a basis for making the decision between using the predicted response and invoking the analyzer functions to obtain a true response as it will be presented in chapter 3 in this thesis. The prediction of the standard error is a main advantage of Kriging over other metamodeling methods since the metamodel can then be dynamically updated based on the responses during a given optimization procedure. Furthermore, as mentioned, Kriging does not require a functional form, though the choice of the correlation function is problem dependent. Simpson et al. (2001) found that Kriging is extremely flexible and suitable for deterministic computer experiments and recommend the use of Kriging metamodels when the number of input variables is less than 50.

After building the metamodels, there is a need to measure the accuracy of these metamodels. In the next subsection, metamodel performance verification step is discussed.

2.5.4 Metamodel Performance Verification

In offline AAO, after creating the metamodel, a set of random samples is generates and the responses are predicted using the metamodels and compared with the true simulation responses. Let $y(x_i)$ be the true response from the simulation and $\hat{y}(x_i)$ be the predicted response from the metamodel for a set of samples with n

individuals. Several errors can be reported such as error for each sample: $Error_i$, relative absolute error: $RError_i$, maximum absolute error: MAE, as follows:

$$Error_i = y(x_i) - \hat{y}(x_i) \tag{2.16}$$

$$RError_i = \frac{|y(x_i) - \hat{y}(x_i)|}{y(x_i)} \times 100\% \tag{2.17}$$

$$MAE = max(|Error_i|), i = 1,...,n \tag{2.18}$$

The root mean square error and relative root mean square error for a set of samples are defined as:

$$RMSE = \left(\frac{1}{n} \sum_{i=1}^{n} Error_i^2 \right)^{1/2}, i = 1,...,n \tag{2.19}$$

$$RRMSE = \left(\frac{1}{n} \sum_{i=1}^{n} RError_i^2 \right)^{1/2} \quad \%, i = 1,...,n \tag{2.20}$$

RMSE and *MAE* consider only the numerical magnitude of the errors. The relative *RMSE* metric is useful when the numerical range of the response i.e., difference between the minimum and the maximum values differs by several orders of magnitude. *RRMSE* is useful in practical engineering examples as demonstrated in this dissertation.

In the next subsection, the different AAO methods used for comparison in this dissertation are briefly discussed.

2.5.5 Overview of ParEGO, PSP, and Forrester's Methods

Numerous AAO approaches have been developed for multiobjective optimization with computationally expensive functions. A few leading approaches

among these that are: ParEGO (Knowles, 2006), PSP (Shan and Wang, 2005), and Forrester's (Forrester et al., 2008). For example, an important strategy in PSP is that a large number of random points are generated in the design space and based on their objective function values obtained from the metamodels, new sample points are selected. In the PSP approach, a sampling guidance function is used to directly sample as many points as possible in order to estimate the entire Pareto optimal frontier. Essentially, PSP uses a version of the objective function as a probability distribution function for guidance in the sampling. More sample points are collected in the areas having lower objective function values while fewer sample points are selected in other areas. PSP employs a global metamodel to estimate the objective function values for the random points and then a combined sorting of the random points and previous sample points is performed. The non-dominated points are observed and used to further improve the metamodel iteratively. In its current form, PSP does not provide a provision for handling constraint functions.

Both ParEGO and Forrester's approaches are based on the concept of Expected Improvement (EI) of the objective functions, in which EI represents the probability that a new design point is better than the current best design points. Using EI, a new design point is located both in the promising areas (where the optimum is expected to be) in the design space and also in the areas with a limited number of sample points and high metamodeling uncertainty. In ParEGO, the expected improvement of multiple objective functions is converted into a single value using randomly generated weighting coefficients. A new sample point is chosen based on maximizing the expected improvement function. Using the random weights, ParEGO

may fail to predict the entire Pareto frontier particularly with a limited number of sample points. Also, ParEGO can only be used for solving unconstraint multi-objective optimization problems. On the other hand, Forrester et al. developed a function for the multi-objective expected improvement based on the multivariate integration of the probability function. The sample points are selected to maximize the multi-objective expected improvement function. Compared to ParEGO, one advantage of Forrester's approach is that it includes a constraint handling technique.

Heat exchanger design optimization problems are examples for computationally expensive engineering problems that require efficient approximation assisted optimization approaches. In the next subsection, different methods used to design heat exchangers are discussed briefly.

2.6 Heat Exchanger Design Methods

Heat exchangers (HXs) are widely used in the processing heat and power, air-conditioning and refrigeration, heat recovery, transportation and manufacturing industries. Such equipment is also used in electronic cooling and for environmental issues such as thermal pollution, waste disposal and sustainable development. Various types of heat exchangers exist such as coil HXs, double tube HXs, shell and tube HXs, plate HXs, and others. A more detailed classification of heat exchangers can be made based on their construction features, modes of heat transfer, and heat duty specifications (Sukhatme and Devotta, 1998; Walker, 1990; Shah and Sekulić, 1998; Kuppan, 2000; Wang et al., 2007). In this section, the basic equations for thermal design of heat exchangers are presented.

There are several techniques for heat exchanger design. Two main methods are: the Logarithmic Mean Temperature Difference (*LMTD*) method and *ε-NTU* method. In both methods, energy balance equations presented in Eq. (2.21) and Eq. (2.22) are used to represent heat transfer between hot and cold streams. In the *LMTD* method, total heat transfer, Q, is calculated using Eq. (2.23), overall heat transfer coefficient, U, is defined in Eq. (2.23) based on the convection heat transfer resistance in both hot and cold streams $\frac{1}{(\eta_o h A_t)}$ where h is the heat transfer coefficient, A_t is total contact area between the solid the fluid and , η_o is the fin efficiency, $R_{contact}$ define contact resistance, R_{wall} is conduction resistance in the wall, R_{foul} is the fouling resistance. F is a temperature correction factor that depends in the HX configuration. LMTD is calculated from Eq. (2.25) for counter flow HX.

$$Q = \dot{m}_h c_{p,h}(T_{h,in} - T_{h,out}) \tag{2.21}$$

$$Q = \dot{m}_c c_{p,c}(T_{c,out} - T_{c,in}) \tag{2.22}$$

$$Q = UA\,(F \times LMTD) \tag{2.23}$$

$$\frac{1}{UA} = [\frac{1}{(\eta_o h A_t)_c} + R_{foul,c} + R_{contact,c} + R_{wall} + R_{contact,h} + R_{foul,h} + \frac{1}{(\eta_o h A_t)_h}] \tag{2.24}$$

$$LMTD = \frac{(T_{h,in} - T_{c,out}) - (T_{h,out} - T_{c,in})}{\ln\left(\frac{T_{h,in} - T_{c,out}}{T_{h,out} - T_{c,in}}\right)} \tag{2.25}$$

In the *ε-NTU* method, the heat transfer rate from the hot fluid to the cold fluid is expressed as:

$$Q = \varepsilon C_{\min}(T_{h,in} - T_{c,in}) \quad \text{where} \quad C_{\min} = \min(\dot{m}_h c_{p,h}, \dot{m}_c c_{p,c}) \tag{2.26}$$

$$NTU = \frac{UA}{\left(\dot{m}c_p\right)_{\min}} \tag{2.27}$$

$$CR = \frac{\left(\dot{m}c_p\right)_{\min}}{\left(\dot{m}c_p\right)_{\max}} \tag{2.28}$$

The HX effectiveness ε, is function of number of transfer units *NTU,* heat capacity ratio *CR,* and HX configuration. Effectiveness ε is a measure of thermal performance of a heat exchanger. It is defined for a given heat exchanger of any flow arrangement as a ratio of the actual heat transfer rate from the hot fluid to the cold fluid to the maximum possible heat transfer rate as given in Eq. (2.26). The heat capacity ratio *CR* is defined as the ratio of smaller to larger heat capacity for the two fluid streams. Number of transfer units *NTU* is defined as a ratio of the overall thermal conductance (*UA*) to the smaller heat capacity rate as given in Eq. (2.27). *NTU* provides a provides a compound measure of the heat exchanger size through the product of heat transfer surface area *A* and the overall heat transfer coefficient *U*. Hence, in general, *NTU* does not necessarily indicate the physical size of the exchanger (Shah and Sekulić, 1998).

For enhanced heat exchanger surfaces there is a need to use CFD simulations to determine the thermal and hydraulic performance of the enhanced surfaces. In the next section, the main governing equations used in CFD simulation are discussed.

2.7 CFD Simulation

Conventionally, extensive experimental investigation is used to find the heat transfer and fluid flow performance for different types of heat exchangers. Recently, with the development in computational capabilities, CFD simulations are used to

predict the thermal and hydraulic performance for enhanced heat exchangers designs (Bergles, 2002). In CFD simulations, the main fluid governing equations are solved numerically. The main governing equations are the continuity, the momentum (Navier-Stokes equations), and the energy as listed in Eq. (2.29) to Eq. (2.31) based on the assumptions used in this thesis as follows:

1. Incompressible and steady state flow
2. Single phase flow, no gravity or any other body force involved
3. Constant wall temperature
4. No fouling of any kind exists in the computational domain
5. Periodicity is established perpendicular to the flow direction
6. Viscous dissipation is negligible in the energy equation
7. All walls are rigid

$$\nabla \cdot \left(\rho \vec{u} \right) = 0 \tag{2.29}$$

$$\nabla \cdot \left(\rho \vec{u} \vec{u} \right) = -\nabla p + \nabla \cdot \left[\mu \left(\nabla \vec{u} + \nabla \vec{u}^{T} - \frac{2}{3} \nabla \cdot \vec{u} \right) \right] \tag{2.30}$$

$$\nabla \cdot \left[\rho \vec{u} \left(h + \frac{u^2}{2} \right) \right] = \nabla \cdot \left(k \nabla T \right) \tag{2.31}$$

where ρ is the fluid density, $\vec{u}$ the velocity vector, p the pressure, h the specific enthalpy, k the thermal conductivity, and T the temperature. In this dissertation, the available CFD commercial package, Fluent® is used with the aforementioned assumptions. The fluid characteristics used in this dissertation are mainly calculated based on default models in Fluent®. By choosing different models, the results may

change based on the fluid used, viscosity models used, Reynolds number, temperature range and wall roughness. For rapid CFD evaluation of different CFD models used in this dissertation, the process of geometry generation, meshing and simulation need to be automated. An automated too, (Abdelaziz, 2009), termed as Parameterized Parallel Computational Fluid Dynamics (PPCFD) is used to carry out CFD analysis automatically in batch mode. More details about PPCFD are discussed in the next section.

For all CFD based examples in this dissertation, the solver was allowed to iterate until convergence or up to a maximum number of iterations. The convergence criteria were based on maximum acceptable normalized residuals defined for each CFD example. Figures 2.8-2.12 present the residual for different CFD cases for different examples presented in this dissertation.

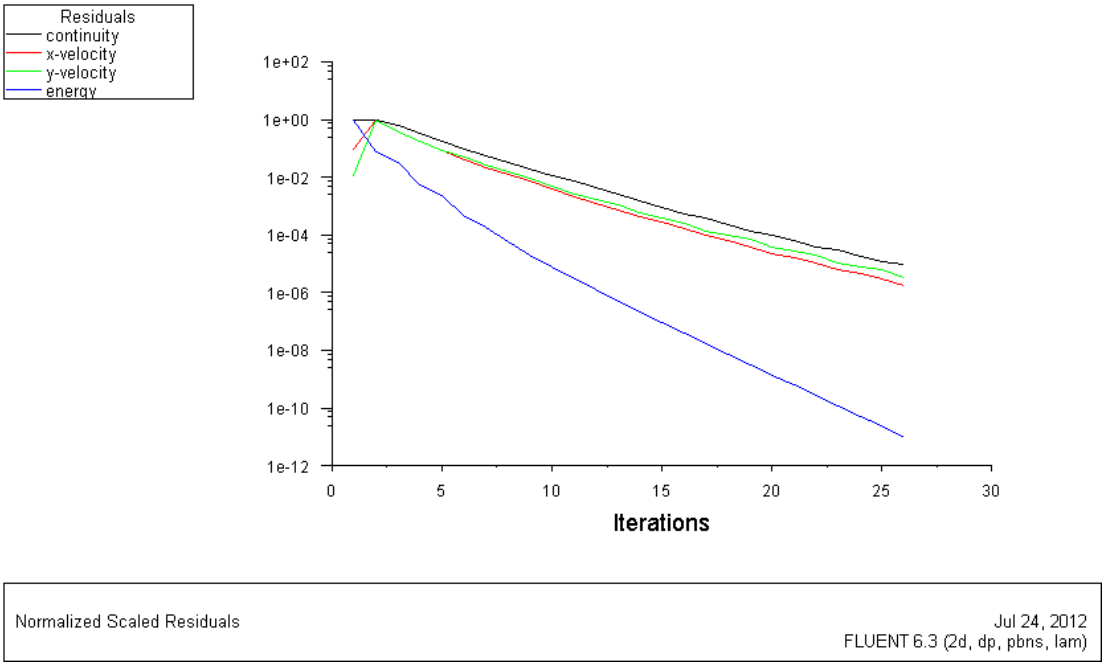

Figure 2.8 Residuals for new generation of air-cooled heat exchanger segment

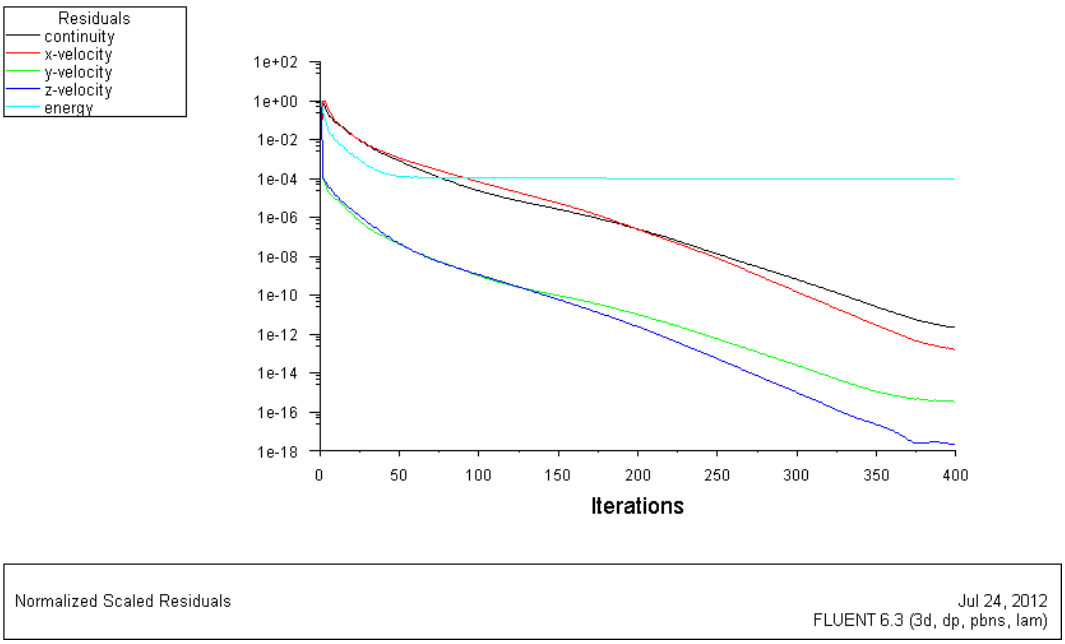

Figure 2.9 Residuals for coldplate model used in electronic cooling

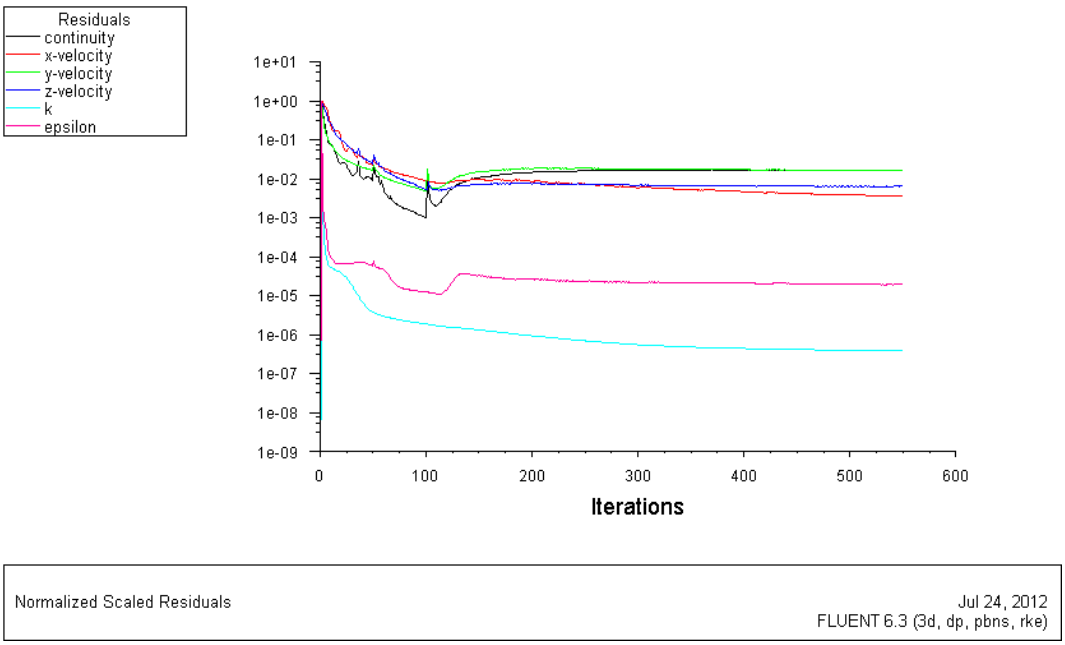

Figure 2.10 Residuals for header used in new generation of air-cooled heat exchanger

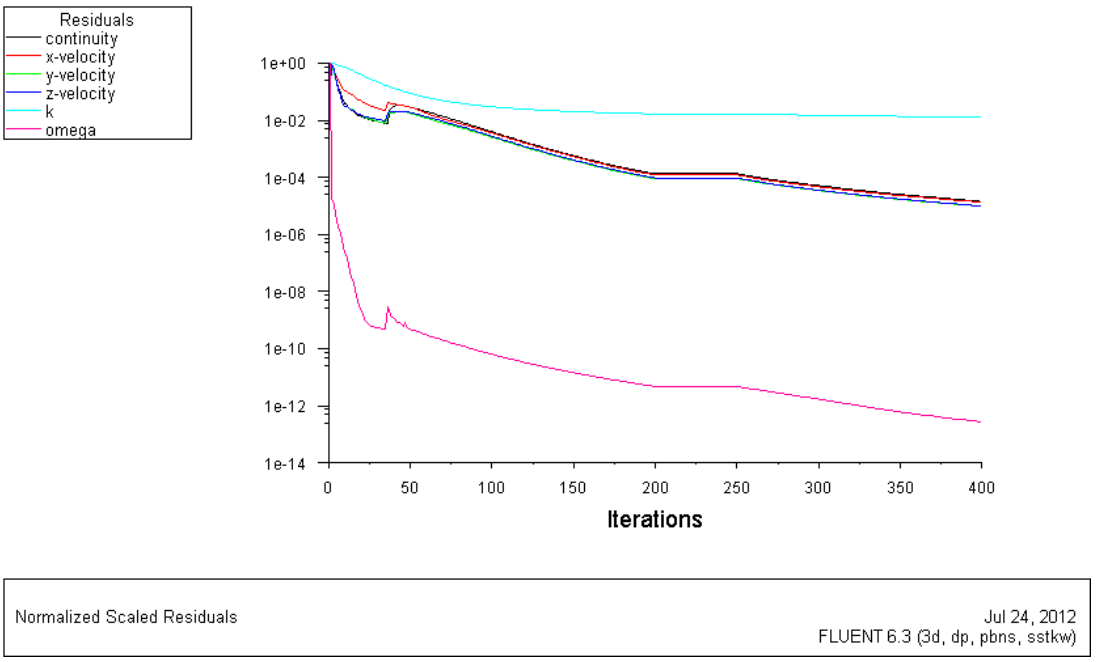

Figure 2.11 Residuals for chevron plate heat exchanger example

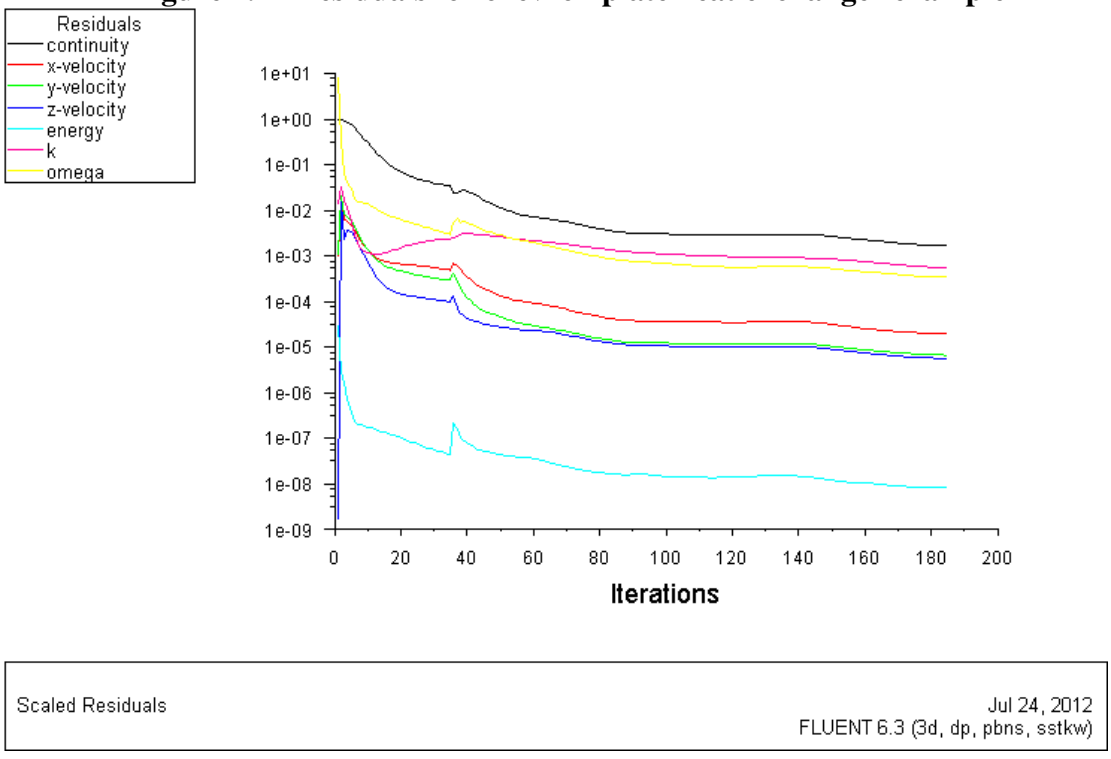

Figure 2.12 Residuals for rollbond plate heat exchanger example

2.8 Parallel Parameterized CFD

Any approximation assisted optimization of a computationally expensive model especially for CFD-based requires a large number of CFD simulations to be executed. In this dissertation, a parallel parameterized CFD (PPCFD) approach (Abdelaziz, 2009) to automatically read the normalized design variables and then generate the corresponding Gambit® journal files. In this step, it is very important to correlate the Gambit® journal files to corresponding design variables. Mesh refinement near the boundaries (boundary layer inflation) applied based on the design dimensions. Also, a finer mesh is applied in locations where higher temperature gradients are expected, such as near the walls, and the thermal and hydraulic entrance regions.

After generating the mesh, the PPCFD program automatically generates Fluent® journal files to read the specified mesh, set the appropriate boundary conditions, model parameters, and material properties. The materials and boundary conditions are defined in the Fluent® journal files.

The main steps in PPCFD can be summarized as follows:

Step 1: reading of the parametric values of all the CFD cases,

Step 2: automatic generation of Gambit® script files and Fluent® script files,

Step 3: running the scripts and performing post processing to summarize the results in terms of relevant thermal and hydraulic performance indicators.

PPCFD is used in this dissertation for all CFD models including new generation of air-cooled HX segment, coldplate, headers for new generation of air-cooled HX, Chevron plate HX, and Rollbond plate HX.

2.9 Summary

In this chapter, the main terminologies and concepts used in this dissertation are briefly discussed. The definitions defined in this chapter can be categorized into two groups: approximation assisted optimization for multiobjective optimization and heat exchanger design for enhanced surfaces using CFD simulations. In the first group, several methods to solve multiobjective optimization problems are discussed followed by dominance concept and quality metrics to measure the quality of the optimum solutions. Then, the multiobjective genetic algorithm is discussed in details as it is used as the optimization approach in this dissertation. Finally, approximation assisted optimization is briefly described with its main steps, e.g., design of experiment, metamodeling, and metamodeling verification metrics followed by a description for three methods from the literature (ParEGO, PSP, and Forrester's). In the second group, different heat exchanger design methods are described followed by the CFD simulation. Finally, PPCFD, a method to couple the CFD simulations with an optimizer is described.

In the next chapter, a new method for online approximation assisted multiobjective optimization is introduced.

Chapter 3: Online Approximation Assisted Multiobjective Optimization (OAAMO)

3.1 Introduction

The material for this chapter is borrowed in part from the papers Saleh et al. (2010b)[1]. In this chapter a new approach for Online Approximation Assisted Multi-objective Optimization, OAAMO, is presented. OAAMO starts with an initial set of sample points to build a metamodel for each objective and constraint function of a multi-objective optimization problem. This metamodel based optimization problem is solved by a Multi-Objective Genetic Algorithm (MOGA) to obtain a set of points. From this set, a few points are selected and added to the current sampled points. The points selected are aimed to (i) sample the region where the multi-objective solutions are expected to be, and (ii) diversify the solution points. OAAMO is compared with (i) AAMO, an offline Approximation Assisted Multi-objective Optimization technique, (ii) ParEGO, an online approximation assisted multi-objective optimization approach from the literature, and (iii) a conventional MOGA. The applicability of OAAMO is also demonstrated with an engineering example for an air-to-refrigerant heat exchanger segment design that involves CFD calculations. The results show that, for the same number of sample points, OAAMO yields a better estimate of the Pareto solutions for most of the examples compared to AAMO and ParEGO. Moreover, compared with MOGA, OAAMO obtains reasonable solutions while reducing significantly the number of functions calls. The goodness of solutions

[1] Saleh, K., Aute, V., Azarm, S., and Radermacher, R., 2010b, "Online Approximation Assisted Multiobjective Optimization with Space Filling, Variance and Pareto Measures," *13th AIAA/ISSMO Multidisciplinary Analysis and Optimization Conference, AIAA-2010,* Fort Worth, TX, USA

obtained from OAAMO is evaluated using two quality metrics from the literature: hyperarea difference and overall Pareto spread, as described chapter 2.

The rest of this chapter is organized as follows: Section 3.2 summarizes the related work from the literature in the area of approximation assisted optimization. An overview of the new approach is provided in Section 3.3. Sections 3.4 and 3.5 introduce numerical examples and results in addition to comparison with ParEGO approach respectively. Section 3.6 presents an engineering example for optimizing air-cooled heat exchanger segment. Section 3.7 provides conclusions and closing remarks.

3.2 Related Work

Most of the existing AAO methods focus on single-objective optimization. A number of methods are reported for multi-objective AAO. Examples of these methods are the Pareto Set Pursuing (Wang and Shan, 2004), multi-criteria sampling (Sasena et al., 2002; Turner et al., 2003) and methods which are based on Efficient Global Optimization (EGO) for single (Jones et al., 1998) and multi-objective optimization (Emmerich et al., 2006; Kean, 2006; Knowles, 2005; Knowles, 2006; Jeong and Obayashi, 2005; Ponweiser et al., 2008). Among these, some methods use a measure like generalized probability of improvement or expected improvement for multi-objective optimization (Emmerich et al., 2006; Kean, 2006). Some of these methods use a single-objective optimization method to maximize the measure of improvement and obtain a sample point. However, such a point may not reflect the best candidate point for the original multi-objective optimization problem (Liu et al., 2008). For instance, ParEGO uses weighting vectors to iteratively convert multiple objective

functions to a single objective function and then chooses the next sample based on maximizing an expected improvement function (Knowles, 2005; Knowles, 2006). ParEGO is computationally expensive for optimization problems with more than ten design variables (Knowles, 2005) and is applicable only to unconstrained optimization problems.

A similar observation can be made in another EGO-based approach by Joeng and Obayashi (2005) where NSGA-II (Deb et al., 2002) is used to optimize an expected improvement of all individual objective functions. However, applying NSGA-II requires thousands of function calls. Similarly, Li et al., (2008) developed a Kriging-based MOGA approach which can require a substantial number of function calls.

One can also find methods in the literature that use quality metrics for guiding the selection of the sample point(s) (e.g., Naujoks et al., 2005; Emmerich et al., 2006; Ponweiser et al., 2008). For instance, a S-Metric Selection based EGO (SMS-EGO) method is reported (Ponweiser et al., 2008) that optimizes the S-metric to select a new sample point. Although SMS-EGO can produce several sample points at every iteration it does not make use of the uncertainty in the metamodel prediction as part of an updating strategy. Accordingly, SMS-EGO may not perform well in predicting optimum solutions (Ponweiser et al., 2008).

The proposed OAAMO has two aims: (i) improving the predictive capability of metamodeling in the region where the optimum solutions are expected to be, and (ii) producing globally accurate and well spread solutions. A few distinct characteristics of OAAMO compared to the related AAO methods are as following:

(1) A significant number of the previous AAO methods only uses a globally accurate metamodel to find optimum solutions (e.g., Koch et al., 2002; Fang et al., 2004; Lian and Liou, 2004; Abdelaziz et al., 2010) which can be computationally expensive. In the proposed approach, online AAO is used to improve the metamodels' performance in the expected optimum region. (2) Some previous approaches (e.g., Knowels, 2006, Wang and Shan, 2004) try to approximate the optimum frontier using an expected improvement measure. Using such a scalar measure based on an aggregate of multiple objectives can change the nature of the original multi-objective optimization problem. However, OAAMO uses the information from the estimated optimum solutions directly and does not use any scalar measure. (3) OAAMO aims at improving the spread, closeness, and accuracy of the solution points while avoiding clustering of the points.

In the next section, the proposed OAAMO approach is described in details.

3.3 Proposed OAAMO

In this section, an overview for OAAMO is presented. In order to update the metamodels and based on intermediate OAAMO runs, OAAMO selects samples with higher Kriging uncertainty to improve the metamodels performance in the expected optimum region. In addition, selecting the sample with minimum variance helps to improve the accuracy in the final optimum solutions. As for the spread and the closeness, selecting the two extreme optimum solutions at each iteration improves the spread while selecting the closest point the ideal point in the objective space helps to improve the closeness. Besides, a space filling filter to avoid samples clustering is considered and to reduce the computational cost of OAAMO approach by avoiding

adding unnecessarily samples. Obviously, each iteration can lead to select several samples. This is suitable for parallel computing environment which can lead to reduce the overall computation time especially with using newly developed workstations.

Furthermore, OAAMO can handle constrained multi-objective problems with taking into account the feasibility of the approximated Pareto solutions. The approach was tested comprehensively for 10 numerical test problems with different number of design variables and constraints and also different Pareto frontier shapes. It resulted in more accurate results compared with ParEGO. In addition, the approach was applied to 2 computationally expensive engineering test problems and the resulting solutions were found to be more accurate compared to offline approximation assisted optimization.

OAAMO is based on an iterative scheme: It starts with an initial set of design points to build metamodels for objectives and constraints of an optimization problem. This metamodel based optimization problem is solved by a Multi-Objective Genetic Algorithm (MOGA) to obtain a set of approximated Pareto solution points. From these Pareto points, five points are selected: The closest point to an ideal point together with the two extreme points in the objective space. In addition the points that have the highest and lowest predicted variance are selected. A space filling filtering scheme is then used to prevent clustering. The collection of points obtained is then used to build and solve the next metamodel based optimization problem and the iterative scheme is repeated until a stopping criterion is met. A limit on the total number of available function calls is used as the stopping criterion.

3.3.1 Overview of Proposed Approach

OAAMO works as follows. It starts with an initial design (a set of points). Next, the Kriging based metamodels are built for the objectives and constraints to create a metamodel assisted multi-objective optimization problem. This problem is solved by MOGA to obtain an estimate of Pareto optimal points. These points with their corresponding predicted variance from the Kriging metamodels are used to select the next sample points. [Although, for simplicity, the description that follows is given based on the objective functions, the effects of the constraints have also been accounted for by using a penalty approach, see e.g., (Kurpati et al., 2002).] The predicted variance is obtained and normalized as follows:

(i) Obtain the variance for the objective functions, say for the case of two-objective functions as f_1 and f_2, for all estimated Pareto points.

(ii) Determine the maximum and minimum values for the variance for f_1 and f_2.

(iii) Calculate the normalized objective variance, i.e., var_{f1} and var_{f2} for f_1 and f_2, respectively. For example, $\text{var}_{f1} = (var_{f1} - var_{f1min})/(var_{f1max} - var_{f1min})$, where var_{f1} is the raw value of the variance for f_1. Also, var_{f1min} and var_{f1max} are the minimum and maximum of the variance for f_1. A similar equation is used to obtain the normalized var_{f2}. Also, a similar procedure is used for normalizing the variance for constraints.

Then the normalized variance var_1 and var_2 are calculated (see Eq.(3.2)) considering the variance in the objectives and constraints.

The normalized objective F_1 (and similarly F_2) is also obtained as follows:

(i) From all the estimated Pareto points obtained so far, identify those with the maximum and minimum of f_1.

(ii) Calculate the normalized objective: $F_1 = (f_1 - f_{1min})/ (f_{1max} - f_{1min})$. A similar equation is used to obtain the normalized for F_2.

Five points from the current estimated Pareto points are selected as follows. In the normalized variance space of objectives, as shown in Figure 3.1(a), a point with the lowest normalized variance for f_1 and f_2, i.e., the closest point to the origin, is selected. An additional point is selected, as shown in Figure 3.1(a), where the normalized variance (e.g., both var_1 and var_2) is large in order to improve the performance of the metamodels globally. Also, in the normalized objective space for the current estimated Pareto points, Figure 3.1(b), the closest point to the ideal point is selected which may be considered as the best point in the objective space. Finally, the two extreme points shown in Figure 3.1(b) in the normalized objective space are selected to improve the diversity of the estimated Pareto frontier. The five points obtained are checked (filtered) with respect to a space filling criterion (described in Section 3.3.3) to prevent clustering. The true responses are then evaluated for the filtered points, these points are added to the current sample points and the metamodels for the objectives and constraints are updated.

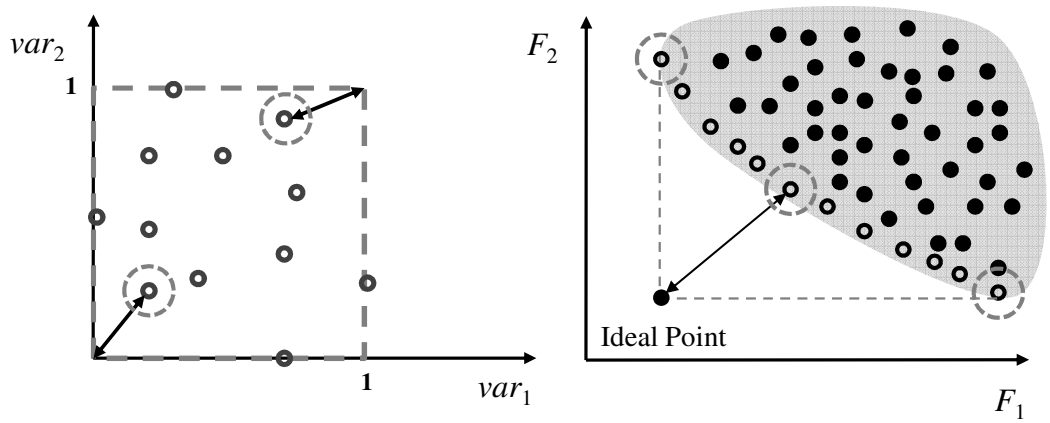

(a) (b)

Figure 3.1 (a) Normalized objective variance space, and (b) normalized objective space

The following sub-sections provide more details on each of the steps summarized above in this section.

3.3.2 Choice of Initial Design

The proposed approach starts with an initial design using maximum entropy design (Shewry and Wynn, 1987). The initial design is used to obtain a representation of the response space and chosen to be a space-filling design with a pre-specified number of points. The initial design is a function of the problem dimension and as such is problem dependent.

3.3.3 Space Filling Metric

In order to avoid the clustering of sample points in the design space, a space filling metric is used (Aute et al., 2008). This space filling metric is based on the Euclidean distance in the design space. The space filling metric used is the maximin distance in the design space as follows. For each experiment in an existing design D,

the minimum non-zero distance of this point from all other points in D is computed. The maximum of these distances is computed and then the space filling metric is set to be equal to one-half of this maximum value. This will ensure that the new sample points will not be placed too close to the existing points. This space filling metric S is independent of the metamodeling technique used. Mathematically, S can be represented as given in Eq. (3.1).

$$\begin{aligned} ds(x_i) &= \min\left(\left\|x_i - x_j\right\|_2\right), \forall\, x_i \in D \wedge (i \neq j) \\ S &= 0.5 \times \max(ds(x_i)), \forall\, x_i \in D \end{aligned} \tag{3.1}$$

3.3.4 Choosing Next Sample Points

Once the optimization problem (with the current metamodels for objectives/constraints) is solved using MOGA, a set of estimated Pareto points is generated. From this set of Pareto points one can select five sample points according to Eq. (3.2), which as mentioned before are filtered to avoid clustering. As mentioned before, points x_1 and x_2 are points in the normalized variance space with the lowest and highest variance respectively and x_3 is a point closest to the ideal point in the normalized objective space in addition to the two extreme points x_4 and x_5 in the normalized objective space where var_1 and var_2 are the normalized objectives variances respectively and F_1 and F_2 are the normalized objectives and F_{ideal} is the ideal point. Although Eq. (3.4) is shown for a bi-objective optimization problem, it can be readily extended to any number of objectives.

$$
\begin{aligned}
&var_1 = \mathrm{var}_{f_1} + \sum_{i=1}^{m} \mathrm{var}_{g_i} \\
&var_2 = \mathrm{var}_{f_2} + \sum_{i=1}^{m} \mathrm{var}_{g_i} \\
&x_1 = \arg\min_x (var_1, var_2) \\
&x_2 = \arg\max_x (var_1, var_2) \\
&x_3 = \arg\min_x \left\| F - F_{ideal} \right\| \ where \ F = (F_1, F_2) \\
&x_4 = \arg\min_x F_1 \\
&x_5 = \arg\min_x F_2 \\
&s.t. \left\| x_i - x_k \right\|_2 \geq S \ \forall \ x_k \in D
\end{aligned}
\tag{3.2}
$$

3.3.5 Design Update

For the design update, the simulation is invoked for the new samples obtained in the last step and then the points are added to the current design *D*. The metamodels are updated and then MOGA solves the corresponding metamodel based optimization problem, producing a new set of Pareto points which will then be sampled according to Eq. (3.2).

3.3.6 Step-by-Step Description of Proposed Approach

Figure 3.2 shows a flowchart for the proposed approach. The stopping criterion used is the maximum number of function calls. The steps in OAAMO are as follows:

Step-1: Generate an initial set of design points using the maximum entropy design method and observe the corresponding responses, i.e., obtain the objectives/constraints values.

Step-2: Develop a metamodel for each objective and constraint function. So, several metamodels are developed in this step.

Step-3: Formulate a multiobjective optimization problem based on the metamodels and solve this problem using MOGA.

Step-4: Obtain Pareto points from Step-3.

Step-5: For all Pareto points calculate the objectives and constraints' variance from Kriging metamodels and select the best point and worst point in the normalized objective variance space. In the normalized objective space, select the point which is closest to the ideal point in addition to the two extreme points.

Step-6: Filter the newly selected points using the space filling filtering scheme as in Eq. (3.1).

Step-7: Evaluate the true response (i.e., run the simulation) for the newly chosen points and then go to Step-2.

Step-8: Repeat Step-2 to Step-7 until a limit on the number of function calls is achieved.

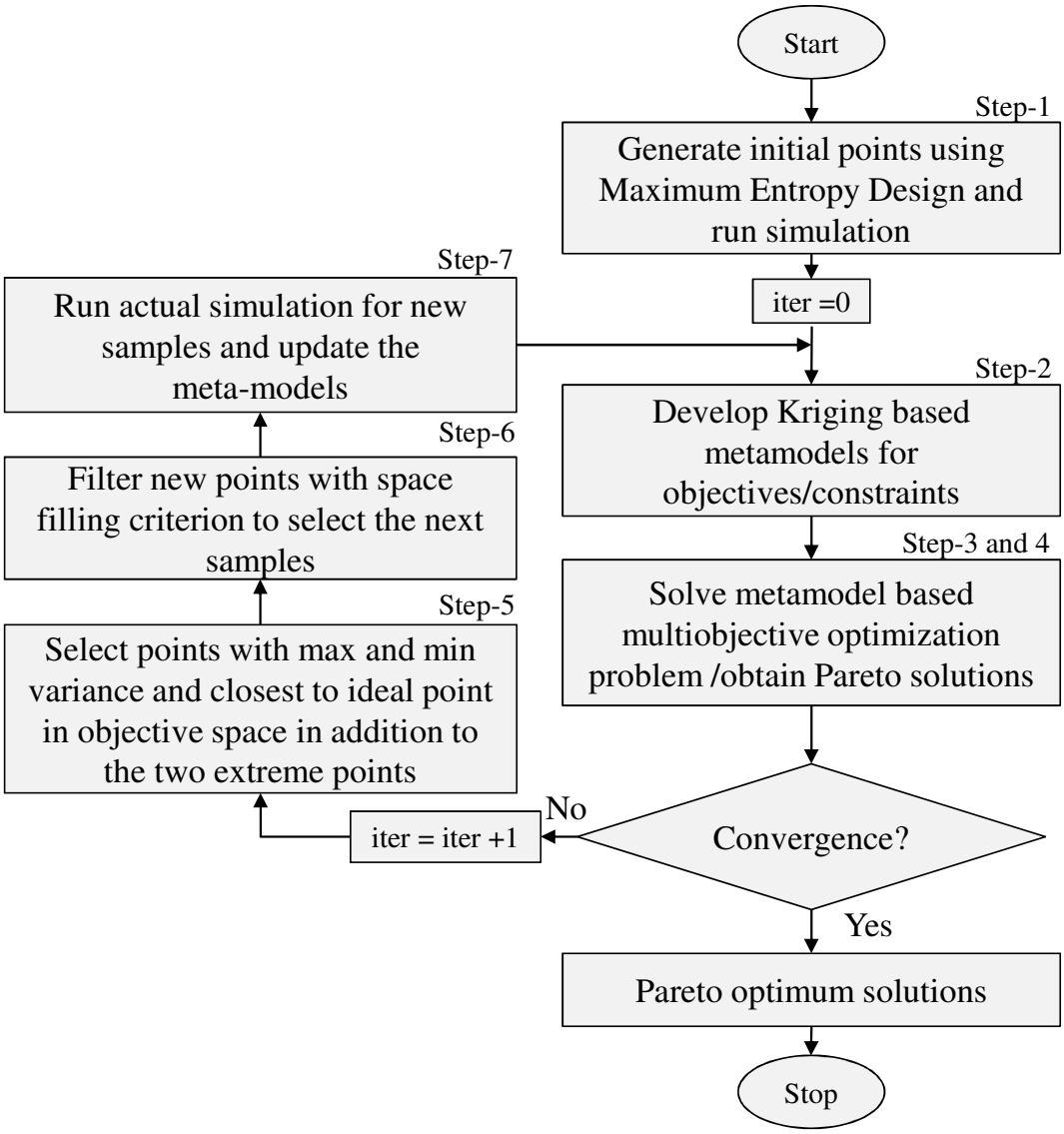

Figure 3.2 Flowchart of OAAMO approach

3.4 Numerical Examples and Results

In this section, the proposed approach is applied to several numerical examples selected from the literature and compared with offline approximation assisted multiobjective optimization approach.

3.4.1 Numerical Examples

The proposed approach is applied to several numerical examples selected from the literature, namely, TNK, CTP, ZDT1,ZDT2, ZDT3 (Deb, 2001), and SR (Azarm and Li, 1989). The formulations of all numerical test problems are listed in Eq. (3.3) to Eq. (3.8). Among others, these examples have different Pareto frontier shapes: concave, convex, and discontinuous. The number of design variables ranges from 2 to 30. Table 3.1 shows the specifications of the test problems including their names as referred to in the literature, problem size, i.e., number of variables, number of points in the initial design, number of new sampled points and number of optimization runs due to stochastic nature of MOGA (MATLAB® 2007a) For the numerical examples, OAAMO is compared with offline approximation assisted optimization, AAMO, and a conventional MOGA. In AAMO, the maximum entropy design method is used to select initial designs and then Multi-response Space Filling Cross Validation Tradeoff (MSFCVT) method (Aute et al., 2008) is used to add sample points until the available number of function calls are exhausted. Then metamodels are built all-at-once (using MSFCVT) for all objectives and constraints and thus an offline metamodel assisted optimization problem is obtained. This problem is then solved with MOGA.

TNK Test Problem

$$
\begin{aligned}
&\text{minimize} \quad f_1(x) = x_1 \\
&\text{minimize} \quad f_2(x) = x_2 \\
&\text{Where} \quad g_1(x) = -x_1^2 - x_2^2 + 1 + 0.1\cos(\arctan(\frac{x_1}{x_2})) \le 0 \\
&\qquad g_2(x) = 2(x_1 - 0.5)^2 + 2(x_2 - 0.5)^2 - 1 \le 0 \\
&\qquad 0 \le x_1 \le \pi, \quad 0 \le x_2 \le \pi
\end{aligned}
\tag{3.3}
$$

SR Test Problem

$$
\begin{aligned}
&\text{minimize} \quad f_1(x) = 0.7854\ a\ x_1 x_2^2 - b + c + d \\
&\text{minimize} \quad f_2(x) = \max\ \{f_{12}, f_{22}\} \\
&\text{where} \quad a = (\frac{10x_3^2}{3} + 14.933 - 43.0934) \\
&\qquad b = 1.508x_1\ (x_6^2 + x_7^2), \\
&\qquad c = 7.477(x_6^3 + x_7^3) \\
&\qquad d = 0.7854(x_4 x_6^2 + x_5 x_7^2) \\
&\qquad g_1(x) = \frac{27}{x_1 x_2^2 x_3} - 1 \le 0, \quad g_2(x) = \frac{397.5}{x_1 x_2^2 x_3^2} - 1 \le 0 \\
&\qquad g_3(x) = \frac{1.93x_4^3}{x_2 x_3 x_6^4} - 1 \le 0, \quad g_4(x) = \frac{1.93x_5^3}{x_2 x_3 x_7^4} - 1 \le 0 \\
&\qquad g_5(x) = \frac{x_2 x_3}{40} - 1 \le 0, \quad g_6(x) = \frac{x_1}{12x_2} - 1 \le 0 \\
&\qquad g_7(x) = 1 - \frac{x_1}{5x_2} \le 0, \quad g_8(x) = 1 - \frac{x_4}{1.9} + \frac{1.5x_6}{1.9} \le 0 \\
&\qquad g_9(x) = 1 - \frac{x_5}{1.9} + \frac{1.1x_6}{1.9} \le 0, \quad g_{10}(x) = \frac{f_{12}}{1800} - 1 \le 0 \\
&\qquad g_{11}(x) = \frac{f_{22}}{1100} - 1 \le 0, \ 2.6 \le x_1 \le 3.6, \ 0.7 \le x_2 \le 0.8
\end{aligned}
\tag{3.4}
$$

CTP Test Problem

$$
\begin{aligned}
&\text{minimize} \quad f_1(x) = x_1 \\
&\text{minimize} \quad f_2(x) = g(x)\left(1 - \sqrt{\frac{f_1(x)}{g(x)}}\right) \\
&\text{Where} \qquad g(x) = \left|1 + \left(\sum_{i=2}^{10} x_i\right)^{0.25}\right| \\
&g_1(x) = \frac{a\left|\sin\left(b\pi\left[\sin(\theta)(f_2(x) - e) + \cos(\theta) f_1(x)\right]^c\right)\right|^d}{\cos(\theta)\left[f_2(x) - e\right] - \sin(\theta) f_1(x)} - 1 \le 0 \\
&\theta = -0.2\pi,\ a = 0.2,\ b = 10,\ c = 1,\ d = 6,\ e = 1 \\
&0 \le x_1 \le 1,\ -5 \le x_i \le 5, \quad i = 2,...,10
\end{aligned}
\tag{3.5}
$$

ZDT1 Test Problem

$$
\begin{aligned}
&\text{minimize} \quad f_1(x) = x_1 \\
&\text{minimize} \quad f_2(x) = g(x) * h(x) \\
&\text{where} \qquad g(x) = 1 + \frac{9\left(\sum_{i=2}^{n} x_i\right)}{n-1} \\
&\qquad\qquad h(x) = 1 - \sqrt{\frac{f_1(x)}{g(x)}} \\
&\qquad\qquad 0 \le x_i \le 1, \quad i = 1,...,30
\end{aligned}
\tag{3.6}
$$

ZTD2 Test Problem

$$
\begin{aligned}
&\text{minimize} \quad f_1(x) = x_1 \\
&\text{minimize} \quad f_2(x) = g(x) * h(x) \\
&\text{Where} \qquad g(x) = 1 + \frac{9\left(\sum_{i=2}^{n} x_i\right)}{n-1} \\
&\qquad\qquad h(x) = 1 - \left(\frac{f_1(x)}{g(x)}\right)^2 \\
&\qquad\qquad 0 \le x_i \le 1, \quad i = 1,...,30
\end{aligned}
\tag{3.7}
$$

ZDT3 Test Problem

$$
\begin{aligned}
&\text{minimize} \quad f_1(x) = x_1 \\
&\text{minimize} \quad f_2(x) = g(x) * h(x) \\
&\text{Where} \quad g(x) = 1 + \frac{9\left(\sum_{i=2}^{n} x_i\right)}{n-1} \\
&\qquad h(x) = 1 - \sqrt{\frac{f_1(x)}{g(x)}} - \left(\frac{f_1(x)}{g(x)}\right)\sin\left(10\pi f_1(x)\right) \\
&\qquad 0 \le x_i \le 1, \quad i = 1,\ldots,30
\end{aligned}
\tag{3.8}
$$

Table 3.1 Test problems data

	# of Design Variables	# of Objectives	# of Constraints	# of Samples in Initial Design	# of New Samples	# of Repeat Runs
TNK	2	2	2	10	10	10
SR	7	2	11	35	35	10
CTP	10	2	1	50	50	10
ZDT1	30	2	0	150	150	10
ZDT2	30	2	0	150	150	10
ZDT3	30	2	0	150	150	10

For all test problems the initial metamodels are built using a set of initial sample points equal to: 5×d, where d is the number of design variables. The total number of available function calls is set to (10×d). The summary of the results including the number of function calls, average and standard deviation for both HD and OS for the six test problems is presented in Table 3.2. For all these test problems, for each generation of MOGA, 100 points (or individuals) are used in the population. For the TNK, SR, and CTP problems, MOGA was run for 200 generations. However for the ZDT1, ZDT2, and ZDT3 problems the number of generations is increased to 500 because there are 30 design variables.

3.4.2 Numerical Results

For all test problems, in order to apply OAAMO, a set of initial design points were generated using MED. This is followed by the actual simulation runs for these design points. After that the Kriging metamodels were built for all objectives and constraints. Next, MOGA was used to solve a corresponding metamodel based multi-objective optimization problem. The obtained Pareto points were tested to select next sample points according to the measures described in Section 3.3. Finally a space filling filtering scheme was applied to the selected points. This procedure was repeated and continued until the stopping criterion was met. The same procedure was used for the other numerical examples: SR, CTP, ZDT1, ZDT2, and ZDT3 as well.

As shown in Tables 3.2-3.4, based on the quality metrics HD and OS, the solutions obtained from OAAMO is comparable with AAMO and MOGA. And, as expected, the total number of function calls is reduced significantly using OAAMO and AAMO compared to MOGA. However, for most of the numerical examples (5 out of 6 examples), the Standard Deviations (STDs) in OAAMO are less than those of AAMO which means solutions obtained from OAAMO are more robust than those obtained from AAMO. In order to compare the performance of OAAMO and AAMO, the errors for the obtained solutions are calculated as given in Eqs. (2.16) – (2.20).

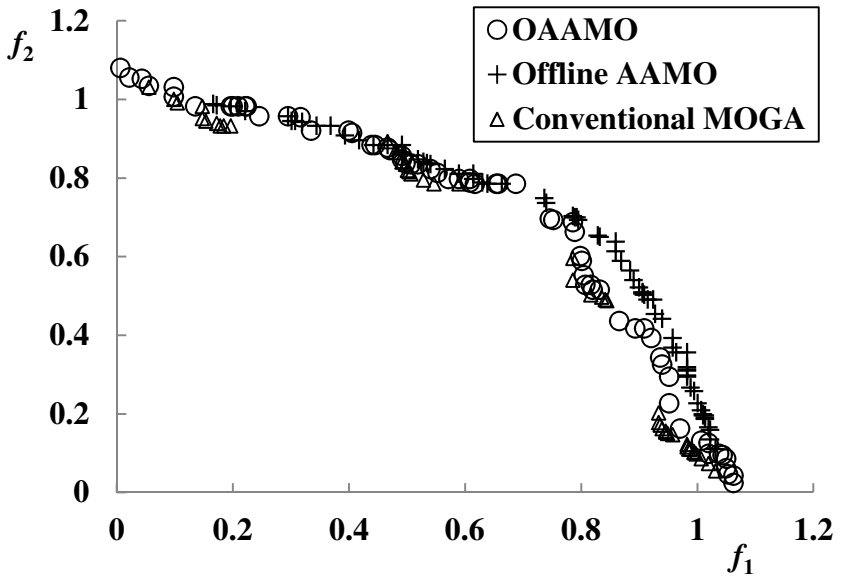
f_2
1.2
1
0.8
0.6
0.4
0.2
0
0
0.2
0.4
0.6
0.8
1
1.2
f_1
OAAMO
Offline AAMO
Conventional MOGA

(a) TNK

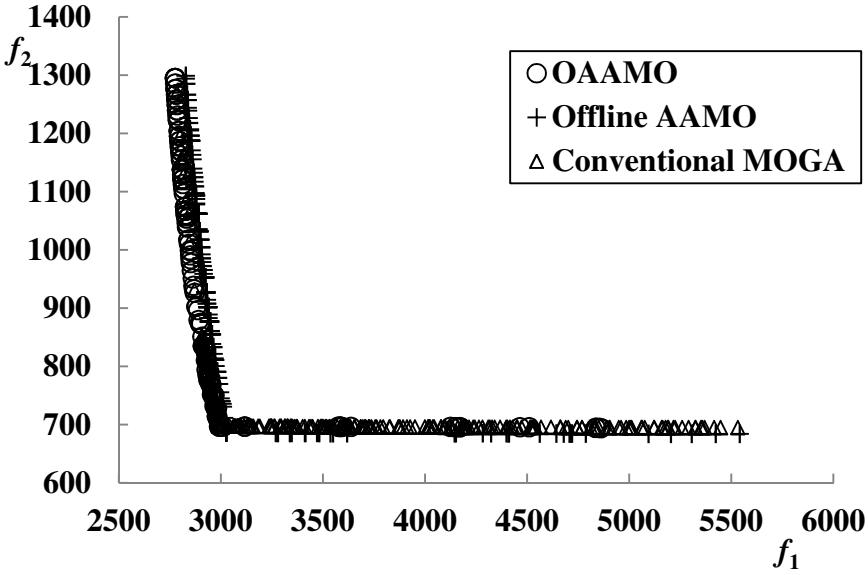
f_2
1400
1300
1200
1100
1000
900
800
700
600
2500
3000
3500
4000
4500
5000
5500
6000
f_1
OAAMO
Offline AAMO
Conventional MOGA

(b) SR

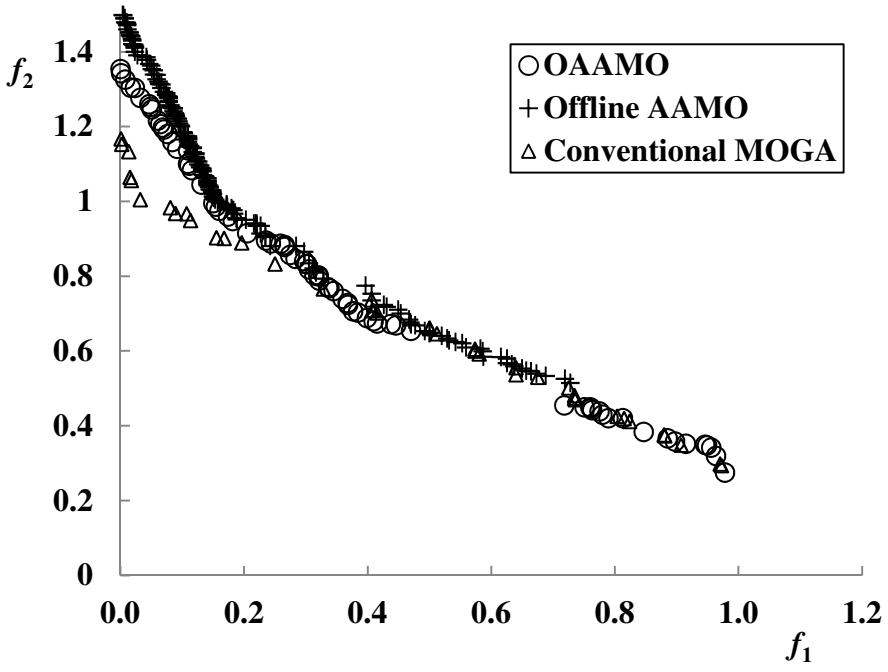
f_2
1.4
1.2
1
0.8
0.6
0.4
0.2
0
0.0
0.2
0.4
0.6
0.8
1.0
1.2
f_1
○OAAMO
＋Offline AAMO
△Conventional MOGA

(c) CTP

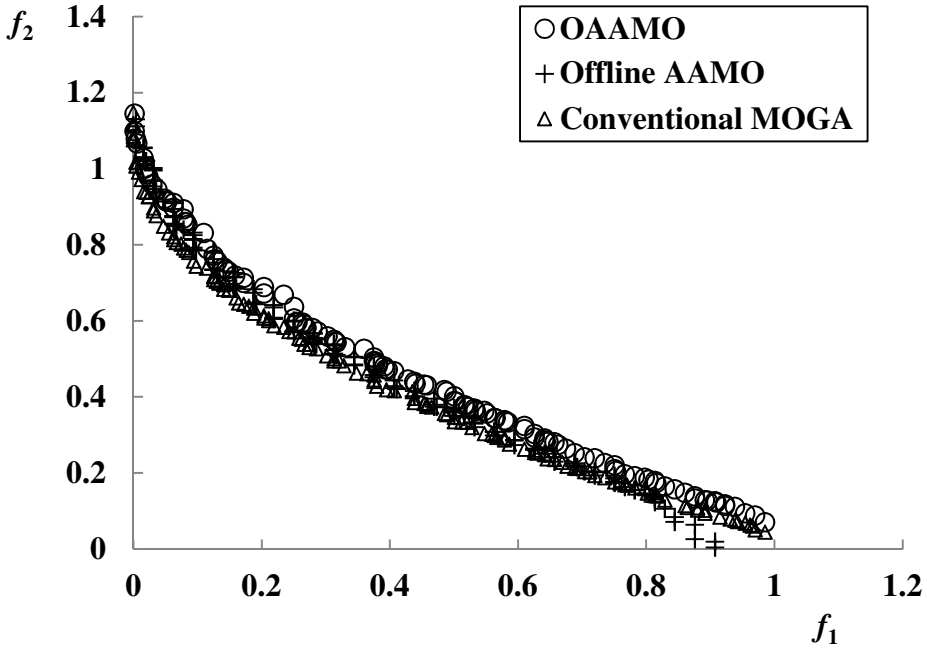
f_2
1.4
1.2
1
0.8
0.6
0.4
0.2
0
0
0.2
0.4
0.6
0.8
1
1.2
f_1
○OAAMO
＋Offline AAMO
△Conventional MOGA

(d) ZDT1

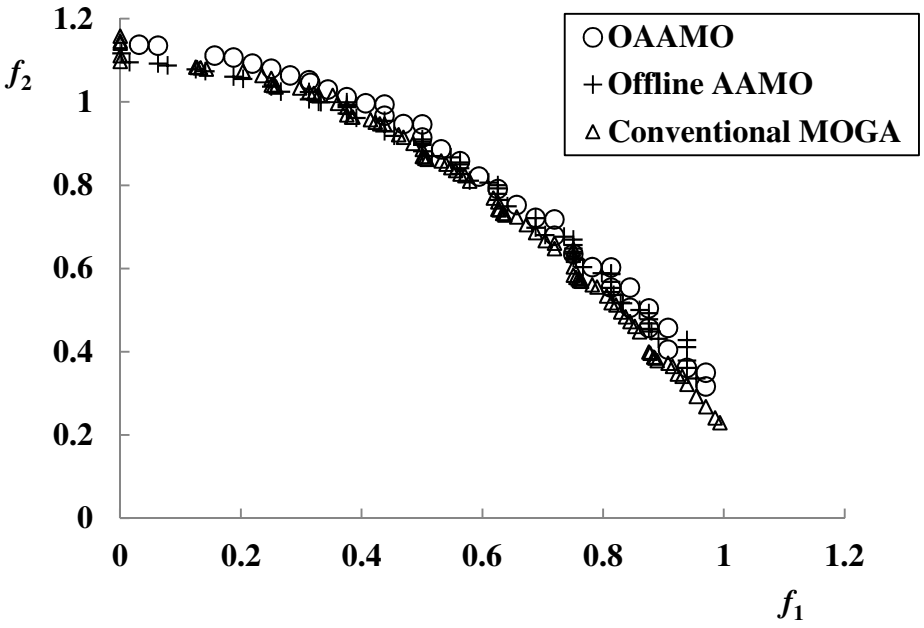

(e) ZDT2

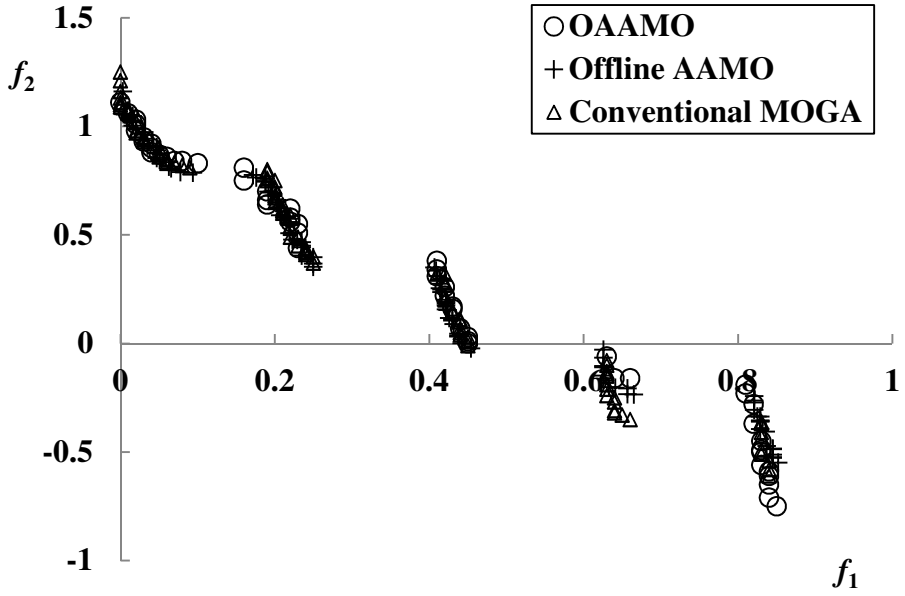

(f) ZDT3

Figure 3.3 Optimal solutions for numerical examples: (a) TNK, (b) SR, (c) CTP, (d) ZDT1, (e) ZDT2, and (f) ZDT3

Table 3.2 OAAMO results for test problems

Test Problem	OAAMO				
	# Fn Calls	HD		OS	
		Average	STD	Average	STD
TNK	20	0.22	0.04	0.83	0.17
SR	70	0.77	0.15	0.52	0.65
CTP	100	0.66	0.03	0.78	0.09
ZDT1	300	0.74	0.04	0.91	0.09
ZDT2	300	0.33	0.06	0.72	0.14
ZDT3	300	0.58	0.03	0.85	0.31

Table 3.3 AAMO results for test problems

Test Problem	AAMO				
	# Fn Calls	HD		OS	
		Average	STD	Average	STD
TNK	20	0.23	0.07	0.54	0.23
SR	70	0.74	0.21	0.98	0.86
CTP	100	0.66	0.03	0.65	0.06
ZDT1	300	0.66	0.05	0.87	0.15
ZDT2	300	0.45	0.07	0.89	0.12
ZDT3	300	0.59	0.05	0.93	0.32

Table 3.4 Conventional MOGA results for test problems

Test Problem	Conventional MOGA				
	# Fn Calls	HD		OS	
		Average	STD	Average	STD
TNK	2100	0.21	0.06	0.78	0.13
SR	2100	0.79	0.17	0.80	0.98
CTP	2100	0.63	0.04	0.76	0.01
ZDT1	5100	0.66	0.01	0.64	0.02
ZDT2	5100	0.32	0.02	0.79	0.09
ZDT3	5100	0.57	0.05	0.81	0.09

A summary of the error results for the numerical test problems is reported in Table 3.5 and Table 3.6. Based on the *RMSE* and *RRMSE*, OAAMO outperforms AAMO for all test problems except TNK. Also, OAAMO results in a smaller STDs compared with AAMO, which again means that OAAMO is more robust and predicts more accurate and consistent results compared with AAMO.

Table 3.5 Pareto verification for OAAMO and AAMO (*RMSE*)

Test Problem	OAAMO				AAMO			
	f_1		f_2		f_1		f_2	
	Mean	STD	Mean	STD	Mean	STD	Mean	STD
TNK	1.9×10^{-5}	0.1×10^{-5}	1.2×10^{-5}	0.2×10^{-5}	1.3×10^{-5}	0.3×10^{-5}	9.6×10^{-6}	0.4×10^{-5}
SR	2.0537	1.82	0.515	0.329	397.48	365.28	210.46	129.126
CTP	0.00	0.00	0.229	0.128	0.00	0.00	0.575	0.339
ZDT1	0.00	0.00	0.012	0.045	0.00	0.00	0. 014	0.015
ZDT2	0.00	0.00	0.004	0.0024	0.00	0.00	0.026	0.0173
ZDT3	0.00	0.00	0.049	0.035	0.453	1.8×10^{-6}	0.672	0.04

Table 3.6 Pareto verification for OAAMO and AAMO (*RRMSE*)

Test Problem	OAAMO				AAMO			
	f_1		f_2		f_1		f_2	
	Mean	STD	Mean	STD	Mean	STD	Mean	STD
TNK	0.002	2×10^{-4}	0.0019	0.4×10^{-8}	0.0014	4×10^{-8}	0.0015	0.4×10^{-5}
SR	0.065	0.012	0.059	0.019	13.204	48.23	22.378	28.89
CTP	0.00	0.00	23.043	2.949	0.00	0.00	37.694	12.78
ZDT1	0.00	0.00	2.842	0.128	0.00	0.00	2.842	0.043
ZDT2	0.00	0.00	0.719	0.001	0.00	0.00	6.475	0.112
ZDT3	0.00	0.00	0.824	0.0288	0.00	0.00	37.529	1.50

3.5 Comparison with ParEGO

In this section, the proposed method OAAMO is compared with ParEGO (Knowels, 2005) for four test problems, all unconstrained, as listed in Eq (3.9) to Eq. (3.12). These test problems have different degrees of difficulty and characteristics. As shown in Figure 3.4, and Table 3.7 and Table 3.8, OAAMO outperforms ParEGO in terms of the average *HD* metric for OKA1, KNO1 and VLMOP2 test problems. In terms of the average *OS* metric, OAAMO performs significantly better than ParEGO for OKA2 and KNO1 problems.

Table 3.9 reports the *RMSE* and *RRMSE* results for OAAMO solutions only. The errors are reported for OAAMO because its solutions are obtained based on metamodels. On the other hand, while ParEGO uses metamodeling internally, the final solutions are obtained based on the observed points and thus no error is reported for its solutions. From these results, it can be concluded that for almost all test problems the accuracy of the OAAMO solutions is reasonable.

OKA1 Test Problem

$$
\begin{aligned}
&\text{minimize} \quad f_1 = x_1' \\
&\text{minimize} \quad f_2 = \sqrt{2\pi} - \sqrt{|x_1'|} + 2|x_2' - 3\cos(x_1') - 3| \\
&\text{Where} \quad x_1' = \cos(\pi/12)x_1 - \sin(\pi/12)x_2 \\
&\qquad\quad x_2' = \sin(\pi/12)x_1 + \cos(\pi/12)x_2 \\
&\qquad\quad x_1 \in [6\sin(\pi/12), 6\sin(\pi/12) + 2\pi\cos(\pi/12)] \\
&\qquad\quad x_2 \in [-2\pi\sin(\pi/12), 6\cos(\pi/12)]
\end{aligned}
\tag{3.9}
$$

OKA2 Test Problem

$$\begin{aligned}
&\text{minimize} \quad f_1 = x_1 \\
&\text{minimize} \quad f_2 = 1 - \frac{1}{4\pi^2}(x_1 + \pi)^2 + \left|x_2 - 5\cos(x_1)\right|^{1/3} + \\
&\qquad\qquad \left|x_3 - 5\sin(x_1)\right|^{1/3} \\
&\text{Where} \quad\quad x_1 \in [-\pi, \pi], x_2, x_3 \in [-5,5]
\end{aligned} \tag{3.10}$$

KNO1 Test Problem

$$\begin{aligned}
&\text{minimize} \quad f_1\ (x) = 20\ -\ r\ \cos\ (f) \\
&\text{minimize} \quad f_2\ (x) = 20\ -\ r\ \sin\ (f) \\
&\text{Where} \quad\quad r = 9 - [3\sin(5/2(x_1 + x_2)^2) + 3\sin(4(x_1 + x_2)) + \\
&\qquad\qquad 5\sin(2(x_1 + x_2) + 2))] \\
&\qquad\qquad f = \pi/12(x_1 - x_2 + 3) \\
&\qquad\qquad x_1, x_2 \in [0,3]
\end{aligned} \tag{3.11}$$

VLMOP2 Test Problem

$$\begin{aligned}
&\text{minimize} \quad f_1 = 1 - \exp\left(-\sum_{i=1}^{n}(x_i - 1/\sqrt{n})^2\right) \\
&\text{minimize} \quad f_2 = 1 + \exp\left(-\sum_{i=1}^{n}(x_i - 1/\sqrt{n})^2\right) \\
&\text{Where} \quad\quad x_1, x_2 \in [-2,2],\ n = 2
\end{aligned} \tag{3.12}$$

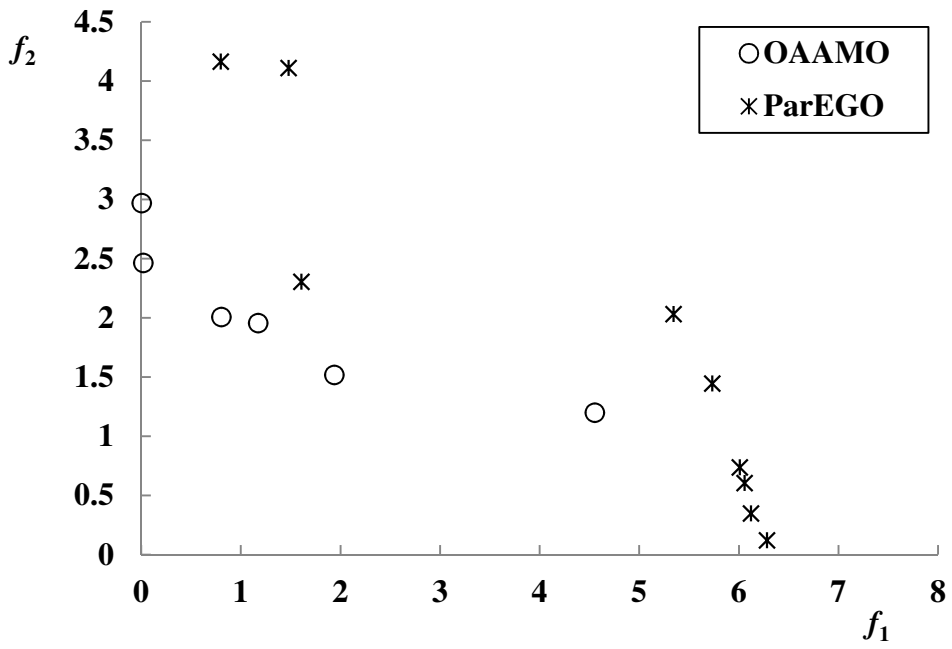
f_2
4.5
4
3.5
3
2.5
2
1.5
1
0.5
0
0
1
2
3
4
5
6
7
8
f_1
OAAMO
ParEGO

(a) OKA1

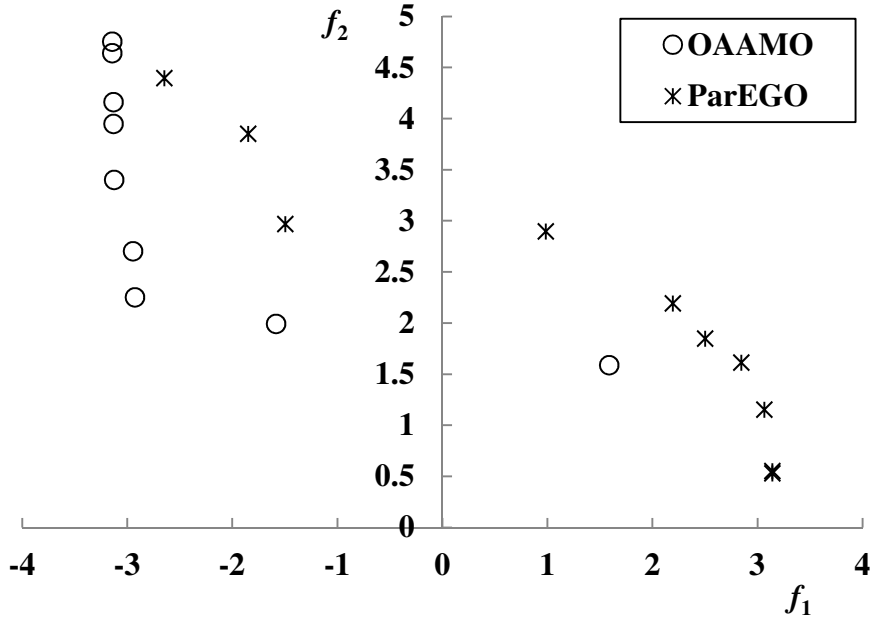
f_2
5
4.5
4
3.5
3
2.5
2
1.5
1
0.5
0
-4
-3
-2
-1
0
1
2
3
4
f_1
OAAMO
ParEGO

(b) OKA2

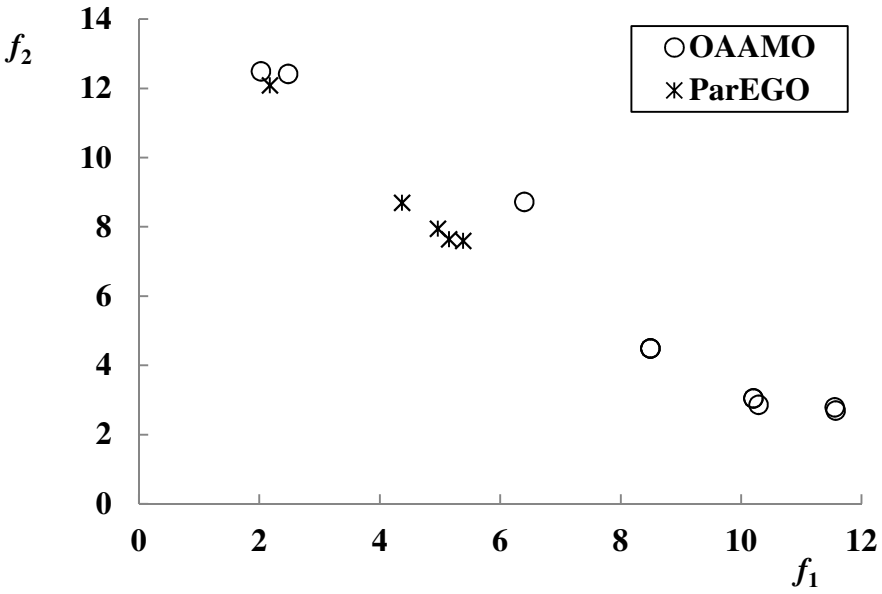

(c) KNO1

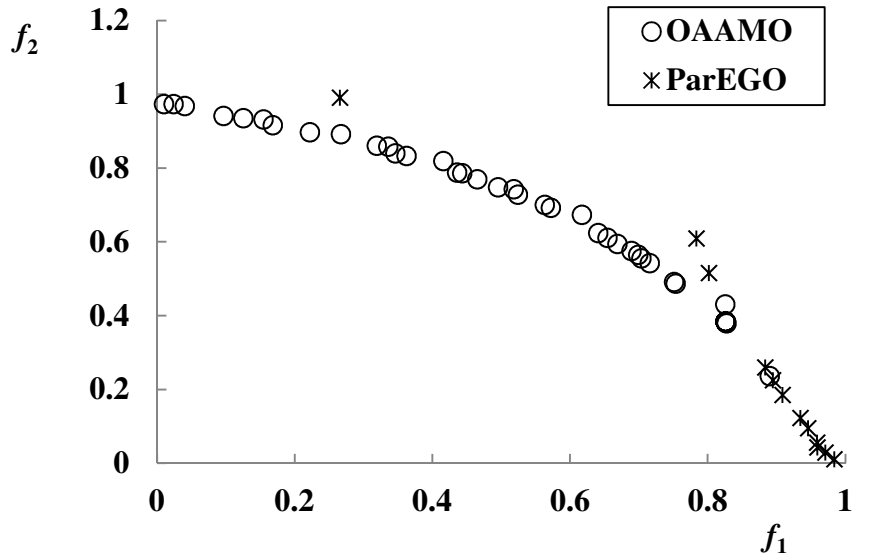

(d) VLMOP2

Figure 3.4 Optimum solution for numerical examples using OAAMO and ParEGO

Table 3.7 OAAMO results

Test Problem	OAAMO				
	#Fn Calls	HD		OS	
		Average	STD	Average	STD
OKA1	20	0.49	0.07	0.35	0.28
OKA2	20	0.61	0.05	0.58	0.29
KNO1	20	0.39	0.13	0.70	0.50
VLMOP2	20	0.61	0.07	0.32	0.11

Table 3.8 ParEGO results

Test Problem	ParEGO				
	#Fn Calls	HD		OS	
		Average	STD	Average	STD
OKA1	20	0.60	0.08	0.44	0.14
OKA2	20	0.59	0.05	0.38	0.17
KNO1	20	0.59	0.09	0.13	0.09
VLMOP2	20	0.68	0.05	0.36	0.18

Table 3.9 Pareto verification for OAAMO

Test Problem	*RMSE*				*RRMSE %*			
	f_1		f_2		f_1		f_2	
	Mean	STD	Mean	STD	Mean	STD	Mean	STD
OKA1	0.05	0.08	0.23	0.12	2.74	3.81	7.94	3.33
OKA2	0.02	0.02	0.30	0.10	1.22	1.08	10.12	4.35
KNO1	0.03	0.04	0.04	0.06	0.19	0.25	0.35	0.42
VLMOP2	0.02	0.01	0.01	0.01	13.17	21.08	3.78	3.99

3.6 Engineering Example

The OAAMO approach was also applied to optimize air-to-refrigerant heat exchanger segment with six design variables as summarized in Table 3.10. A commercially available CFD simulation tool (Fluent, 2007) was used to evaluate the actual values of objectives and constraints.

The initial metamodels are built using an initial design with 30 samples. 100 individuals in the population in each generation of MOGA are used with the total number of generations is set equal to 500. For the engineering example, OAAMO is

just compared against AAMO since the computational time for solving these two examples was prohibitively large to solve them directly with MOGA. Only 60 actual simulations were used with OAAMO or AAMO.

3.6.1 Air Cooled Heat Exchanger Segment Model

A schematic of a cross-flow air-to-refrigerant heat exchanger (Abdelaziz et al., 2010) is shown in Figure 3.5(a) and corresponding heat exchanger segment in Figure 3.5(b). The performance measures for this heat exchanger element are the air side heat transfer coefficient and the air side pressure drop. The overall goal is to find via optimization the best segment design that provides a heat exchanger segment with higher air side heat transfer coefficient and lower pressure drop.

The different dimensions or design variables which dictate the air side performance of the element are marked in Figure 5(c). The corresponding temperature distribution is shown in Figure 5(d) for inline arrangement when there is no offset. The air side heat transfer and pressure drop are obtained by solving the continuity and momentum equations using CFD.

Overall, this air to refrigerant heat exchanger problem has six input variables and two responses. For the purpose of this study, individual metamodels are developed for each response. The six design variables are as follows (see Figure 3.5): Tube internal diameter, center to center vertical and horizontal spacing, the number of ports, offset, and the inlet air velocity. The time required for each simulation is approximately 5 minutes on a Dual 2 GHz Xeon workstation.

Table 3.10 Test problems data

Test Problem	# of Design Variables	Initial Design	New Samples	Repeat Runs
HXSegment	6	30	30	10

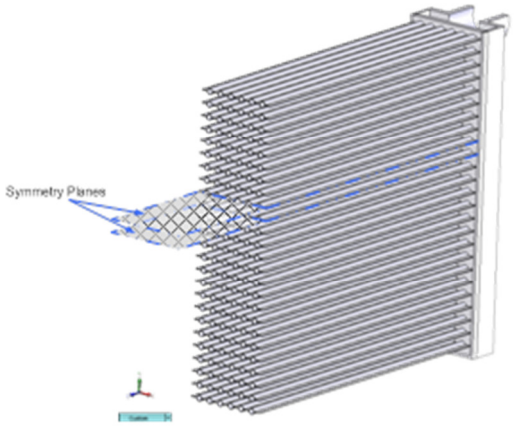

(a)

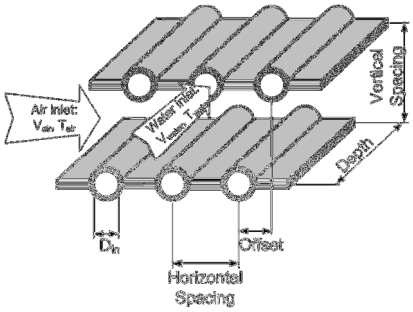

(b)

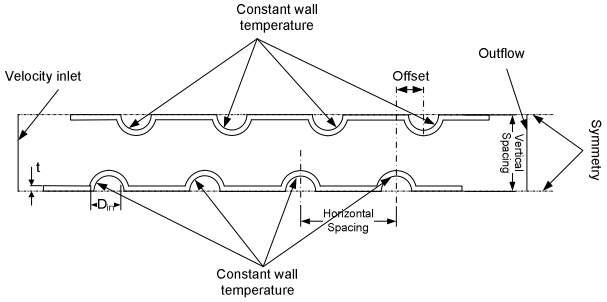

(c)

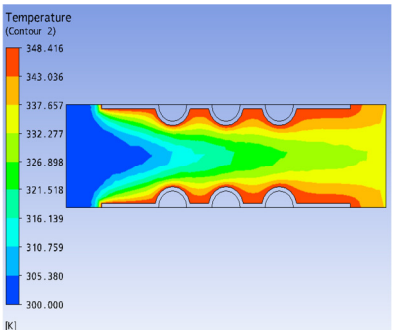

(d)

Figure 3.5 (a) Air to refrigerant heat exchanger, (b) heat exchanger segment Schematic, (c) computational domain and (d) sample results (Abdelaziz et al., 2010)

3.6.2 Air Cooled Heat Exchanger Segment Optimization Problem Definition

The input variables used to build the metamodel and their limits are given in Table 3.11. The outer diameter, the tube thickness and the horizontal and the vertical spacing are a function of the inner diameter. Thus accounting for inner diameter also accounts for outer diameter, thickness and spacing. The vertical and horizontal spacing needs to be accounted for, since it has a direct influence on the air-side heat transfer and pressure drop. Since the limits imposed on the inner diameter differ by an order of magnitude, it is imperative to have the limits on the other design variables scale accordingly. The velocity limit was chosen based on the velocity limits for conventional air-conditioning applications. All design variables are normalized within the interval [0, 1] when used in the DOE and metamodel development. The optimization problem for the heat exchanger segment can be summarized as shown in Eq. (3.13).

Table 3.11 Design Variables for Heat Exchanger Segment Optimization

Design Variable	Lower Limit	Upper Limit
Inner diameter, D_{in}	0.1mm	1mm
Horizontal spacing, *Hs* [mm]	$1.5 \times D_{out}$	$6.0 \times D_{out}$
Vertical spacing, *Vs* [mm]	$2 \times D_{out}$	$4 \times D_{out}$
Depth, *w* [mm]	Function of D_{in}	Function of D_{in}
Offset, *l* [mm]	Function of *Hs*	Function of *Hs*
Air velocity, *v* [m/s]	1.0	3.0

$$\begin{aligned} &minimize \quad f_1(x) = AirHTC \\ &minimize \quad f_2(x) = \Delta P_{air} \\ &subject\ to: \ \Delta P_{air} \le 50\,kPa \\ &\qquad\qquad AirHTC \ge 100\ W/m^2K \end{aligned} \tag{3.13}$$

3.6.3 Results

Two different metamodels were built for the two responses or objectives, one for Air pressure drop (ΔP_{air}) and the other for Air Heat Transfer Coefficient (*AirHTC)*. Kriging with logarithmic response (to avoid negative values during prediction) was used to develop the metamodels. For AAMO, a non-adaptive approach was used and 60 samples were generated using the MED method.

Figure 3.6 shows the obtained Pareto sets for OAAMO and AAMO. As observed from Figure 3.6, OAAMO resulted in an improved Pareto set such that it obtains solutions with higher heat transfer coefficient and lower pressure drop than AAMO. CFD verification for the Pareto set also shows smaller errors for the OAAMO compared to AAMO, see Table 3.12.

Table 3.12 Relative Errors in Pareto Solutions from OAAMO and AAMO for Heat Exchanger Segment

RError	OAAMO		AAMO	
	ΔP_{air} %	*AirHTC %*	ΔP_{air} %	*AirHTC %*
Average	1.20	0.30	4.62	2.34
Max	6.30	1.70	8.94	4.89
Min	0.02	0.01	0.06	0.16
STD	1.99	0.54	1.52	2.63

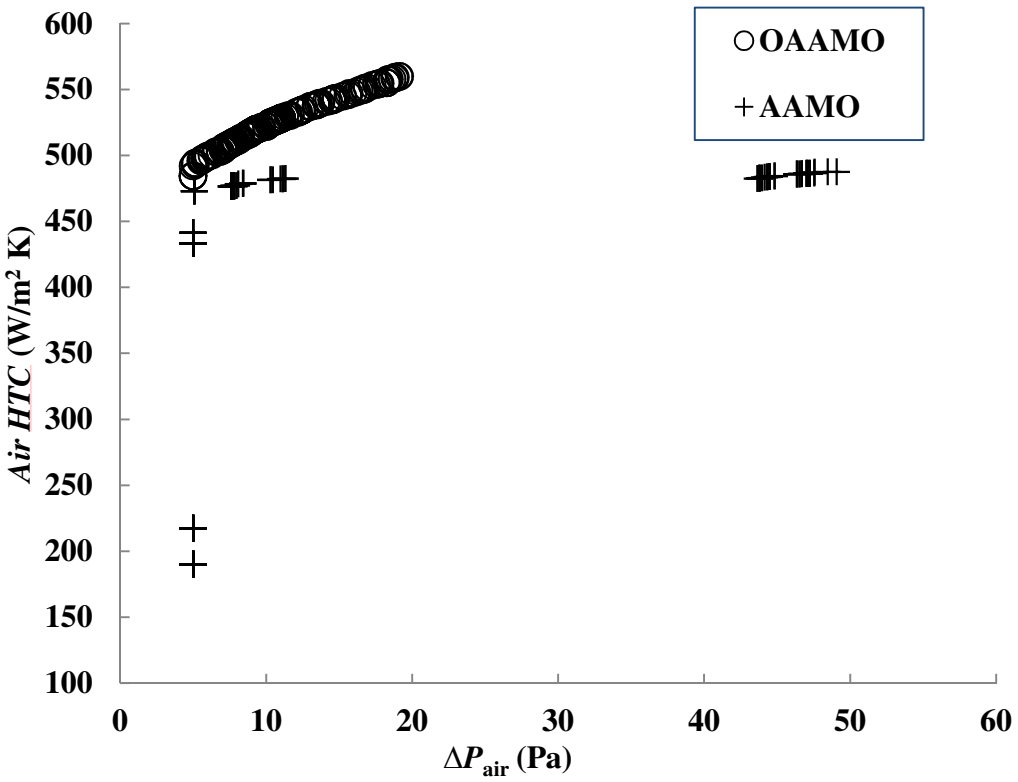

Figure 3.6 Comparison between OAAMO and AAMO for heat exchanger segment optimization

3.7 Summary

In this chapter, a new online approximation assisted multiobjective optimization approach called OAAMO is presented. In the proposed approach, metamodels of objectives and constraints are iteratively developed and updated in concert with an optimizer. This updating of the metamodels is based on selecting a few (five) sample points from an estimated set of Pareto solutions obtained in each iteration of the approach. An accumulation of these sample points together with an initial design form a set of samples for building metamodels. The five selected points include: (i) two points with the lowest and highest (normalized) predicted variance in

the normalized objective functions' variance space, (ii) three points from the current estimated Pareto points (two end points and one in the middle). A space filling filter is applied to prevent any clustering of the samples. The proposed approach is applied to a total of 10 numerical and an engineering test problems with different degrees of difficulty. The OAAMO solutions are compared with AAMO, ParEGO and MOGA. Based on the results obtained, it is concluded that OAAMO obtains a better estimate of the Pareto solutions for most of the examples compared to AAMO and ParEGO. Moreover, compared with MOGA, OAAMO obtains reasonable solutions while reducing significantly the number of functions calls.

In the next chapter, a new global and local search based approach is proposed for multiobjective optimization. The new approach is mainly developed to reduce further the computational cost by eliminating the verification of final optimum solutions. In addition, the new approach always delivers feasible solutions.

Chapter 4: Approximation Assisted Multiobjective Optimization with Combined Global and Local Metamodeling

4.1 Introduction

The approximation assisted multiobjective optimization with global and local metamodeling approach of this chapter is presented in Hu et al., (2012)[2,3].

In this chapter, a new approximation assisted multiobjective optimization approach is developed. Both global and local metamodels for objective and constraint functions are used. Numerical example is used to compare the proposed approach with previous approaches in the literature. Additionally, the proposed approach is applied to a CFD-based engineering design example. It is found that the proposed approach is able to estimate Pareto optimum points reasonably well while significantly reducing the number of function evaluations.

The rest of this chapter is organized as follows: Section Section 4.2 summaries the related work from the literature. An overview of the new approach is provided in Section 4.3. Sections 4.4 introduce numerical example and results in addition to comparison with approaches from the literature. Section 4.5 presents an engineering example for optimizing coldplate device that is used for electronic cooling. Section 4.6 provides conclusions and closing remarks.

---

[2] Hu W., Saleh, K., and Azarm, S., 2012a, "Approximation Assisted Optimization with Combined Global and Local Metamodeling," ASME *2012 International Design Engineering Technical Conference, IDETC 2012*, August 12-12, 2012, Chicago, IL, USA.

[3] Hu W., Saleh, K., Azarm, S., and Mosier, G., 2012b, "Approximation Assisted Optimization with Combined Global and Local Metamodeling," *Manuscript Submitted to Journal of Mechanical Design*, June 5, 2012.

4.2 Related Work

As introduced early in Chapter 3, Approximation Assisted Optimization (AAO) is widely used in engineering design problems to replace computationally intensive simulations with metamodeling. Traditional AAO approaches employ global metamodeling for exploring an entire design space. Recent research works in AAO report on using local metamodeling to focus on promising regions of the design space. However, very limited works have been reported that combine local and global metamodeling within AAO. A summary of the related work in the area of using global and local metamodeling in approximation assisted optimization is provided in the this section.

According to the coverage of design space by a metamodel, AAO can be categorized as either a global or local approach. A global AAO uses a metamodel to estimate each objective and constraint function for the entire design space (Sasena et al., 2002; Huang et al., 2006). A local AAO approach focuses on certain local regions in the design space and constructs the metamodels in those focused regions for the objective and constraint functions (Fonseca et al., 2010; Picheny et al., 2010; Pilat and Neruda, 2011). For example, local approximation with a Taylor expansion has been used based on a coarsely sampled global space (Haftka, 1991). Also, work has been reported with only one cluster to focus on an expected optimum region for single-objective optimization (Wang and Simpson, 2004). Both global and local AAOs have their advantages and limitations. A global AAO is useful in exploring the entire design space and obtaining a global optimal solution. While for local AAO, since the focus is on a relatively small region in the design space, a higher accuracy

of solutions can be achieved. But AAO with local metamodeling alone is not capable of exploring the entire design space and may be stuck at a local optimum or suboptimal solutions.

In this chapter, a newly developed online approximation assisted multiobjective optimization approach is presented. The proposed approach combines global and local metamodels to significantly improve metamodeling accuracy while using fewer sample points during AAO. The basic idea is to screen a set of randomly generated points by using metamodels and select the non-dominated ones. The observed non-dominated points are grouped in multiple clustered regions in the design space and then local metamodels of objective/constraint functions are constructed in each region. The observed points are also used to update the metamodels and this procedure is repeated until a pre-specified number of sample points is exhausted. One numerical and one engineering examples are tested with this approach. The results from the numerical example are compared with several well-known previous approaches, namely ParEGO (Knowles, 2006), PSP (Shan and Wang, 2005) and Forrester's approach (Forrester et al., 2008).

A few distinct characteristics of the proposed approach compared to the related AAO methods in the literature are: (1) The majority of previous AAO methods focus either on global or local metamodeling and very few consider using both global and local metamodel with multiobjective optimization. In the proposed approach, online sample points are iteratively placed in both global and local design spaces and consequently used to construct multiple metamodels to explore the design space. Combining global and local metamodels with AAO allows the proposed

approach to explore the entire design space better, while focusing on promising local regions. (2) While a previous approach (Wilson et al., 2001) uses a clustering method to support the refinement of a local optimum region for single-objective optimization, the proposed approach identifies a number of clusters in the promising local design spaces for a multiobjective optimization problem. This multiple clustered regions are helpful for the proposed approach to estimate better a wider range of Pareto solutions. (3) An adaptive procedure is developed in the proposed approach to determine the number and location of clusters according to a "spread distance" of the non-dominated points. Since the spread distance is calibrated in both design variable and objective space, the clusters are able to quickly identify the most promising region and further improve the non-dominated points iteratively. (4) The clusters in the proposed approach are located around the current best design points. In this way, the local metamodels significantly enhance the accuracy of metamodeling and predictive capability of the approach. In addition, the best design point is always observed and is feasible. As such, there is no need to verify the final solutions separately. In the next section, the details of the proposed approach are presented.

4.3 Proposed Approximation Assisted Multiobjective Optimization with Combined Global and Local Approach

The following sub-sections provide details on the global and local search methodology, the adaptive clustering technique and the steps in the proposed approach.

4.3.1 Overview of Proposed Approach

The approach starts with global metamodels for objective and constraint functions and using them it selects the most promising points from a large number of randomly generated points. The actual simulation for the selected points is run, which means their actual objective/constraint function values are computed. Based on these values, the "best" points are grouped in multiple clustered regions in the design space and then local metamodels of objective/constraint functions are constructed in each region. All observed points are also used to iteratively update the metamodels. In this way, the predictive capabilities of the metamodels are progressively improved as the optimizer approaches the Pareto optimum frontier. An advantage of the proposed approach is that the most promising points are observed and that there is no need to verify the final solutions separately.

4.3.2 Global and Local Search

The main goal of the proposed approach is to find a good estimate of the global Pareto optimum design points while reducing the total number of function calls. In order to achieve this, both global and local metamodeling and search of the design space are considered. Iteratively, global metamodels are built for the entire design space while a large number of random points are generated and evaluated using the global metamodels. The global metamodels are iteratively updated to better estimate global optimum design points and to avoid getting stuck at local optimum solutions. Additionally, after non-dominated points are obtained, clusters are defined and local metamodels are built in each cluster. For each cluster, random points are also generated and evaluated (according to the objective/constraint functions) based

on the local metamodels. The method for creating clusters and iteratively and adaptively updating them is described next.

4.3.3 K-Means Clustering

In the proposed approach, the purpose of clustering is to divide a population of non-dominated points into a few groups or subpopulations (Seber, 1984; Hastie et al., 2001). Each of these groups consists of non-dominated points which are close to each other in the design space. When using metamodels to estimate the objective and constraint functions, the response over the entire design space can be highly non-linear and multi-modal. However, the non-dominated points in one cluster can be selected to have more similar responses for the estimated objective and constraint functions. Therefore, using a clustering method that divides the non-dominated points into different clusters and constructing local metamodels for each cluster can significantly improve the accuracy of the metamodels.

In this approach, a standard K-means clustering method (Seber, 1984) is used to divide a set of N non-dominated points $\mathbf{x}_j$ (j = 1, 2, … N) and determine the location of cluster centers. In K-means clustering, the mean value of the K cluster centers $\mathbf{c}_k$ (k=1, 2,… K) are determined so that the within-cluster sum of the distances between the non-dominated points and center of the cluster are minimized, as expressed in Eq. (4.1):

$$\min \sum_{k=1}^{K} \sum_{j=1}^{N} \| \mathbf{x}_j - \mathbf{c}_k \| \tag{4.1}$$

where the quantity ||•|| computes the Euclidean distance for the inside term. Since the K-means cluster method minimizes the Euclidean distances of the elements within the

same cluster, different clustering results can be identified with different values of K. In the next section, an adaptive method is developed to determine the value of K.

After the non-dominated points are clustered, a rectangle (or a hyper-box in multiple dimensions) is formed around each cluster, enclosing all the non-dominated points within the cluster. The boundary of the rectangle is extended by adding a small margin around the rectangle. This will allow the proposed approach to better explore the design space adjacent to the current clusters. Within the rectangle for each cluster, a local metamodel for the objective and constraint functions is constructed using the non-dominated points (which are all observed). The details of the cluster-based metamodeling are discussed in the next section.

4.3.4 Adaptive Clustering

The number of clusters is mainly identified based on the number of non-dominated points and the distance between the non-dominated points in the design space. The number of clusters helps to improve the spread of the final optimum designs while avoiding sample crowding in the design space. The steps to determine the number of clusters are listed below:

Step 1: Start with one cluster, k=1.

Step 2: Use the K-means clustering approach (Seber, 1984) to determine k clusters and the centers of these clusters ck (k=1, 2, …, K)

Step 3: Calculate the maximum in-cluster distance $d_{\max}$. First, the maximum in cluster distance for cluster k, d_k, is computed:

$$d_k = \max_{j \in S_k} \| \mathbf{x}_j - \mathrm{c}_k \| \tag{4.2}$$

where c_k represent the center (or centroid) for cluster k and Sk represents the set of all the points $\mathbf{x}_j$ inside the cluster k. Among all the maximum in-cluster distances d_k (k=1, 2, …, K), the maximum in-cluster distance for different clusters, $d_{\max}$, is obtained:

$$d_{\max} = \max_k (d_k) \tag{4.3}$$

Step 4: Check the stopping condition, with $D_{\max}$ being a user specified maximum acceptable in-cluster distance:

$$d_{\max} \leq D_{\max} \tag{4.4}$$

If this condition is not satisfied, increase the number of clusters by one: $k = k+1$, and return to Step 2. Otherwise, the number of clusters equals to k.

The quantity $D_{\max}$ is a problem dependent parameter. It represents an upper bound for an acceptable distance between any sample point and centroid of a cluster. Typically, a smaller $D_{\max}$ results in more clusters and thus better accuracy of the metamodels and solutions. However, this smaller value also increases the number of function calls needed in the proposed approach.

4.3.5 Sample Selection

The initial samples are generated using a space filling sampling technique such as the Maximum Entropy Design (MED) or Latin Hypercube Sampling (LHS) method (Koehler and Owen, 1996). After the non-dominated random points are identified, one new sample from the non-dominated set is selected based on the spread distance. The spread distance is computed using a Euclidean distance between a non-dominated (candidate) point and the existing sample points considering both design and objective space. In calculating the spread distance, the design variables

and objectives are scaled between 0 and 1. The spread distance in the design space is given by the following equation:

$$d_{\mathbf{x}} = \max_{i \in S} \| \mathbf{x} - \mathbf{x}^i \| \tag{4.5}$$

where $\mathbf{x}$ and $\mathbf{x}^i$ represent a candidate point and a sample point, respectively. The max in Eq. (4.5) is over all existing sample points where S refers to the sample set. Similarly, the distance in the objective function space is expressed as:

$$d_{\mathbf{f}} = \max_{i \in S} \| \mathbf{f} - \mathbf{f}^i \| \tag{4.6}$$

A weighted sum of both distances Eqs. (4.6) and (4.7) is used to account for the closeness (or spread distance) in both spaces:

$$\gamma = 1/2 d_{\mathbf{x}} + 1/2 d_{\mathbf{f}} \tag{4.7}$$

A non-dominated random point with the largest γ value is selected as a new sample point in every iteration of the proposed approach.

4.3.6 Step-by-Step Description of Proposed Approach

Figure 4.1 shows a flowchart for the proposed approach. The steps are described as in the following.

Step 1: Initialize

Create an initial set of sample points (or samples), run the simulation and calculate the responses (for objectives and constraints).

Step 2: Build Global Metamodels

Build a global metamodel for each objective and constraint function.

Step 3: Generate Global Random Points

Generate random samples in the entire design space and estimate the responses using the global metamodels obtained in Step 2; combine initial samples and the random points into a universal sample set.

Step 4: Identify Global Non-Dominated (ND) Points

Identify the ND points from the universal set of points from Step 3 and observe (or compute the objectives/constraints for) the non-dominated points that are not observed yet.

Step 5: Create Clusters and Local Metamodels

Create a few clusters based on the non-dominated points as described in Section 4.3.3; place additional samples (if necessary) in each cluster to build locally accurate metamodels for objectives and constraints.

Step 6: Generate Local Random Points in Clusters

Generate random points in each cluster and estimate their response using local metamodels; again combine existing samples and the random points in the clusters into a universal sample set.

Step 7: Identify Local Non-Dominated (ND) Points

Identify the non-dominated points from the universal set in Step 6 and observe the non-dominated points that are not observed before.

Step 8: Repeat and Stop

Repeat steps 2-7 until a certain stopping criterion is satisfied.

The stopping criterion can be based on one or more of the following criteria: (i) No change in clusters (location and size) for several iterations. (ii) Total number of

available function calls is exhausted. (iii) No change to the non-dominated points for a number of iterations.

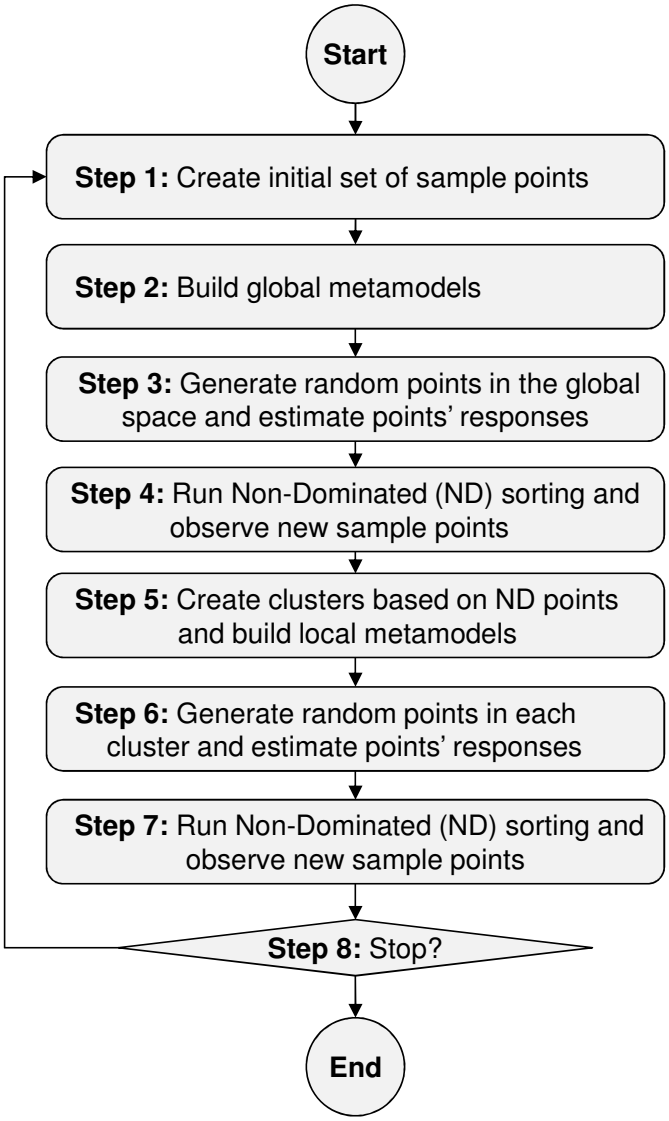

Figure 4.1 Flowchart of the proposed approach

4.4 Numerical Examples and Results

In this section, the two-variable two-objective ZDT3 example from the literature (Shan and Wang, 2005) is chosen to demonstrate the approach. The formulation of the optimization problem is:

$$
\begin{aligned}
&\min \quad f_1 = x_1 \\
&\min \quad f_2 = u[1-\sqrt{x_1 / u} - (x_1 / u)\sin(10\pi x_1)] \\
&s.t.: \quad x_1, x_2 \in [0,\ 1] \\
&\text{where} \quad u = 1+9x_2
\end{aligned}
\tag{4.8}
$$

As summarized in Table 4.1, a response surface metamodeling technique is used in this example. The values of initial and total number sample points are 6 and 20 respectively. The maximum in-cluster distance $D_{\max}$ which adaptively determines the number of clusters, is 0.07.

Table 4.1. Number of samples and maximum in-cluster distance for ZDT3 example

	Metamodel	# of total samples	# of initial samples	Max. in-cluster dist.
ZDT3	Kriging	20	6	0.07
Coldplate	Kriging	30	10	0.09

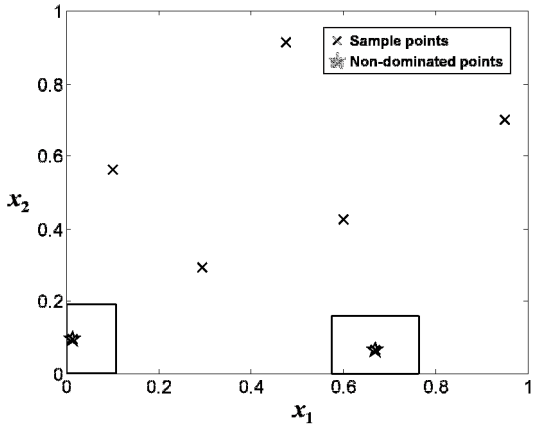

(a)

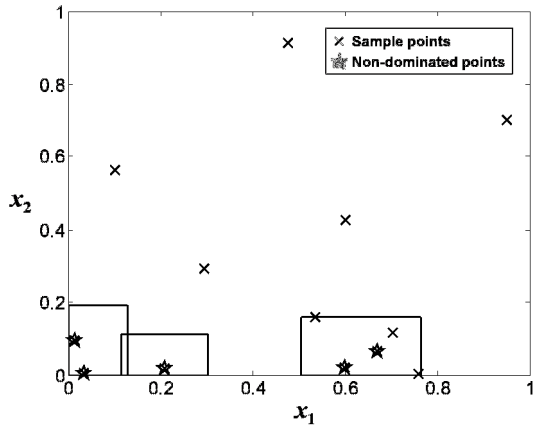

(b)

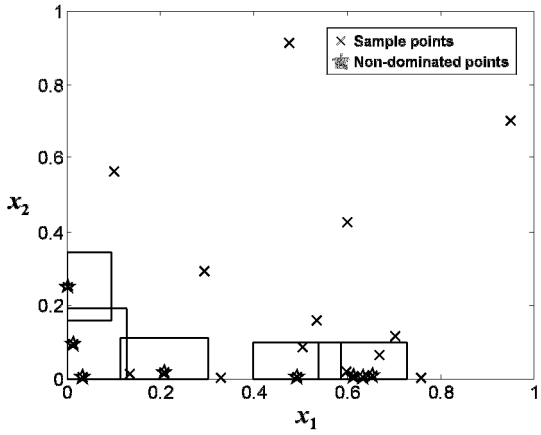

(c)

Figure 4.2 Number of sample points (N) and Non-Dominated (ND) points with clusters (a) N=7 ND=2, (b) N=13 ND=5, and (c) N=20 ND=9

Following the steps of the proposed approach, 6 initial sample points are placed in the global design space in the beginning. Based on these sample points, a global metamodel for each objective function is constructed. Next, 200 random points are generated in the global design space and both objective function values are estimated using their global metamodels. The global random points are then combined with the current sample points, and the non-dominated points are identified. Among the non-dominated points, some points might have already been

observed from the existing sample set. For the unobserved non-dominated points, one point is selected based on the spread distance in both design and objective space as discussed earlier in Section 4.3.5. Consequently, the selected point is observed.

In Figure 4.2 (a), the initial 6 sample points and the newly observed non-dominated point are shown in the design variables space. As can be seen, only two non-dominated points are identified. The non-dominated points are clustered adaptively based on the maximum in-cluster distance, where the rectangle represents the boundary of the clusters. As shown in Figure 4.2 (a), two clusters are identified and the local metamodel is constructed for each cluster using the sample points within the clusters. In the following, 100 random points are generated in each cluster and their objective function values are estimated using the local metamodels. Finally, the local random points are combined with the sample (observed) points, and the non-dominated points are identified. Again one sample is selected based on the spread distance and if a selected non-dominated random point is not observed, it should be observed. After that, the iteration counter is increased by one and the previous steps are repeated. Figure 4.2 (b) and (c) shows the progressive improvement of the sample points and non-dominated points from an intermediate iteration and the final iteration for the illustrative example. It can be seen from the figure that both the area and location of the rectangles (or clusters) change iteratively. Because only a limited number of sample points are used, the optimization is stopped when the total number of sample points (i.e., 20) is exhausted. One interesting observation is the overlapping of clusters in Figures 4.2. This happens because a small $D_{\max}$ value is used which allow more clusters to be adaptively created, and also because the area of each cluster

is extended with a margin. However, this overlap effect does not degrade the performance of the proposed approach.

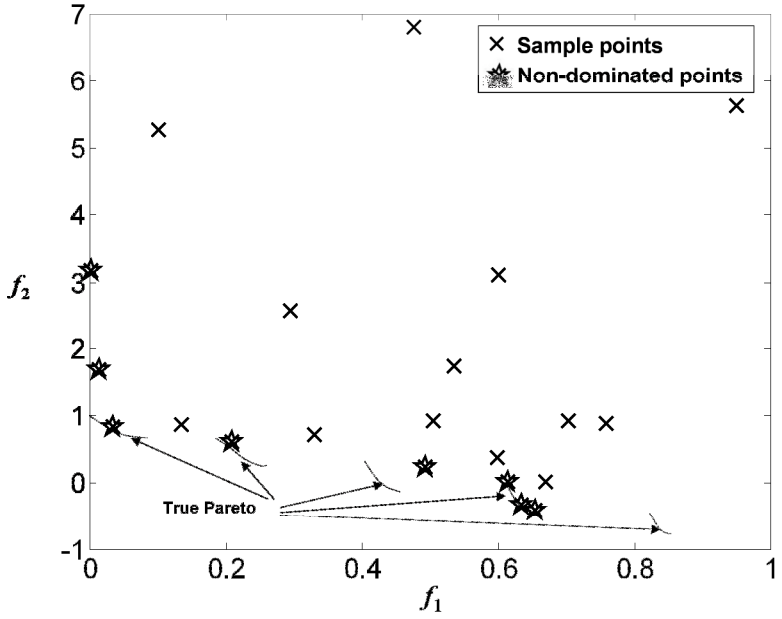

Figure 4.3 Optimal solution for ZDT3 test problem

The final non-dominated points based on 20 sample points are shown in the design variable space in Figure 4.2(c). The same set of sample points and non-dominated points are also plotted in the objective space in Figure 4.3. The true Pareto frontier is also shown in the same figure for comparison. It can be seen that the majority of the sample points are located around the true Pareto and the proposed approach identified a reasonable set of optimum solutions in terms of closeness as well as the spread in the objective function space.

Then the results obtained from the proposed approach are compared with three approaches from the literature, PSP (Shan and Wang, 2005), Forrester (Forrester et al., 2008), and ParEGO (Knowles, 2006). The summary of the comparison is presented in Table 4.2. and Figure 4.4. Considering the randomness of initial sample

points generated by the LHS, all compared approaches are run for 10 times for with the same number of initial and total number of sample points as shown in Table 4.1. HD, and overall spread, OS in addition to the number of non-dominated points obtained from each approach are used in the comparison. The attainment surfaces for the best and worst non-dominated solutions based on the HD value from each approach are shown in the objective function space in Figure 4.4. Table 4.2 summarizes the mean and standard deviation of the number of non-dominated points, HD and OS.

Table 4.2 Number ND points and quality metrics for numerical and engineering examples

	Approach	#ND pts. Mean/std.	HD Mean/std.	OS Mean/std.
ZDT3	Proposed	7/1	0.19/0.02	0.37/0.15
	PSP	7/1	0.21/0.02	0.36/0.27
	Forrester	6/2	0.22/0.02	0.87/0.37
	ParEGO	6/2	0.20/0.06	0.22/0.16
Coldplate	Proposed	11/1	0.43/0.01	0.36/0.13
	Forrester	9/1	0.42/0.01	0.65/0.08

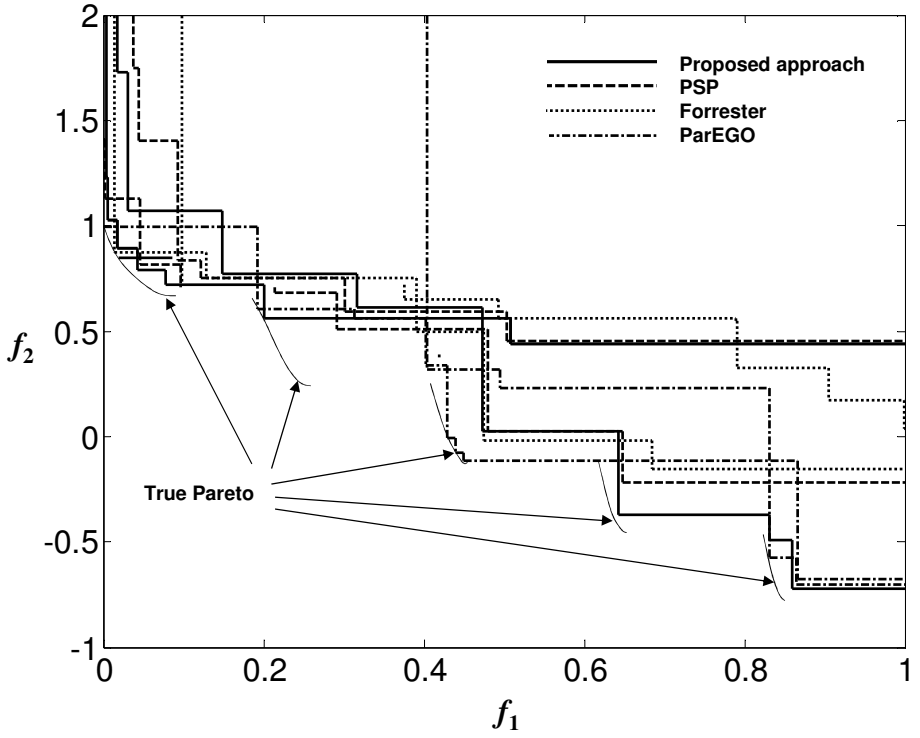

Figure 4.4 Optimal solutions for numerical examples ZDT3

4.5 Engineering Example

The proposed approach is applied to optimize the design of a microchannel coldplate. The coldplate schematic is shown in Figure 4.5(a) (Saleh et al., 2010). The objectives considered are: minimizing the maximum channel temperature $T_{\max}$ while minimizing the refrigerant pressure drop ΔP inside the channel as formulated in Eq. (4.9).

$$
\begin{aligned}
&\min\ f_1 = T_{\max} \\
&\min f_2 = \Delta P \\
&\text{s.t.: } T_{\max} < 600\,\text{K} \\
&\quad \Delta P\ < 4\times10^4\ \text{Pa} \\
&\quad T_{out} - T_{in} < 14\ \text{K}
\end{aligned}
\tag{4.9}
$$

Table 4.3 Design Variables for Coldplate Optimization

Design Variable	Lower Limit	Upper Limit
Channel height, H [mm]	0.8	2.0
Channel width, W [mm]	5.0	70.0
Refrigerant velocity, *v* [m/s]	0.5	3.0

In this example, three design variables are considered as shown in Table 4.3: channel height H, channel width W, and refrigerant velocity ν. The constraints are the allowed refrigerant pressure drop inside the channel and limitation on both maximum channel wall temperature (material constraint) and temperature difference between outlet and inlet of the channel. Only half of the channel, as shown in Figure 4.5(b), is simulated as there is symmetry at the center of the channel. Parallel parameterized CFD (PPCFD) approach (Abdelaziz et al., 2010) is used to automatically read the normalized design variables and then generate the corresponding Gambit® and Fluent® journal files (Fluent, 2007).

Because all constraint functions in the coldplate example are obtained from an expensive CFD simulation, the PSP and ParEGO approaches are not applied to this example since both approaches cannot handle constraints. However, the Forrester's approach is applied and the results of both the proposed approach and Forester's approach are given in Figure 7 where the non-dominated solutions from the best and worst runs from both approaches are shown. The number of non-dominated points and the quality of the non-dominated solutions are shown in the last two rows of

Table 4.2. Note that the proposed obtains slightly more number of non-dominated points compared with the Forrester's approach. On the other hand Forrester's diversity is slightly better than the proposed approach. In terms of the attainments surfaces, the two approaches are comparable.

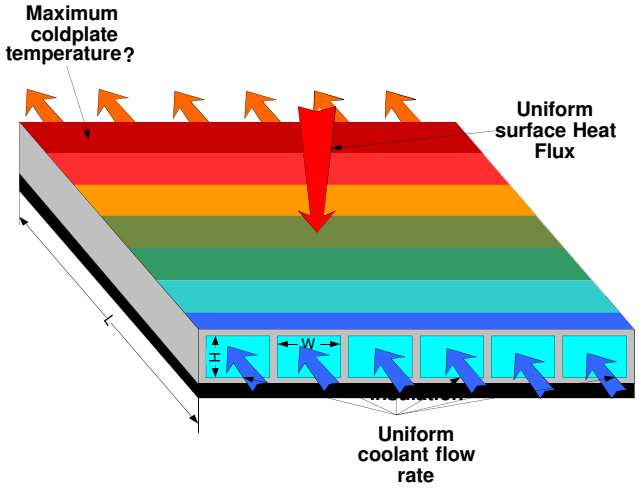

(a)

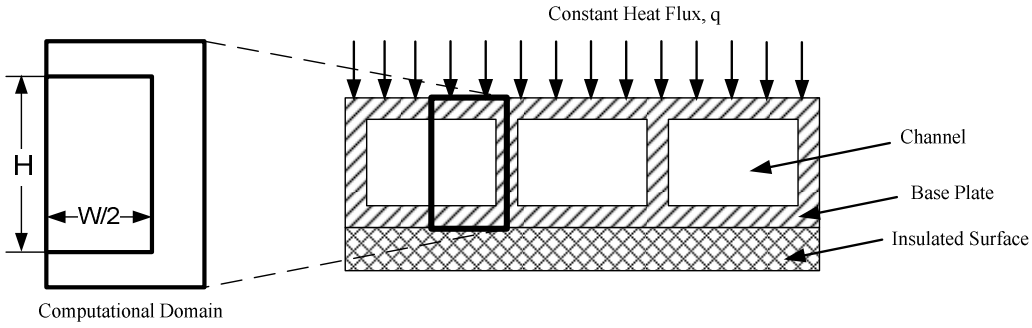

(b)

Figure 4.5 Coldplate (a) Schematic (b) Computational domain (Saleh et al., 2010)

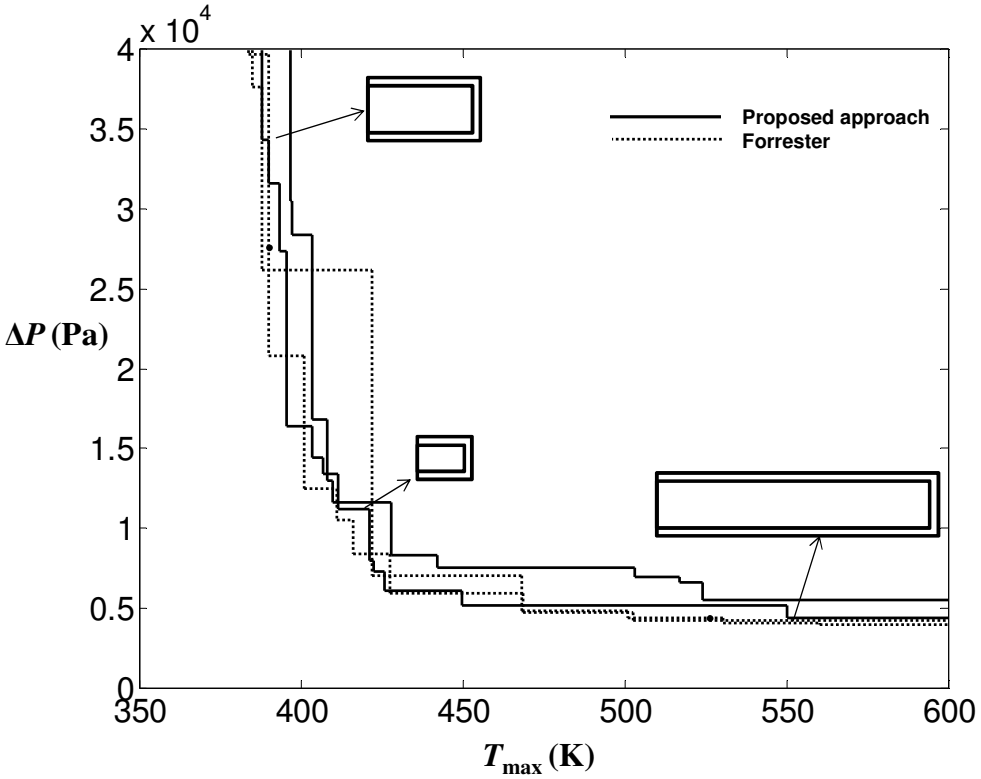

Figure 4.6 Optimal solution for coldplate example

In terms of the coldplate design itself, it can be depicted from the results in Table 4.4 that for a smaller channel width and high refrigerant velocity the pressure drop constraint tends to approach the upper bound while the maximum temperature is significantly reduced. This trend can be seen in the upper left corner in Figure 4.6. However for the maximum channel width and intermediate refrigerant velocities the pressure drop is significantly reduced while the temperature increased as the surface is subjected to the constant heat flux.

Table 4.4 Optimum solutions for coldplate example

W mm	H mm	ν m/s	T_{max} K	ΔP Pa
5.20	1.04	2.57	388.21	34344.28
5.88	1.12	2.69	390.05	31629.56
5.33	1.11	2.31	393.48	27373.30
5.12	1.80	2.65	395.68	16341.62
5.89	1.67	2.30	403.68	14450.23
6.65	1.78	2.37	407.12	13429.33
6.51	1.84	2.10	411.72	11169.17
5.93	1.83	1.55	421.38	7999.49
5.34	1.85	1.41	422.53	7281.43
5.09	1.97	1.29	426.01	6090.60
9.61	1.99	1.29	449.77	5155.07
46.33	1.98	1.25	550.26	4384.63

4.6 Summary

A new and novel online approximation assisted multiobjective optimization approach is developed and presented in this chapter. The approach iteratively uses and updates both global and local metamodels for the objective and constraint functions in its pursuit for Pareto optimum solutions. The global metamodels allow the approach to explore the entire design space while a number of local metamodels focus on promising regions with higher accuracy. These promising regions are determined based on a number of clusters using a newly developed clustering scheme. This scheme is adaptive and dynamically determines the number of clusters, their size and location in the design space.

The proposed approach considers both objective and constraint functions as being computationally expensive and as such it can be used in a wide range of engineering design optimization applications. Both numerical and engineering examples are tested using the proposed approach. A CFD coldplate design example is

demonstrated with the proposed approach as well. It is found that a reasonable set of optimum design solutions are obtained with a few number of CFD simulations.

In the next chapter, a new framework for applying OAAMO to heat exchanger design problems with multiscale simulations is presented.

Chapter 5: Online Approximation Assisted Multiobjective Optimization for Problems with Multiscale Simulation (OAAMOMS)

5.1 Introduction

In this chapter, an online multiobjective approximation assisted optimization approach is used to design a novel air-cooled heat exchanger using a multiscale simulation. The material of this chapter is essentially the same as that given in the paper by Saleh et al. (2011a)[4].

In OAAMOMS, design optimization is performed using multiobjective genetic algorithm while the computational cost is reduced significantly by applying an online approximation technique. Higher model fidelity is achieved by applying the multiscale heat exchanger simulation method. This approach uses a CFD technique on the segment level coupled with ε-*NTU* solver for the entire heat exchanger performance evaluation.

The rest of this chapter is organized as follows: Section 5.2 summaries the related work from the literature. An overview of the new approach is provided in Section 5.3. Sections 5.4 presents an engineering example for applying the new approach to optimize a new generation of air-cooled heat exchanger with comparison with offline approximation assisted multiobjective optimization based approach. Section 5.5 provides conclusions and closing remarks.

[4]Saleh, K., Radermacher, R., Aute, V., and Azarm, S., 2011a, "Online Approximation Assisted Optimization of a Novel Air-Cooled Heat Exchanger," *10th IEA Heat Pump Conference*, Tokyo, Japan, Paper No. 00272.

5.2 Related Work

Conventional heat transfer and pressure drop correlations for air side in air-cooled heat exchangers (HXs) cannot be used for new heat exchangers configurations. In addition, experimental investigations require developing several prototype designs which can be expensive, time consuming and do not ensure finding optimum design solutions. Consequently, numerical models using CFD simulations are considered to predict amount of heat transfer and pressure drop of the new HX configuration (Sunden, 2007). Computationally, it can be difficult to build an accurate CFD model for the entire heat exchanger. Therefore, there is a need to use multiscale simulation to overcome this problem. Multiscale means that the CFD simulation used at the heat exchanger segment level, to predict the thermal and hydraulic performance, is coupled with the entire heat exchanger simulation tool such as ε-*NTU* method.

Previously, experimental results have been used to predict the hydraulic and thermal performance in the area of HX design (Kays and London, 1998). Recently, many works reported using CFD simulations to predict the heat transfer and hydraulic performance. Bergles (2002) recommended using numerical techniques for the prediction of thermal performance for new HXs geometries. According to Sunden (2007), there are two different ways to use CFD in heat exchangers simulation. The first approach uses large scale or coarse-mesh schemes with local averaging or porous medium to predict the flow distribution within the heat exchanger by the method of flow and thermal resistance. In the second approach, periodic modules with the heat exchanger are used with fine meshes to predict the heat transfer and friction

coefficients with high accuracy (Romero-Mendez et al., 2000; Li et al., 2006; Wu and Tao, 2007; De Losier et al., 2007; Abdelaziz et al., 2010). In the next sub-section, the work reported in the literature for heat exchangers' optimization is discussed.

5.2.1 Heat Exchanger Optimization

In the area of heat exchanger optimization, most CFD studies have focused on segment level optimization. Few studies used approximation assisted optimization for the entire heat exchanger design (Lee et al., 2001). Some existing methods have used curve fitting to correlate the response from CFD calculations inside the optimization step. Other methods use DOE, metamodeling, and optimization in heat exchanger design applications (Jing et al., 2005; Park and Moon, 2005; Park et al., 2006). The most recent work in the area of heat exchanger optimization using multiscale simulation was based on adaptive DOE which was used to build offline metamodels for both air heat transfer coefficient and air pressure drop (Aute et al., 2008 and Abdelaziz et al., 2010). The main advantage of using offline metamodels is the ability to work with different optimization objectives, derived from the same metamodel. In other words, based on offline metamodels, different optimization problems can be solved with the same metamodels. However, the metamodels used for offline metamodel assisted optimization should be globally accurate. This means additional CFD simulations will be required to achieve a reasonable level of global accuracy.

However, in many instances, an optimization task is very narrowly defined. For instance, manufacturer aims at reducing the heat exchanger weight and reducing the pumping power for aerospace applications. There might be many constraints on the heat exchanger dimensions, aspect ratios, as well as the pumping power, the weight

and so on. This means, in terms of optimization, both the objectives and the constraints are well known. In such cases, we just need to improve the performance of metamodels near the expected optimum region. Therefore, online approximation assisted multiobjective optimization is a better choice for such cases.

In the proposed approach, the online approximation assisted optimization presented in chapter 3 is applied to heat exchanger design. More specifically, the proposed approach in chapter 3 is used to integrate the use of CFD for segment level simulation with the *ε-NTU* model (Shah and Sekulić 2003) to evaluate the performance of the entire heat exchanger. Metamodels are used for the optimization to replace the computationally expensive CFD simulations. The metamodels are updated in the direction of improving their performance in the region where the optimum heat exchanger design solutions are expected to be. In addition, the solutions from online approximation are compared with solutions from offline approach (Abdelaziz et al., 2010). As will be shown for the case studies considered, the current results show that the online approximation approach outperforms the offline approximation approach in terms of reducing the computational time significantly and obtaining more accurate solutions.

5.2.2 CoilDesigner Solver

CoilDesigner is a control volume based simulation tool that can simulate the performance of air-to-refrigerant and refrigerant-to-refrigerant heat exchangers (Jiang et al., 2006). The solver discretizes the individual tubes in a heat exchanger into smaller heat exchanger elements termed as segments. CoilDesigner internally uses this discretization on the segment level along with the *ε-NTU* method (Shah and

Sekulic, 2003) of heat transfer calculations which helps to account for the changes in transport properties (density and viscosity) during evaporation and condensation processes resulting in accurate prediction of the entire heat exchanger performance. CoilDesigner is described in more details with experimental validation in Jiang et al. (2006) and more recently in Singh et al. (2008). Optimization of heat exchangers using MOGA with CoilDesigner has been described and demonstrated in Aute et al. (2004), Abdelaziz et al. (2010). It is important to note that CoilDesigner uses correlations for air and refrigerant side heat transfer and pressure drop calculations. This makes CoilDesigner very flexible, because once a correlation is available for a given geometry, CoilDesigner can be used to simulate the coil performance using the particular tube/fin geometry. Correlations are generally based on experimental data sets, but in cases where experimental data is not available for new heat exchangers, the heat transfer and pressure drop characteristics can be obtained using CFD simulation. That can help to use CoilDesigner to explore the performance of new heat exchangers without significant change in the solver itself.

CoilDesigner requires detailed geometrical and design information to evaluate performance of heat exchangers. This information includes tube diameters, thickness, fin thickness, tube horizontal and vertical spacing, tube length, number of parallel tubes. The results predicted by CoilDesigner include the overall heat load, refrigerant side heat transfer coefficients, refrigerant side pressure drop, outlet refrigerant and air conditions, the volume of heat exchanger, material weight.

5.2.3 Multiscale Simulation

In order to reduce the time associated with simulating the new heat exchanger designs, multiscale simulation concept is introduced by Abdelaziz et al. (2010) as shown in Figure 5.1. In multiscale simulation, CFD simulations are performed in heat exchanger (HX) segment level to predict the thermal and hydraulic performance of the new enhanced HX surfaces whereas a segmented based *ε-NTU* solver such as CoilDesigner is used to predict the performance of the entire heat exchanger. In order to apply the multiscale simulation approach, the following assumptions should be satisfied (Abdelaziz et al., 2010):

1- Heat Exchangers are periodic in nature

2- Symmetry planes should be identified

3- Neglecting the side wall effects

4- The overall heat transfer coefficient is mainly depending on the airside performance

5- Constant wall temperature for liquid inside the tubes

6- Constant air properties and constant liquid in tube properties

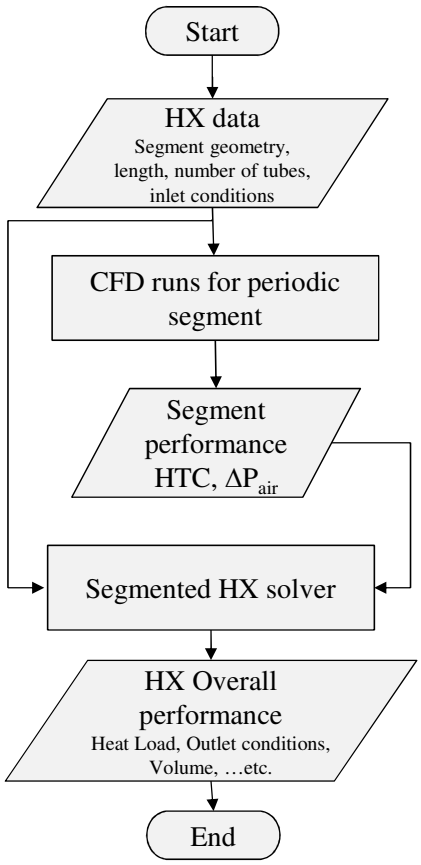

Figure 5.1 Multiscale simulation for heat exchangers (HXs)

5.3 Proposed Online Approximation Assisted Optimization for Problems with Multiscale Simulation (OAAMOMS)

5.3.1 Overview

The OAAMO approach presented in chapter 3 is combined with a multiscale simulation technique (Abdelaziz et al., 2010) in order to reduce the computational time and improve the accuracy of the predict optimum results. The new approach, OAAMOMS, integrates CFD simulations on the segment level with a conventional segmented heat exchanger simulation tool to reduce the computational time while improving the accuracy of the optimum designs. The commercial CFD package,

Fluent® (Fluent 6.3.26) is used and integrated with segmented *ε-NTU* solver, CoilDesigner (Jiang et al., 2006) to simulate the overall heat exchanger performance. CFD is used to calculate the segment air heat transfer coefficient and air pressure drop which are used later in *ε-NTU* solver to predict the entire heat exchanger performance.

5.3.2 Step-by-Step Description of Proposed Approach

The flowchart for the overall approach is presented in Figure 5.2. The air-cooled HX segment model used in this section is described in Section 3.6. After developing a robust CFD model that is valid for the entire range of design variables, a set of initial designs is selected based on the maximum entropy DOE method. Afterwards, CFD runs using Parallel Parameterized CFD (PPCFD) described in Section 2.8 is used.

Based on PPCFD results, metamodels are built for both air heat transfer coefficient (*AirHTC*) and air pressure drop (ΔP_{air}) using the Kriging metamodeling method. Having the metamodels, CoilDesigner can be used to predict the *AirHTC* and ΔP_{air} based on the metamodels. After that, MOGA is used to optimize two design objectives: to minimize HX volume and minimize the air side total pressure drop based on CoilDesigner simulations. Subsequently, the obtained optimum design solutions are filtered using OAAMO approach presented in chapter 3 to select the new set of to update the metamodels. CFD simulations are performed for the new selected candidates using PPCFD. Thereafter, metamodels are updated. The previous steps are repeated several times until a certain stopping criterion is met. In this study, a limit on total number of CFD runs is used as the stopping criterion. Finally, the optimum solutions are verified using CFD simulations.

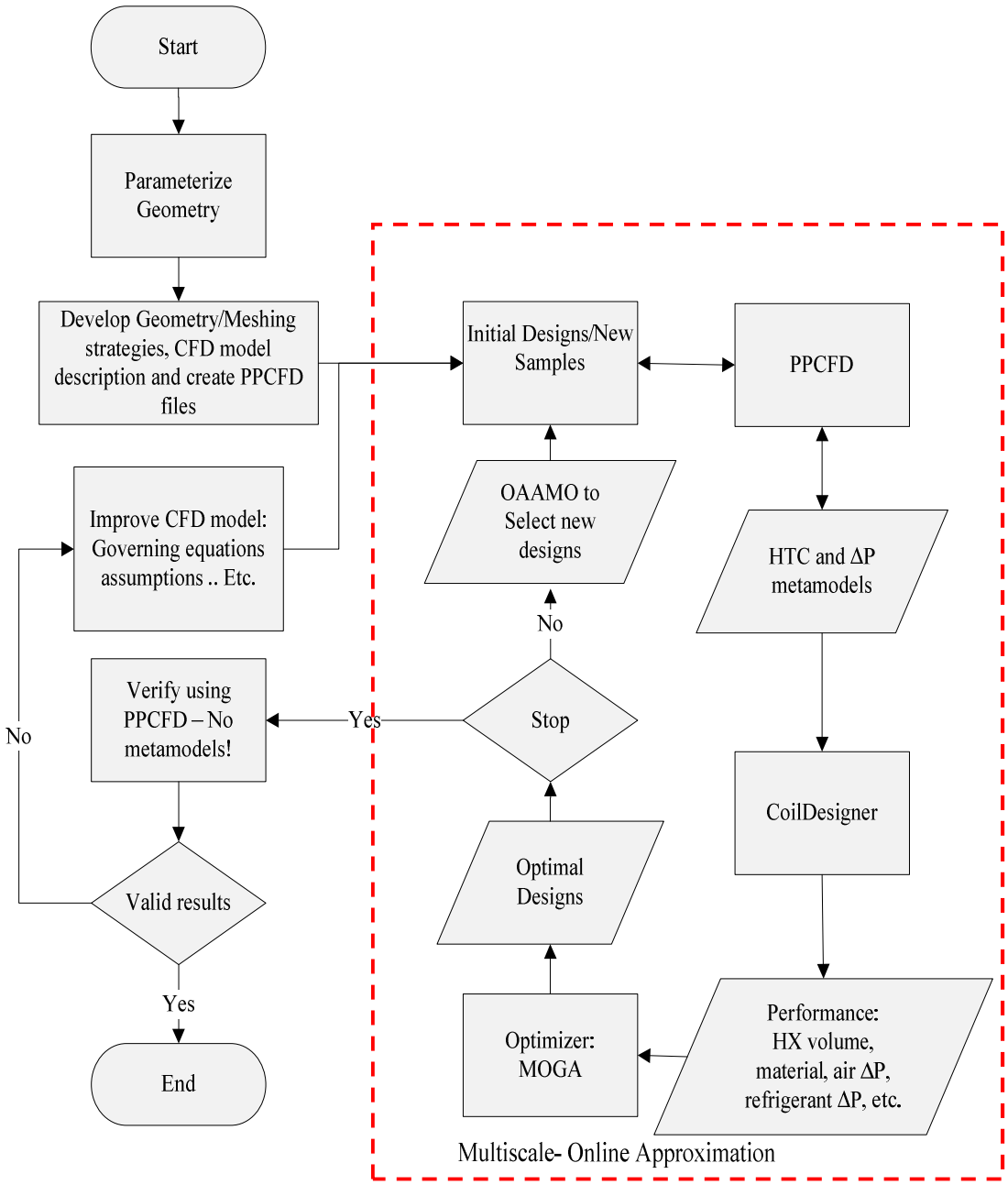

Figure 5.2 Flowchart of OAAMOMS

The prescribed approach is generic. It can be used with any online approximation assisted optimization technique. In addition, it can be applied for any HX type with any segmented based solver such as *ε-NTU* or *LMTD* solver with a great reduction in the computational time required. In the next section an example is used to demonstrate an application of the approach for finding optimum designs of a new generation of air-cooled HXs including a comparison with an offline approach.

5.4 New Generation of Air-Cooled Heat Exchangers Example

In this section, the online approximation assisted multiobjective optimization for problems multiscale simulation approach (OAAMOMS) described earlier in this chapter is used to design a novel air-cooled HX.

5.4.1 Problem Definition

The optimization problem objectives for this design are to minimize HX volume and to minimize the air side pressure drop. These two objectives are conflicting. The HX design is based on segment configuration shown in Figure 3.5 (Abdelaziz et al., 2010). There are six design variables as shown in Table 5.1.

Table 5.1 Design Variables for Heat Exchanger Segment Optimization

Design Variable	Lower Limit	Upper Limit
Inner diameter, D_{in}[mm]	0.2	0.7
Horizontal spacing, *Hs* [mm]	$1.5 \times D_{out}$	$6.0 \times D_{out}$
Vertical spacing, *Vs*[mm]	$2 \times D_{out}$	$4 \times D_{out}$
Number of Ports	3	19
Offset, *l* [mm]	$0 \times Hs$	$1 \times Hs$
Air velocity, *v* [m/s]	0.5	3.0

The optimization problem can be summarized as shown in Eq. (5.1)3. The main objectives are to minimize both the HX volume and the air side pressure drop. This is subjected to certain constraints on the pressure drop for air side. Also, the aspect ratio which is the ratio between the tube length (L) and the coil height ($N_t \times Vs$) is constrained. There is one more limitation on the HX volume.

$$\begin{aligned} &\min \ \ HX\,Volume \\ &\min \ \ HX\ \Delta P_{air} \\ &\text{s.t.:} \ \ HX\ \Delta P_{air} < 100\,Pa \\ &\qquad 0.25 < Aspect\ Ratio < 4 \\ &\qquad 1000 < Q < 1050\,W \\ &\qquad HX\,Volum < 240\ cm^3 \end{aligned} \tag{5.1}$$

5.4.2 Solution Procedure

The solution starts with CFD model development that is valid for the entire design space. Then MED method is used to generate a set of initial designs. In this particular problem, 65 samples are used in order to fill the design space boundaries with initial designs. Then, PPCFD runs. The results are used to build a metamodels for both ΔP_{air} and *AirHTC*. Afterward, MOGA runs with a population of 150 with 200 generations to find the optimum designs. The objectives/constraints evaluations are based on CoilDesigner to evaluate the performance of the entire HX. In lieu of CoilDesigner runs, metamodels are used to predict both ΔP_{air} and *AirHTC* on the segment level. After obtaining some intermediate optimum solutions, OAAMO approach is applied to filter some of the optimum solutions and select the next set of samples to update the metamodels in the expected optimum region. The results are presented at intermediate iterations in the next section.

5.4.3 Results and Comparison with Offline Multiscale Simulation

In this section, the results obtained from applying OAAMOMS approach are presented. Firstly, after running MOGA based on 65 samples, the optimum solutions, i.e., the approximated Pareto solutions, are presented as Iteration #1 as shown in Figure 5.3. Next, after different updates of the metamodels based on intermediate MOGA runs, the results are presented for a total number of samples of 95 and 120 respectively.

As it is apparent from the results, better solutions can be obtained using fewer number of CFD simulations. To compare the results with offline multiscale approximation approach, an offline metamodels are built for both ΔP_{air} and *AirHTC* using 500 samples based on MED method. As it can be depicted from the results, OAAMOMS approach resulted in better optimum designs in terms of closeness and spread compared with offline approach based on MED designs. Approximately 76% CFD simulations are saved when using the OAAMOMS approach.

In addition, OAAMOMS approach is compared with offline approach based on adaptive sampling. The adaptive sampling technique used in this comparison is MSFCVT (Aute, 2009). As it can be illustrated from Figure 5.4, the results are comparable. However using OAAMOMS, we can save 60% of the computational simulations in addition to obtaining better optimum frontier in terms of spread.

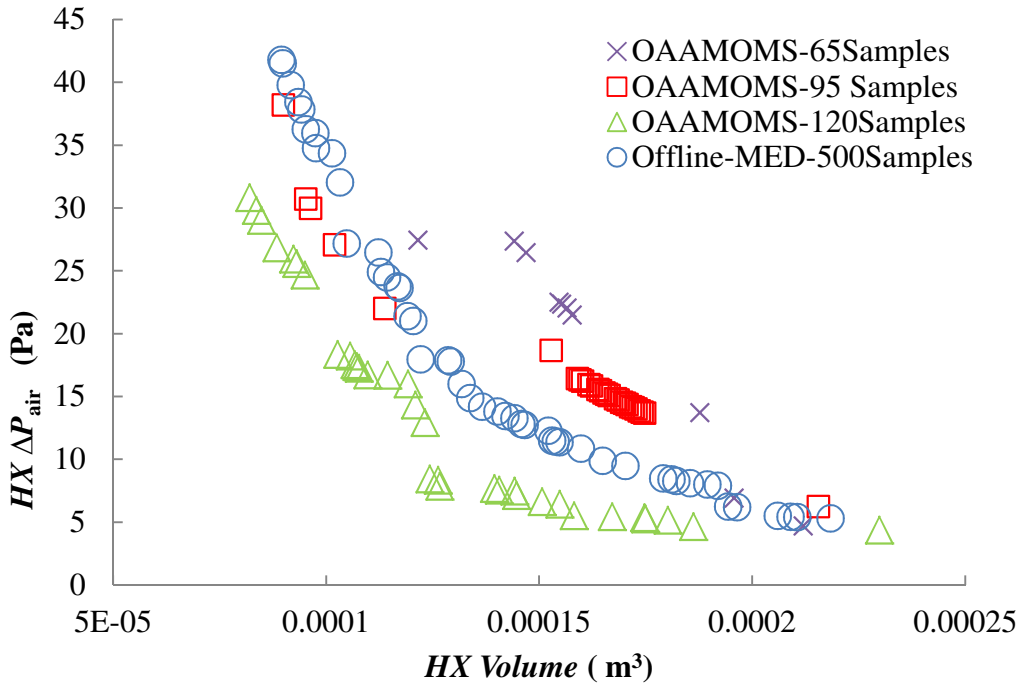

Figure 5.3 Online multiscale approximation results at different iterations and comparison with Offline results using MED

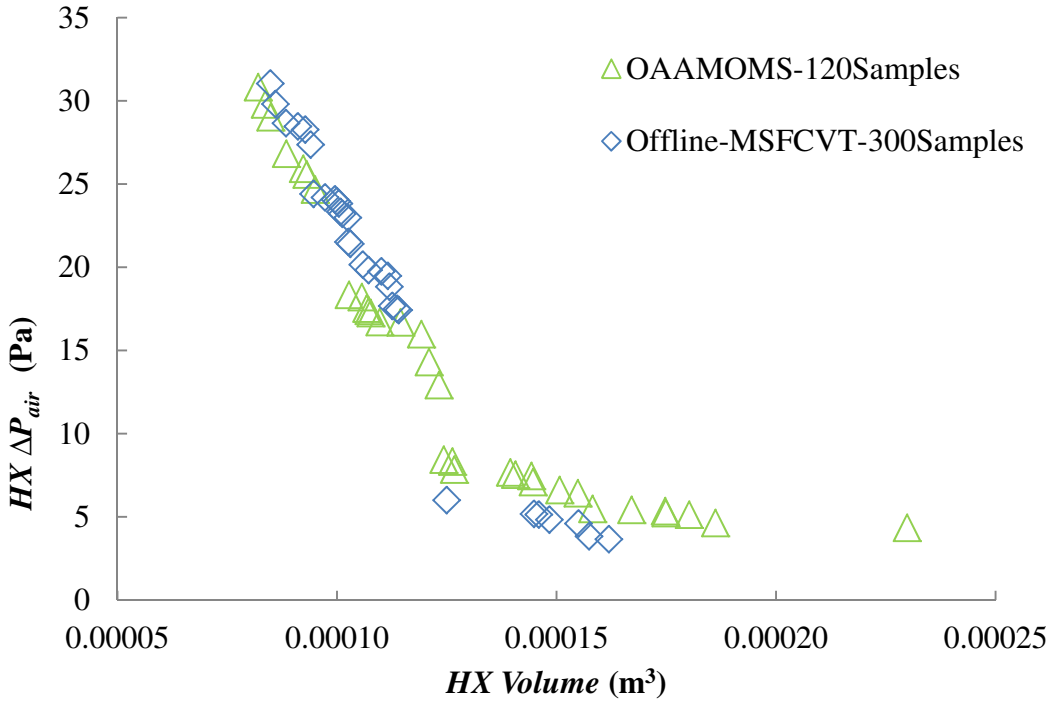

Figure 5.4 Online multiscale approximation results vs. Adaptive Offline results using MSFCVT method

5.4.4 Pareto Solutions Verification

In order to verify the accuracy of the obtained results, all Pareto solutions are verified using CFD runs. The errors in predicting air side pressure drop (ΔP_{air}) and air heat transfer coefficient (*AirHTC*) are summarized in Table 5.2. The definition of error metrics used is given in Section 2.5.2. By examining the results, it is clear that the performance of the metamodels is improved by adding more samples in the expected optimum region using OAAMOMS approach. Comparing with offline line based multiscale simulation using both adaptive sampling, MSFCVT, with 300 samples, and space filling sampling technique, MED, with 500 samples, OAAMOMS gives acceptable and comparable accurate results while reducing significantly the computational cost. This is the main advantage of using OAAMOMS approach. In case of limitation in the computational resources, OAAMOMS gives reasonably accurate results in shorter time. By adding more samples the accuracy of the obtained results is improved.

Table 5.2 Optimum solution verification

Method (Number of Samples)	***RMSE***		***RRMSE***	
	ΔP_{air} (Pa)	***AirHTC* (W/m^2 K)**	**ΔP_{air} %**	***AirHTC* %**
OAAMOMS (120)	3.80	18.32	16.7	14.82
Offline-MED (500)	8.78	2.56	20.78	2.698
Offline-MSFCVT (300)	8.58	15.51	30.41	12.75

5.5 Summary

A new approach for online multiscale approximated assisted optimization for problems with multiscale simulations such as heat exchanger is presented in this chapter. The approach combines adaptive update of metamodels for air heat transfer coefficient and air pressure drop on the segment level with the entire heat exchanger simulation for new generation of air-cooled heat exchangers. The approach resulted in a significant reduction of computational cost compared with offline approximation techniques. The accuracy of the results is comparable with offline approximation results. The online multiscale approximation approach can save more than 60 % of the computational time required to obtain similar results as the offline multiscale approximation techniques. The approach is generic in nature and can be applied to any similar heat exchanger optimization.

In the next chapter, online approximation assisted optimization is used to optimize headers for a new generation of air-cooled heat exchangers.

Chapter 6: Header Optimization for New Generation of Air-Cooled Heat Exchangers using NURBS

6.1 Introduction

The material presented in this chapter is presented with slight modification in Saleh et al., (2012a)[5] for the header optimization and in Saleh et al. (2012b)[6] for the 1 kW integrated heat exchanger module optimization presented in Section 6.7.

In this chapter, an online multiobjective approximation assisted optimization approach is used to design optimum headers for compact air cooled heat exchangers. A CFD model is developed to predict single-phase fluid flow in headers with multiple parallel ports. This CFD model applies the porous jump interior condition in order to reduce the computational domain. In addition, Non Uniform Rational B-Splines (NURBS) are used to define and manipulate the header outer shape with the purpose of reducing the mass flow rate maldistribution. Design optimization is performed using a multiobjective genetic algorithm while the computational cost due to CFD analysis is reduced significantly by applying an online approximation technique. Optimization is performed to reduce both the mass flow rate maldistribution in different ports and the header frontal area with respect to the total heat exchanger frontal area. The optimization results predicted from metamodels are verified using CFD runs with high accuracy of prediction. Finally design guidelines are provided based on the optimization results and the effect of header shape is presented.

---

[5] Saleh, K., Abdelaziz, O., Aute, V., Radermacher, R., and Azarm, S., 2012a, "Approximation Assisted Optimization of Headers for New Generation of Air-Cooled Heat Exchangers," *Applied Thermal Engineering Journal* (2012) http://dx.doi.org/10.1016/j.applthermaleng.2012.06.007

[6] Saleh, K., Abdelaziz, O., Aute, V., Radermacher, R., and Azarm, S., 2012b, "New Generation of Air Cooled Heat Exchanger 1 kW Module Design Optimization, " *14th International Refrigeration and Air-Conditioning Conference at Purdue*, IN, USA, Paper No. 2178

The rest of this chapter is organized as follows: Section 6.2 provides introduction and motivation for using online approximation assisted multiobjective optimization for header optimization and summaries the related work from the literature. In Section 6.3, the details of the new CFD model developed for header simulation is presented. Section 6.4 describes in detail the online approximation assisted multiobjective header design optimization approach. Section 6.5 summarizes the results obtained with CFD verification and proposes some design guidelines for headers. Section 6.6 discusses the effect of NURBS. Finally, Section 6.7 presents the efforts to optimize 1 kW integrated heat exchanger module based on the header optimization results.

6.2 Related Work

Headers play an important role in the refrigerant flow distribution in heat exchangers in addition to providing structural strength and stability to the tubes and fins. Properly designed headers strive to achieve uniform flow distribution with minimum additional volume, material and pressure drop. In the case of novel Heat Exchanger (HX) designs such as those with a large number of parallel flow channels, header design becomes an important challenge. In air-cooled heat exchangers, large headers also reduce the effective frontal face area of the heat exchanger thereby reducing heat transfer.

Current development in the area of air-cooled HX resulted in using channels in the range of micro or mini scale. As a result, reducing the maldistribution of mass flow rate entering different channels is an important issue in order to reduce the deterioration in heat transfer while reducing the pressure drop on the refrigerant side.

Remarkable attention has been paid to designing better HX headers to reduce the mass flow rate maldistribution.

However, most of work in the literature used traditional header design approaches and parametric studies to find a better design. In this way, such a design may not be an optimum solution to header design. In addition, the technique of approximation assisted optimization has not been applied to find optimum header designs.

Generally speaking, current industrial practice is mainly focused on CFD simulations to predict the flow maldistribution in the headers of heat exchangers with high agreement with experimental results (Shah, 2006). Recent research in the area of HX header design can be classified into two categories, viz., (1) numerical analysis, and (2) experimental work. Researchers focused mainly on plate heat exchangers to minimize the variance in velocity distribution at each channel or to reduce the mass flow rate maldistribution factors by experimental and numerical approaches (Jiao et al., 2003; Zhang and Li, 2003; Wen and Li, 2004; Jiao and Baek, 2005; Wen et al., 2007). The effect of varying geometry and operating conditions on refrigerant distribution in minichannel evaporator manifolds were experimentally explored to provide design guidelines (Hwang et al., 2007). CFD models were developed to take into account the effect of flow maldistribution on plate HX, e.g., (Galeazzo et al., 2006). Few efforts were focused on finding optimum HX header designs for other types of HXs. For instance, cross flow microchannel evaporator was analyzed to minimize the flow maldistribution for two phase fluid and resulted in novel radial header design instead of conventional longitudinal header (Kulkarni et

al., 2004). Constructal Theory (Bejan, 1997; Bejan, 2000; Bejan and Lorente, 2006) was used to design new fluid distributions in order to reduce the pressure drop by minimizing the viscous dissipation and the residence time simultaneously (Tondeur and Luo, 2004; Luo and Tondeur, 2005). However, for mini and micro channels, it is unclear whether using the traditional round tube (4mm-10mm diameter) correlations for pressure drop would yield adequate results or not. For example, maldistribution in air-cooled HX was studied for 32 tubes of diameter 25.65 mm and different flow velocities between 1 and 2.5 m/s to decrease the standard deviation of mass flow rate in tubes (Habib et al., 2008). However, the results of that research cannot be applied to mini (10 μm ~200 μm) or micro (200 μm~3 mm) scale tubes (Kandlikar et al., 2006). Therefore there is a need for more accurate method to predict the pressure drop and flow maldistribution inside headers used for a HX with mini and micro channels.

In order to optimize the header design such that the refrigerant pressure drop will decrease while decreasing the header size, it is important to have the flexibility to change the header shape. Non Uniform Rational B-Splines (NURBS) are mathematical models commonly used for generating and representing curves and surfaces and can offer great flexibility and precision for handling both analytic and freeform shapes (Piegl and Tiller, 1997). NURBS can be used to define the shape of the heat exchanger inlet and outlet manifolds or headers. This flexibility of numerically representing header shapes can greatly facilitate optimization of header designs.

The research described in this chapter has two objectives. The first is to develop a new CFD model for fluid flow inside headers for compact heat exchangers using NURBS to represent the header geometry. The second objective is to develop an approach to optimize header designs so as to minimize the refrigerant maldistribution inside the tubes and at the same time reduce the frontal area of the header. The header frontal area is considered an obstacle to the air flow for new generations of air-cooled HX that use mini and micro scale tubes.

6.3 Proposed Approach

In this section, the proposed approach to optimize headers for new generation of air-cooled heat exchangers is presented. First, the CFD model is presented. Then the application problem is elaborated. Finally, the optimization procedure is discussed.

6.3.1 Header CFD Model with NURBS

Traditional CFD simulations of HX including headers would suggest that the entire HX shown in Figure 6.1 (Abdelaziz, 2009) be included in the computational domain. A common simplification would be to model just a periodic section of the HX assuming symmetry planes as denoted in Figure 6.1. This would result in a significant reduction in the computational domain. The HX shown in Figure 6.1 is modeled by considering 1 port per tube as shown in Figure 6.1. This assumption is valid only in the case of neglected side wall effects; i.e. the shear at the side walls is neglected such as in tubes with larger number of ports. The approach used here suggests the use of the porous jump interior boundary conditions to represent the

tubes. Hence, the computational domain can further be reduced as shown in Figure 6.2. In this case, the CFD solver artificially creates a pressure jump across the faces representing the tubes. This modeling approach will not be able to capture the vena contracta and the flow dynamics in the tubes; however, it will be able to account for the effect of overall pressure drop in each flow channel on the mass flow rate distribution (Abdelaziz, 2009).

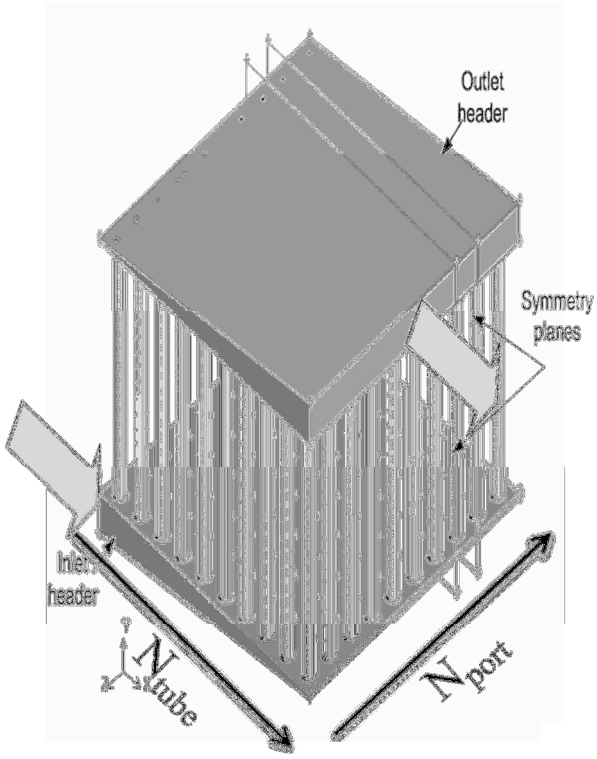

Figure 6.1 Computational domain for a compact heat exchanger Made of 10 × 10 ports (Abdelaziz, 2009)

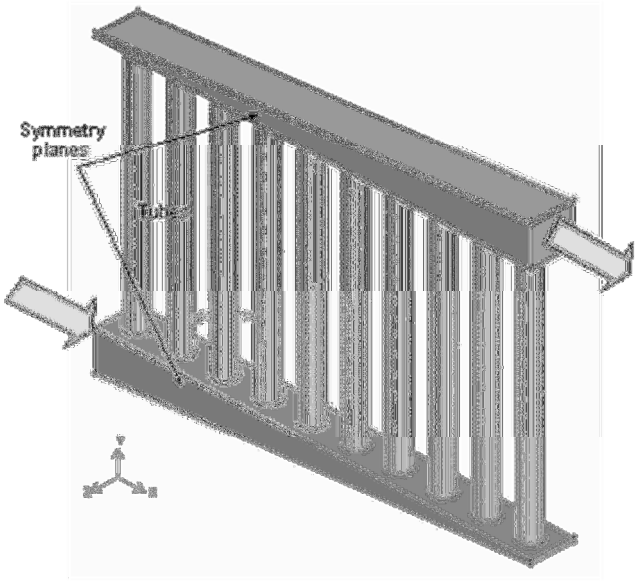

Figure 6.2 Conventional computational domain simplification (Abdelaziz, 2009)

The aforementioned CFD model was modified by adding NURBS to change the surface of the header as shown in Figure 6.3. Non-uniform rational basis spline (NURBS) is a mathematical model commonly used in computer graphics for generating and representing curves and surfaces which offers great flexibility and precision for handling both analytic (surfaces defined by common mathematical formulae) and modeled shapes. NURBS is commonly used in computer-aided design (CAD), manufacturing (CAM), and engineering (CAE) and are part of numerous industry wide used standards. The shape of the surface is determined by control points. In Fluent (2007), there is an option to create curves based on NURBS. In the current CFD model, NURBS is used to change the shape of the header outer surface by connecting control points as defined in Figure 6.3.

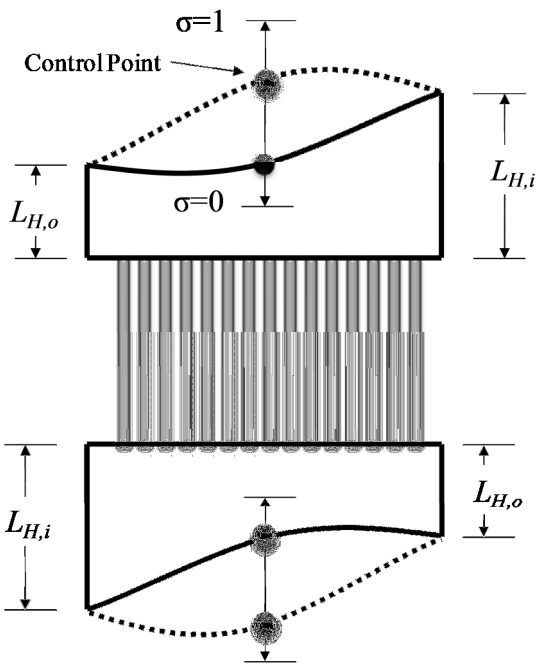

Figure 6.3 New header geometry represented with NURBS

According to Fluent (2007), the porous jump condition is capable of modeling a thin porous media based on the velocity pressure-drop characteristics. The pressure drop across the porous jump condition is correlated to the average velocity through the cell faces as shown in Eq. (6.1) where μ is the laminar fluid viscosity, α is the permeability of the medium, C_2 is the pressure-jump coefficient, v is the velocity normal to the porous face, and Δm is the thickness of the medium which equal to the tube length, L, in the current simulation. The first term in Eq. (6.1) represents an inertial loss term that is required for actual porous media; and can be neglected in HX header simulations. The second term represents the pressure drop due to skin friction which is fundamental to finding the accurate mass flow rate distributions.

$$\Delta P = -\left(\frac{\mu}{\alpha} v + C_2 \frac{1}{2} \rho v^2\right) \Delta m \tag{6.1}$$

$$\Delta P = \Delta P^* \frac{\rho v^2}{2} \tag{6.2}$$

$$x^+ = \frac{\mathrm{L/D}}{\mathrm{Re}} \tag{6.3}$$

$$\Delta P^* = 4x^+ \left[\frac{3.44}{\sqrt{x^+}} + \frac{1.25\left(4x^+\right)^{-1} + 16 - 3.44\left(x^+\right)^{-0.5}}{1 + 0.00021\left(x^+\right)^{-2}} \right] \tag{6.4}$$

$$C_2 = \frac{\left(4x^+\right)}{L} \left[\frac{3.44}{\sqrt{x^+}} + \frac{1.25\left(4x^+\right)^{-1} + 16 - 3.44\left(x^+\right)^{-0.5}}{1 + 0.00021\left(x^+\right)^{-2}} \right] \tag{6.5}$$

In order to find the value for C_2, the pressure drop correlation of interest should be considered. An investigation of single phase water flow in microtubes (Abdelaziz, 2009) suggests the use of (Shah and London, 1978) correlation. Solving Eq. (6.1) along with the pressure drop correlation given in Eq.(6.2) and Eq.(6.4), the value of C_2 can be evaluated as shown in Eq.(6.5). This shows the dependence of C_2 on x^+ and the tube length L. The quantity x^+ is a dimensionless number representing the ratio between (L/D) and Re as given in Eq.(6.3). Hence, C_2 varies as the flow conditions change. Accordingly, it is required to update the value of C_2 for each port periodically while the solver is iterating. The solution procedure used is as follows:

1. Set the solver controls, boundary conditions, and initialize the flow.
2. Use average mass flow rate per port assuming uniform flow distribution to calculate C_2, initial according to Eq.(6.5) to set all porous jumps in the header.
3. Set the solver to iterate for 100 iterations.

4. Re-calculate the C_2 coefficient for each port based on the current value of mass flow rate pert porous jump, refine the mesh based on pressure gradients and let the solver run for 20 iterations and repeat 20 times (400 iterations total).

5. Set the solver to run for 100 iterations.

6. Re-calculate the C_2 coefficient for each port based on the current value of mass flow rate, refine the mesh based on pressure gradients and let the solver run for 100 iterations and repeat 5 times (500 iterations total).

The procedure listed above provides a means for Fluent® to update the pressure drop coefficient of the porous jump. This is achieved through the use of Scheme programming language (Dybvig, 2003) which is supported within the Fluent® text interface.

The CFD simulations were automated using the PPCFD approach (Abdelaziz et al., 2010). The mesh was generated using either hexahedral or tetrahedral elements based on the design complexity. In the case of low aspect ratio headers, hexahedral mesh elements were used and the boundary layer was carefully accounted for by ensuring that enough elements covered the boundary layer. On the other hand, for large aspect ratios, tetrahedral mesh was easier to generate. In the case of tetrahedral mesh generation, the mesh was further refined in Fluent® using the adapt boundary tool to split the elements near the walls. An additional mesh adaptation step was introduced to the solving procedure listed above to allow Fluent® to refine the grid in areas of high pressure gradient before Step-4.

The CFD simulations resulted in a distribution of mass flow rates across the different tubes. The relative standard deviation in mass flow rate per tube was used as a measure of flow uniformity. As for the CFD simulations, PPCFD automatically generates Fluent® script files to define the problem and the appropriate solver settings. The CFD simulations did not consider energy equation. The no-slip boundary conditions were set for all walls and a pressure outlet condition was used for the water outlet port. Inlet velocity boundary condition was used for the water inlet header. Symmetry planes were identified as shown in Figure 6.2. The flow channels were simulated using the porous jump interior boundary conditions with updated pressure loss coefficient using Scheme programming language as discussed earlier. Second order upwind discretization schemes were used for the governing equations and SIMPLEC algorithm (Van Doormaal and Raithby, 1984) was used for the pressure coupling. The convergence criterion was based on maximum acceptable normalized residuals of 10^{-5} for all equations (Abdelaziz, 2009).

6.3.2 Problem Definition

In optimizing the header shape, the header total height ($L_{H,i} + L_{H,o}$), the header size ration ($L_{H,i} / L_{H,o}$), and the location of the NURBS control point (σ) are defined as the three design variables as shown in Table 6.1. In the current study a particular heat exchanger is considered with different parameters including tube length, tube diameter, horizontal spacing and vertical spacing, and average water velocity as presented in Table 6.2. Two objectives are considered, (a) minimizing refrigerant mass flow rate relative standard deviation (σ_{MFR}), and (b) minimizing the header

frontal area with respect to the total heat exchanger frontal area (Area Ratio). The first objective addresses the reduction of pressure drop and better heat transfer distribution along the tubes which is necessary to avoid the deterioration in heat transfer inside the HX. The second objective reduces the obstruction in the air flow direction which enables more compact HX design. The optimization problem definition is given in Eq. (6.6).

$$\begin{aligned} &\min \quad \sigma_{MFR} \\ &\min \quad \text{Area Ratio} \\ &\text{subject to:} \\ &\qquad \Delta P_{total} \le 1000\,\text{Pa} \\ &\qquad \text{Area Ratio} \le 0.06 \end{aligned} \tag{6.6}$$

Table 6.1 Air-cooled heat exchanger design variables for header optimization

Design Variables	Lower limit	Upper Limit
$(L_{H,i} + L_{H,o})$	0.002 m	0.01 m
$(L_{H,i}/L_{H,o})$	1	16
σ	0	1

where $\sigma = 0$ at control point height equal to 0.5 $L_{H,o}$ while $\sigma = 1$ at control point height equal to 1.5 $L_{H,i}$

Table 6.2 Design parameters for header optimization

Design parameter	Value
Tube length	0.1 m
Tube inner diameter	0.4 mm
Horizontal spacing	0.8 mm
Vertical spacing	0.8 mm
Average water velocity per port	0.5 m/s

6.3.3 Proposed Optimization Approach

The overall approach for online approximation assisted optimization of headers using NURBS is summarized in the flowchart of Figure 6.4. A 3D CFD model is first established for a header; NURBS is used to represent the outer shape of the header as shown in Figure 6.3. Several CFD cases are generated and tested to study the applicability of Gambit® and Fluent® journals for the entire design space. Next, initial samples are selected using Maximum Entropy Design (MED) method. CFD analysis is conducted using PPCFD (Abdelaziz et al., 2010) for the selected initial samples.

Afterwards, metamodels are built for refrigerant mass flow rates and total pressure drop. Then the optimization is carried out based on the metamodels. Next, a previously developed Online Approximation Assisted Multiobjective Optimization (OAAMO) approach presented in chapter 3 is used to select new samples among the current optimum designs in order to update the metamodels with the purpose of improving the accuracy in the expected optimum region. Finally the metamodels are updated by adding new samples to improve the performance in the expected optimum region and then optimization is carried out based on the updated metamodels. The summary of optimum header design is presented in the next section.

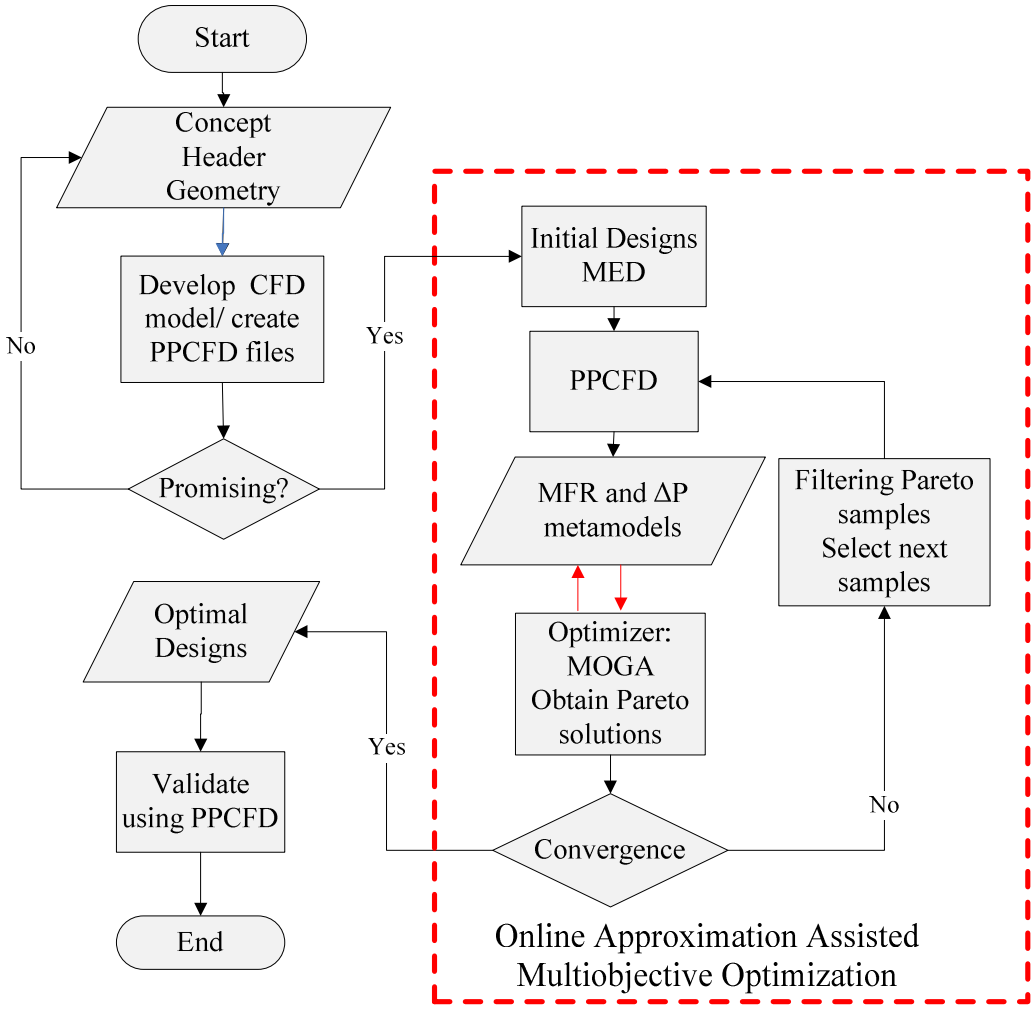

Figure 6.4 Header online approximation assisted multiobjective optimization flowchart

6.4 Results and Discussion

The results from solving the optimization problem are shown in Figure 6.5 in the form of a Pareto set. As expected, there is a tradeoff between the two objectives. In order to minimize the pressure drop, the mass flow rate standard deviation should be minimized. To achieve this target, both the header height and the header size ratio should be increased. On the other hand, by increasing both the header height and the

header size ratio, the area ratio will increase. In addition, the position of the control point varies significantly amongst the different designs in the Pareto set.

A comparison of three optimum designs (Case-1, Case-2, and Case-3), as shown in Figure 6.5 is presented in Table 6.3. As seen from Table 6.3, when decreasing both the header total size ($L_{H,i} + L_{H,o}$) and the control point height ratio ($\sigma = 0.1$), the area ratio decreases while the pressure drop increases significantly as it can be seen in Case-1. Whereas increasing the header total size and shifting the position of the control point up ($\sigma = 0.24$), the pressure drop decreases while the area ratio increases as shown in Case-2. For higher header total size and higher control point height ratio ($\sigma = 0.68$), the pressure drop reduces significantly while the area ratio increases to the upper limit as noticed in Case-3. The CFD verifications for these cases are presented in Table 6.4. During verification, full 3D CFD simulations are performed for the three cases and the output is compared to the results predicted by the metamodels used in optimization. The relative error in predicting the pressure drop and the mass flow rate standard deviation is acceptable and less than 7.5% which proves the accuracy of the online approximation assisted optimization as it is shown in Table 6.4.

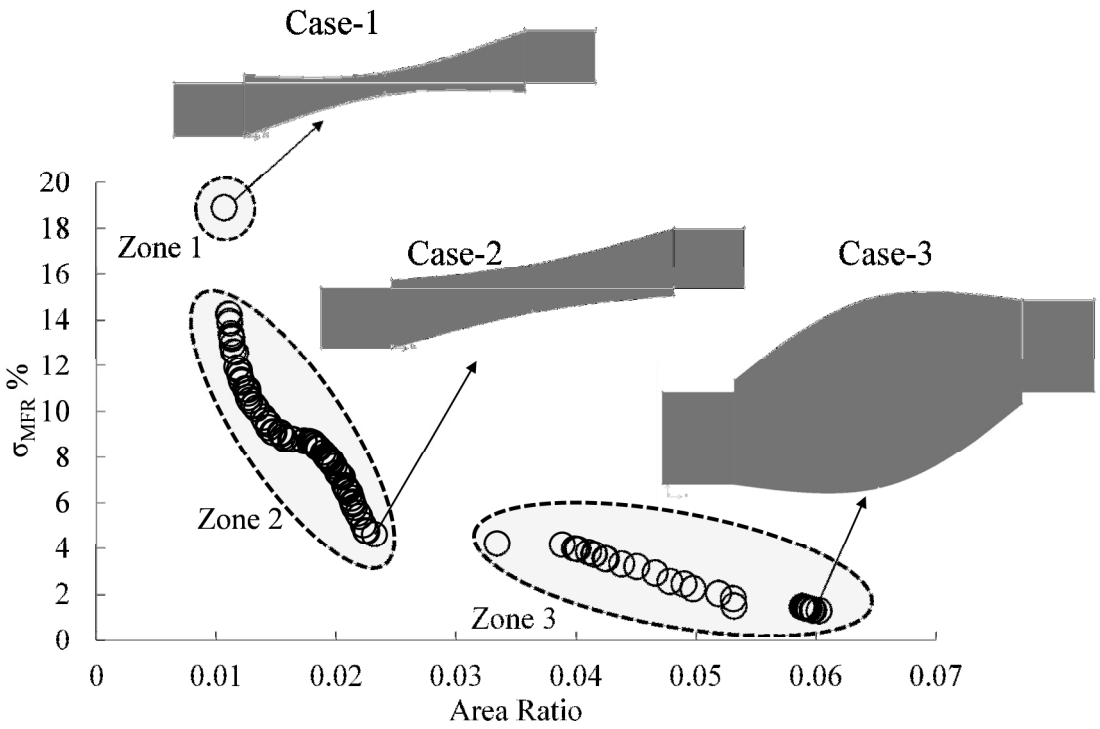

Figure 6.5 Header optimum designs, refrigerant mass flow rate relative standard deviation (σ_{MFR}) vs. Area Ratio

Table 6.3 Design data and objectives for verification Pareto designs

	$L_{H,i} + L_{H,o}$ (m)	$L_{H,i}/L_{H,o}$	σ	Area Ratio	σ_{MFR} %
Case-1	0.00201	6.21	0.1	0.0107	18.89
Case-2	0.00301	7.95	0.24	0.0232	4.61
Case-3	0.00669	7.96	0.68	0.0598	1.32

Table 6.4 CFD verification for of selected Pareto designs

	Relative Error %	
	ΔP_{total}	σ_{MFR}
Case-1	3.45	6.74
Case-2	5.47	3.52
Case-3	4.32	7.21

6.5 Header Design Guidelines

The optimum frontier can be divided into three zones as shown in Figure 6.5. Selected optimum designs representing different zones are given in Table 6.5. For Zone 1, the header total size ($L_{H,i} + L_{H,o}$) is minimum however the header size ratio ($L_{H,i}/L_{H,o}$) is very large and the control point height ratio ($\sigma = 0$). That leads to reduce significantly the area ratio. On the other hand, the mass flow rate relative standard division is very large as well as the pressure drop. This zone is recommended if the designer mainly needs to reduce the total volume and the pressure drop is not a solid constraint. Zone 2 represents very well the relation between the header size ratio ($L_{H,i}/L_{H,o}$) and the height of the control point (σ). For approximately the same header total size, with increasing both the header size ratio and the height of the control point, the area ratio increases from 1% to 2 % which helps to reduce the maldistribution inside the header and the pressure drop by more than 60 %. As for Zone 3, increasing the header total size and reducing both the header size ratio and the height of the control point result in reducing significantly the maldistribution and total pressure drop by approximately 67 %. However the area ratio increases by approximately 78%.

In summary, for reducing the pressure drop inside the headers while reducing the header area ratio with respect to the entire heat exchanger frontal area, one can find two different scenarios. First scenario, in case of limited total header size, designer should increase the header size ratio and increase the height of the control point in order to reduce the maldistribution as it is shown in Zone 2 in Figure 6.5. Second scenario, if there is no limitation on the header total size, it is recommended

to use larger header size which will help to reduce the refrigerant pressure drop but it should be considered that the larger header size and hence the larger area ratio will result in increasing the obstacles and the pressure drop in the air side.

Table 6.5 Design data and objectives for selected Pareto designs

	$L_{H,i} + L_{H,o}$ (m)	$L_{H,i}/L_{H,o}$	σ	Area Ratio	σ_{MFR} %	ΔP_{total} (Pa)
Zone 1	0.00200	13.038	0	0.011	0.19	18.90
Zone 2	0.00200	9.384	0.006	0.011	0.13	13.38
	0.00200	8.551	0.033	0.012	0.12	11.54
	0.00201	8.542	0.061	0.013	0.11	10.76
	0.00201	8.534	0.151	0.015	0.09	9.26
	0.00206	10.642	0.277	0.017	0.09	8.65
	0.00201	14.010	0.402	0.020	0.08	7.60
	0.00201	14.846	0.451	0.021	0.06	6.39
	0.00203	15.746	0.486	0.022	0.05	5.03
Zone 3	0.00208	15.853	0.995	0.033	0.04	4.22
	0.00508	10.845	0.500	0.040	0.04	3.92
	0.00574	9.973	0.495	0.047	0.03	2.90
	0.00589	9.079	0.498	0.050	0.02	2.24
	0.00598	8.488	0.496	0.053	0.02	1.78
	0.00989	3.877	0.137	0.059	0.01	1.39

6.6 Effect of Control Point Height Ratio

For Case-2, the effect of the control point height ratio (NURBS) is predicted from the metamodels as shown in Figure 6.6. By changing the control point position, the area ratio changes and the pressure drop changes as well. As shown in Figure 6.6, with increasing value of σ, the pressure drop will decrease to a certain minimum value at (σ = 0.24) beyond which flow separation occurs at walls. As a result, eddies are formed resulting in a slightly increased in pressure drop. With further increasing in the value of σ, the pressure drop decreases because of the increase in the header area.

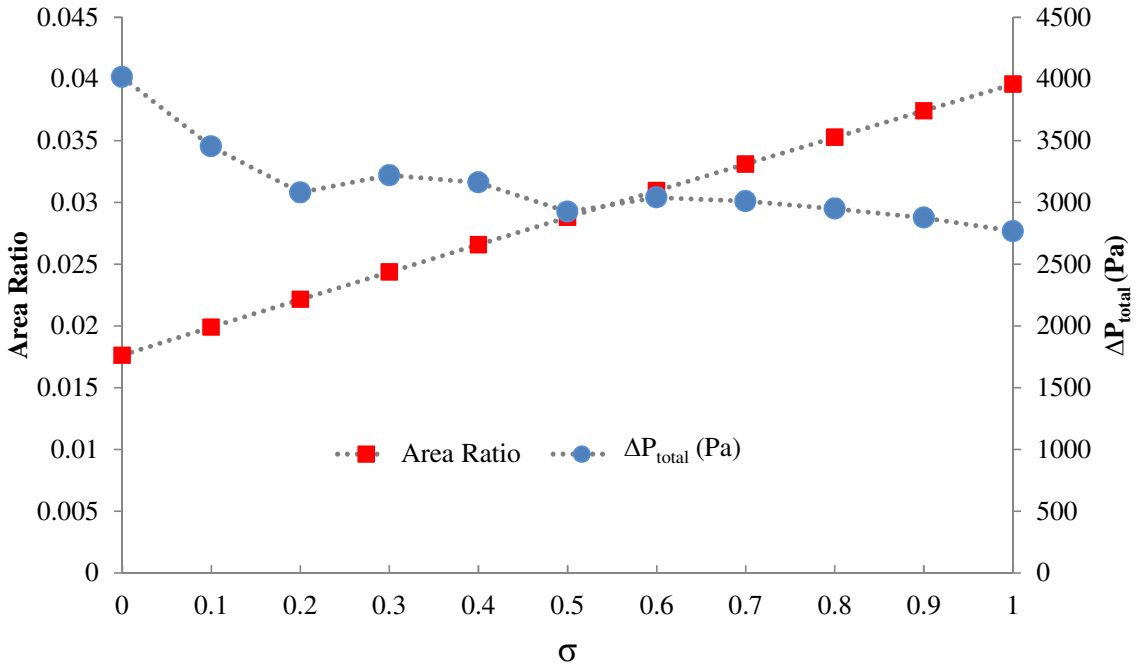

Figure 6.6 Effect of changing control point position on the area ratio and total pressure drop for Case-2

In order to further understand the effect of the control point position, a separate 3D CFD parametric study was conducted for a heat exchanger with only 5 tubes. The header design parameters are the same as the ones listed in Table 6.2 and the design variables are given in Table 6.6. It is evident from Figure 6.7 and Figure 6.8 that beyond the control point position value of 0.2, there is a slightly small change in both the mass flow rate relative standard deviation and the pressure drop. This approximately corresponds to the case of a straight line, i.e., the header surface is flat. Therefore using headers with a flat surface is a good option if both the header total height and the header size ratio are optimized as well, leading to reduced pressure drop and mass flow maldistribution. As it can be seen from the results, there is a tradeoff between the location of the control point, the header total height and the

header size ratio. One should consider the effect of these three variables while optimization the header shape in order to reduce the total pressure drop and to reduce the header area ratio.

Table 6.6 Header design variables for control point position parametric study

Design Variables	value
$(L_{H,i} + L_{H,o})$	0.002 m
$(L_{H,i}/L_{H,o})$	4
σ	0, 0.1, .., 1

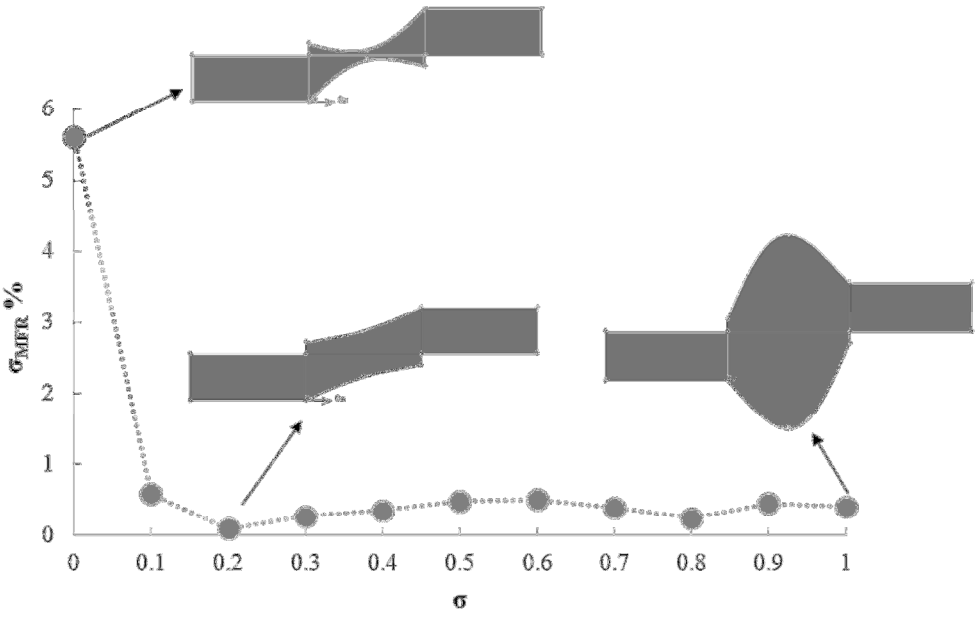

Figure 6.7 Effect of changing control point position on the mass flow rate relative standard deviation

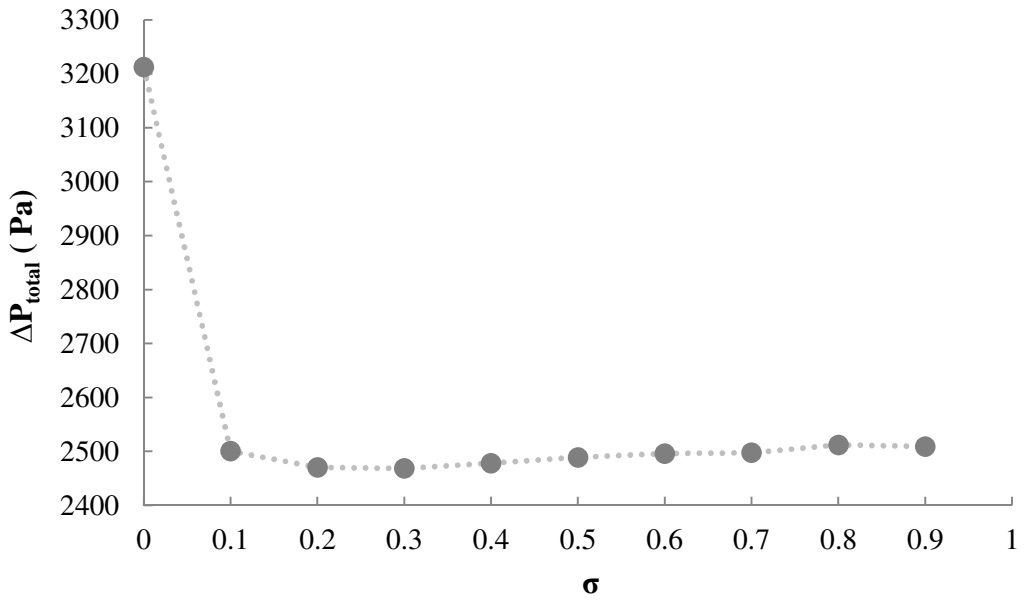

Figure 6.8 Effect of changing control point position on pressure drop

6.7 1 kW integrated Heat Exchanger Module

In this section we will introduce the efforts to integrate 1 kW heat exchanger module with headers based on the previous header optimization results presented in this chapter. The schematic of the integrated module is presented in Figure 6.1. The number of tubes on the flow direction is called N_{tube}; however the number of tubes in the perpendicular direction is called N_{port} as shown in Figure 6.1. The header total height ($L_{H,i} + L_{H,o}$) and the header size ratio ($L_{H,i} / L_{H,o}$) are two important variables that can affect the refrigerant distribution inside the tubes.

6.7.1 Integrated Heat Exchanger Module and Results

In the current header simulation, blocked geometry technique is used with hexahedral mesh to simulate the flow distribution inside the inlet and outlet headers. The main advantage of using the blocked geometry with hexahedral mesh is to reduce the number of cells significantly. This reduction enables solving the header

simulation problem in shorter time compared to the conventional meshing strategies. The heat exchanger considered in this study is fixed and the characteristics presented in Table 6.7. The selected header in this study is mainly based on the optimization results presented early in this chapter. Some results for header simulations with different header size ratios, ($L_{H,i}$ /$L_{H,o}$), as defined in ranged from 1 to 8 as shown in Figure 6.9 The results show improved performance with header size ratios of 4 and 5.

Table 6.7 Heat exchanger design data

Design parameter	**value**
Number of tubes (N_{tube})	69
Number of ports (N_{port})	17
Horizontal spacing (H.S.)	0.875 mm
Vertical spacing (V.S.)	1.24 mm
Refrigerant MFR	0.025 kg /s
Tube length (L)	120.073 mm
Tube inner diameter (D_{in})	0.467 mm
Air Pressure Drop(ΔP_{air})	52.88 Pa

In this section SR is referring to size ratios ($L_{H,i}$ /$L_{H,o}$), where SR1, SR2, SR4, SR5, SR8 are referring to headers with size ratios equal to 1, 2 ,4 ,5 ,and 8 respectively. H1, H2, and H3 refer to three different headers design as it is presented in Table 6.8. Integrated module results for the three headers (H1, H2, and H3) are presented in Table 6.8.

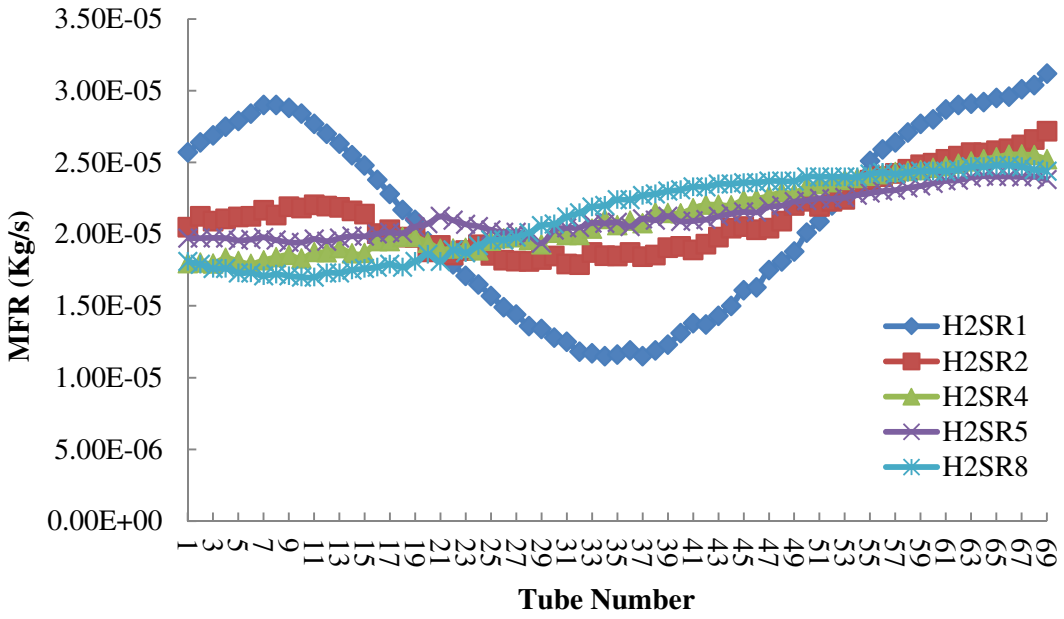

Figure 6.8 Mass flow rate (MFR) distribution for different header configurations

Table 6.8 Integrated module results

Design	Heat Load (W)	Total Volume (cc)	Material Volume (cc)	ΔP_{ref} (Pa)	Header Height (mm)	SR	Area Ratio	σ_{MFR}%
H1	1000.08	185.87	23.02	422.43	16.21	5.00	0.119	12.2
H2	999.56	184.01	22.89	432.37	14.86	10.00	0.110	14.4
H3	1001.21	174.72	22.2	481.91	8.11	5.00	0.063	7.06

As observed from Figure 6.9 and Figure 6.10, there is a tradeoff between the total volume and the refrigerant pressure drop. In H1, the refrigerant pressure drop is minimum however the total volume is maximum. The main reason behind the reduction of the pressure drop is the large header which also causes the increase in the total volume. On the other hand, H3 has the smallest header height with the minimum total volume however the refrigerant pressure drop is maximized. As for the air side pressure drop and heat transfer coefficient, it is the same for all cases as the heat exchanger configuration is fixed as given in Table 6.7. The effect of changing the header size ratio (SR) is presented in the next section.

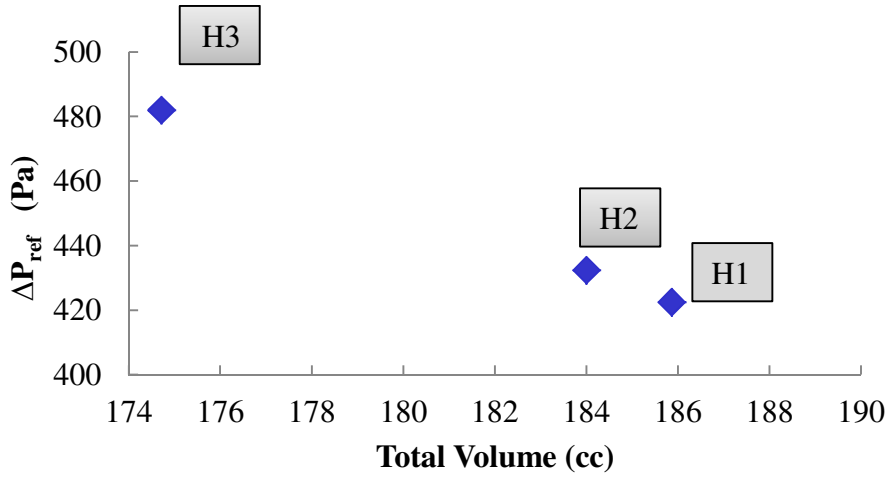

Figure 6.9 Refrigerant pressure drop versus total module volume

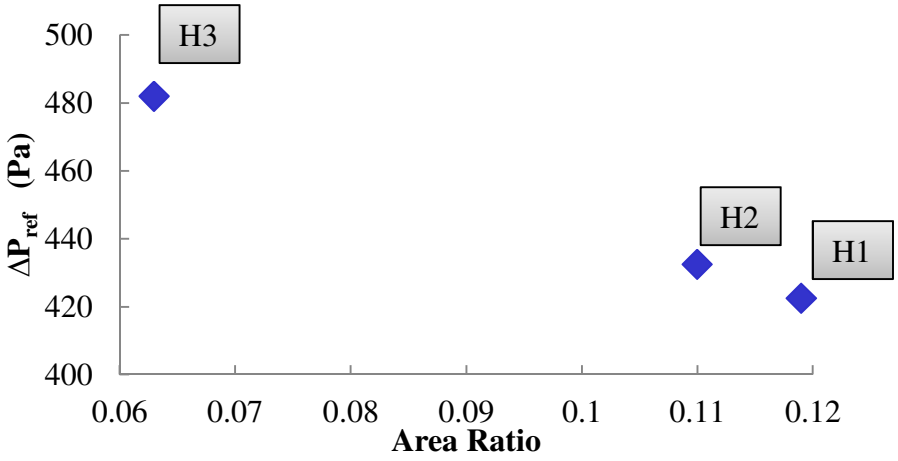

Figure 6.10 Refrigerant pressure drop versus area ratio

6.7.2 Header Size Ratio Parametric Study

Additional investigation for header size ratio effects is performed for H1, H2 and H3 are shown in Figures 6.11-6.16 and Tables 6.9-6.11 respectively. 3D-CFD simulations are performed for different header size ratios. Then heat exchanger solver for each case was run. Finally overall integrated module solver used to obtain the integrated heat exchanger module performance. The results show the impact of header size ratio on the module performance. For H1, the results are shown in Table

6.9. and Figures 6.11 and 6.12. It can be concluded that an optimum header size ratio of 2 is obtained for H1 design. At this optimum value the refrigerant pressure drop is minimum at 400.266 Pa with total module volume of 185.874 cc.

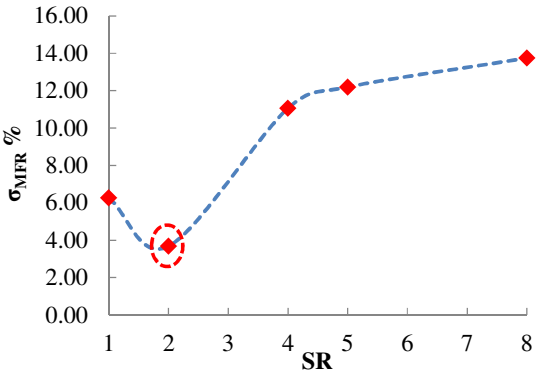

Figure 6.11 Refrigerant MFR standard deviation versus header size ratio for H1

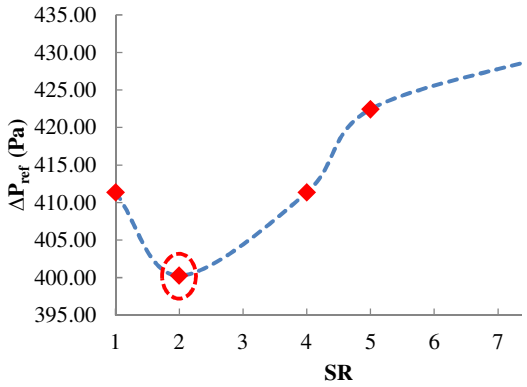

Figure 6.12 Refrigerant pressure drop versus header size ratio for H1

Table 6.9 Parametric study results for header H1

SR	Heat Load (W)	Total Volume (cc)	ΔP_{ref} (Pa)	Header Height (mm)	Area Ratio	σ_{MFR} %
1	1001.202	185.874	411.350	16.210	0.119	6.260
2	1001.624	185.874	400.266	16.210	0.119	3.680
4	1000.480	185.874	411.350	16.210	0.119	11.060
5	1000.080	185.874	422.430	16.210	0.119	12.200
8	999.682	185.874	430.045	16.210	0.119	13.751

Similarly, the results for H2 are presented in Table 6.10 and Figures 6.13 and 6.14. However, the optimum header size ratio is changed to be 5 as it can be depicted from the figures. Likewise, H3 parametric study results are presented in Table 6.11 and Figures 6.15 and 6.16. where the optimum header size ratio is equal to 5 too.

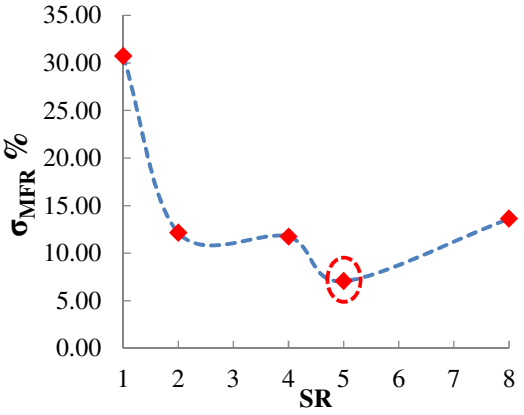

Figure 6.13 Refrigerant MFR standard deviation versus header size ratio for H2

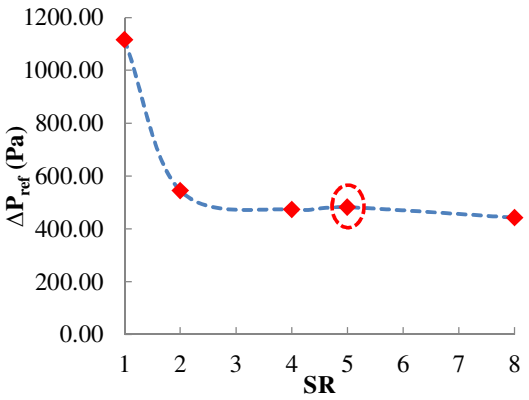

Figure 6.14 Refrigerant pressure drop versus header size ratio for H2

Table 6.10 Parametric study results for header H2

SR	Heat Load (W)	Total Volume (cc)	ΔP_{ref} (Pa)	Header Height (mm)	Area Ratio	σ_{MFR} %
1	991.395	174.721	22.193	1116.122	8.110	0.063
2	1000.197	174.721	22.194	544.780	8.110	0.063
4	999.820	174.721	22.195	472.837	8.110	0.063
5	1001.210	174.720	22.200	481.910	8.110	0.063
8	999.817	174.721	22.197	442.827	8.110	0.063

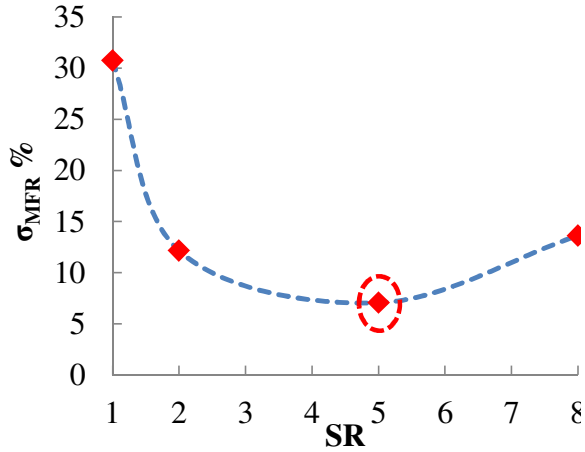

Figure 6.15 Refrigerant MFR standard deviation versus header size ratio for H2

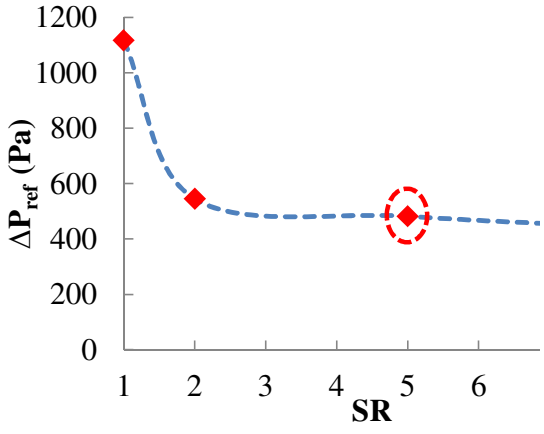

Figure 6.16 Refrigerant pressure drop versus header size ratio for H2

Table 6.11 Parametric study results for header H3

SR	Heat Load (W)	Total Volume (cc)	ΔP_{ref} (Pa)	Header Height (mm)	Area Ratio	σ_{MFR}%
1	991.395	174.721	1116.122	8.11	0.063	30.725
2	1000.197	174.721	544.78	8.11	0.063	12.143
5	1001.21	174.72	481.91	8.11	0.063	7.06
8	999.817	174.721	442.827	8.11	0.063	13.622

In summary, an optimized 1 kW air-cooled heat exchanger module is presented in this section. Two different designs can be considered; the first design leads to minimize the header frontal area however the refrigerant mass flow rate maldistribution will increase. The alternative design has a low refrigerant mass flow rate maldistribution while increasing the header frontal area. Optimum designs with area ratio between 1 % and 12 % are presented. The corresponding refrigerant mass flow rate relative standard deviation is between 1 % and 14 %. The heat exchanger solver accounts for the variation in refrigerant mass flow rates inside the tubes calculated based on the header 3D-CFD simulation. The results confirmed the importance of header total height and header size ratio on the final design. Using headers with larger height and low header size ratio improves the refrigerant mass flow rate distribution and reduces the refrigerant pressure drop while increasing the total module volume. On the other hand, headers with smaller height need larger header size ratio and lead to increased pressure drop while reducing the module total volume.

6.8 Summary

In this chapter, 3D-CFD model is used and modified for headers used in next generation of air-cooled heat exchangers based on mini and micro tubes. The model

uses porous jump condition to represent the pressure drop inside the tubes in order to reduce the computational domain. The porous-jump parameters are updated during the CFD solver iterations using Scheme programming language. In addition, NURBS are used to represent and manipulate the header shape in order to reduce the mass flow rate maldistribution inside the header. Then a systematic and generic approach for header optimization is developed using online approximation assisted multiobjective optimization that enables to find more accurate optimum header designs while significantly reducing the computational cost. Based on the results obtained, there is a tradeoff between header area ratio and refrigerant mass flow rate relative standard deviation. Increasing the mass flow relative standard deviation also results in increased pressure drop and vice-versa. A proper header design can be selected to optimize the header total size, the header size ratio, and the header outer shape. For instance, some of the optimum designed obtained had mass flow rate standard deviations of less than 2% and other designs had headers area ratio less than 2%. The three extreme designs were validated using CFD simulations. The error in the predicted total pressure drop was less than 6% and that for the mass flow rate relative standard deviation was less than 8%, thus verifying the acceptable accuracy of the metamodels. In addition, design guidelines are presented to reduce the pressure drop and the header area ratio based on the optimum results. Using online approximation assisted optimization enables to find the optimum solutions while significantly reducing the computational cost. Only 25 CFD simulations were required for building the metamodels, compared to several thousands of actual CFD simulations that would be required when conventional MOGA is used. In addition,

several CFD simulations were needed to verify the optimized results. The approach proposed in this chapter is generic and can be used to find optimum headers designs for other types of heat exchangers and to study the effect of changing the header outer surface on both the total pressure drop and header total volume. In addition, parametric studies are accomplished to optimize 1-kW integrated heat exchanger and header module.

In the next section, more applications are presented to demonstrate the advantage of using online approximation assisted multiobjective optimization (OAAMO) for optimization of several types of heat exchangers and thermal devices.

Chapter 7: Applications: Coldplate, Chevron Plate Heat Exchanger, and Rollbond Plate Heat Exchanger

7.1 Introduction

In this chapter additional applications of OAAMO and offline AAMO for design of different heat exchangers and thermal devices are presented. These applications include: design of a coldplate used for electronic cooling and design of two different types of plate heat exchangers.

This is chapter is divided into three sections corresponding to the aforementioned applications. In Section 7.2, coldplate optimization using OAAMO is presented including a comparison with offline AAMO results. The material in Section 7.2 was published in Saleh et al (2010a)[7], and Saleh et al. (2011b)[8]. In Section 7.3, Chevron type plate heat exchanger is presented based on the materials published in Han et al (2011)[9] and Saleh et al. (2012c)[10]. Rollbond plate heat exchanger optimization is presented in Section 7.4 based on the material published in Lee et al. (2012)[11]. Finally, in Section 7.5, a summary of the lessons learned from using OAAMO and offline AAMO for optimization of different types of heat exchangers is briefly discussed.

---

[7]Saleh, K., Abdelaziz, O., Aute, V., Radermacher, R., and Azarm, S., 2010a, "Microchannel Approximation Assisted Design Optimization and CFD Verification," *13th International Refrigeration and Air-Conditioning Conference at Purdue*, IN, USA, Paper No. 2312.

[8]Saleh, K., Aute, V., Radermacher, R., and Azarm, S., 2011b, "Online Approximation Assisted Optimization and CFD verification of Microchannel Designs," *Thermal &Fluid Analysis Workshop (TFAWS),* Newport News, VA, USA, Paper No. TFAWS2011-AT-007

[9] Han, W., Saleh, K., Aute, V., Ding, G., Hwang, Y., and Radermacher, R., 2011, "Numerical Simulation and Optimization of Single Phase Turbulent Flow in Chevron-type Plate Heat Exchanger with Sinusoidal Corrugations," *HVAC & R Research*, Vol. 17, No. 2, pp.186-197.

[10]Saleh, K., Aute, V., Radermacher, R., and Azarm, S., 2012c, "Plate Heat Exchanger Optimization Using Different Approximation Assisted Multiobjective Optimization Techniques," *14th International Refrigeration and Air-Conditioning Conference at Purdue*, IN, USA, p.2188.

[11]Lee, H., Saleh, K., Hwang Y., and Radermacher, R., 2012, "Optimization of Novel Heat Exchanger Design for the Application of Low Temperature Lift Heat Pump," *Energy Journal*, Vol. 42, pp.204-212

7.2 Coldplate Optimization

Developing an optimized compact heat exchanger is crucial for many applications. In general, two objectives mainly are considered while designing a heat exchanger for naval and aeronautics applications. These two objectives focus on minimizing heat exchanger volume as well as minimizing the total pressure drop. Conventionally, designers used exhaustive search and other trial-and-error methods to find the best heat exchanger design. However, it is very difficult to apply exhaustive search if the heat exchanger model is computationally expensive, i.e., it takes several hours or even days to run one single simulation. Also, it is computationally prohibitive in cases of dealing with large number of design variables and design objectives. In addition, using some conventional optimization approaches such as multiobjective genetic algorithms and other heuristic optimization techniques can help reduce the total number of simulations needed but still it is not feasible to apply these techniques for large scale design problems. Therefore, using approximation assisted optimization techniques can help to reduce the computational time associated with the optimization process.

This section considers a microchannel design optimization problem with the objective of minimizing the maximum channel temperature while minimizing the refrigerant pressure drop inside the channels. This is a two-objective optimization problem resulting in a tradeoff between the aforementioned two conflicting objectives. In order to find optimally compact heat exchanger designs, mini and microchannel geometries are being considered. The goal in this study is to evaluate the potential in designing high heat density microchannels for a given application and

at the same time reduce the computational effort required to do so. Online approximation assisted optimization technique, described in chapter 3, OAAMO, is applied to optimally design a microchannel with single phase flow and constant heat flux. A comparison with offline AAMO built using space filling sampling technique (MED) described in chapter 2, and a Kriging metamodeling method are used to build metamodels for the maximum temperature, fluid outlet temperature, and pressure drop inside the channels based on CFD analysis. A multi-objective genetic algorithm (MOGA) is used as the optimizer. The solutions present the effect of changing the channel dimensions and the coolant flow rate on controlling both the channel maximum temperature and pressure drop. The optimum solutions are verified using CFD simulations. It is observed that online approximation assisted optimization obtains reasonably accurate optimum design solutions while reducing significantly the computational time.

7.2.1 Related Work

Optimum microchannel heat sink design can lead to significant improvements in the performance and heat density. In most electronic cooling devices there is high heat flux as it can be seen in many industrial applications such as high heat load optical components, power electronics, plasma facing components, X-ray medical devices and hybrid vehicle power electronics. Microchannel structures have been shown to generate significant heat transfer rates from extremely small volumes (Tuckerman and Pease, 1981; Sobhan and Garimella, 2001).

Microchannel optimization studies can be found in the recent literature reflecting the increasing interest in the practical implementation of such systems

(Chong et al., 2002; Liu and Garimella, 2005; Gopinath et al, 2005; Cetegen et al., 2009). Previous work has used Multi-Objective Genetic Algorithm (MOGA) to optimize the selection of a heat sink (Gopinath et al, 2005; Foli et al., 2006; Cetegen et al., 2009), including combining CFD analysis with an analytical method and multi-objective genetic algorithm were described (Foli et al., 2006). Simple duct flow correlations were used to predict the heat transfer coefficient and friction coefficients (Gopinath et al., 2005). In the next section, the CFD model for the coldplate is presented.

7.2.2 CFD Model

An essential step to optimize any heat exchanger or thermal device using approximation assisted optimization technique is to automatically generate all CFD cases. In this study, parallel parameterized CFD (PPCFD) approach (Abdelaziz et al., 2010), described in chapter 2 is used to automatically read the normalized design variables and then generate the corresponding Gambit® journal files. The microchannel model is presented in Figure 7.1. Mesh refinement near the boundaries (boundary layer inflation) is applied. Also, a finer mesh is applied in locations where higher temperature gradients are expected, such as near the channel walls, as shown in Figure 7.2.

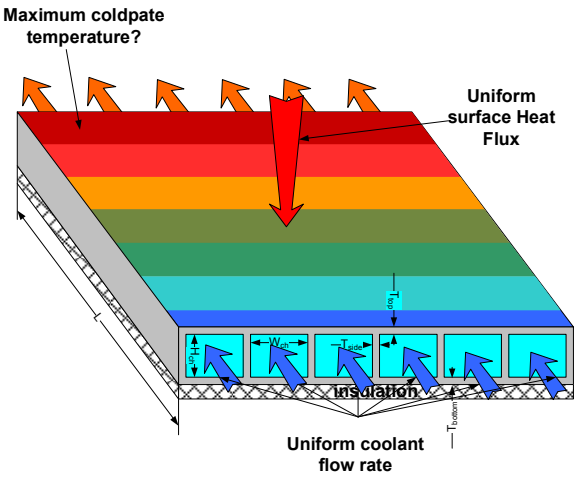

(a)

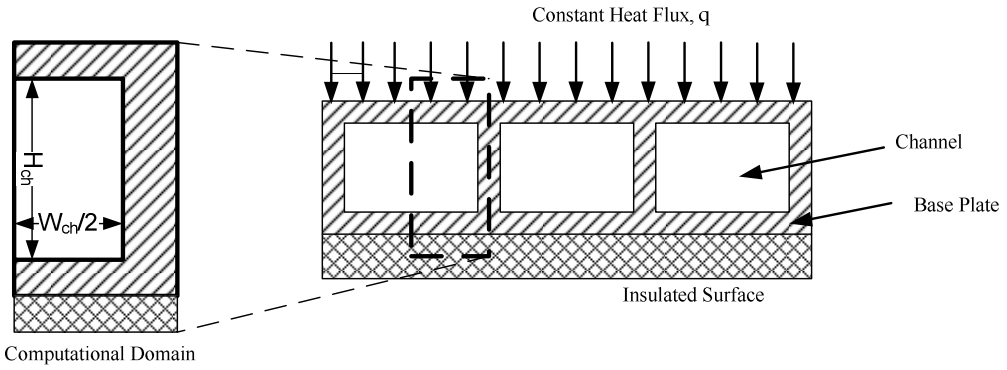

(b)

Figure 7.1 Coldplate (a) Schematic (b) Computational domain

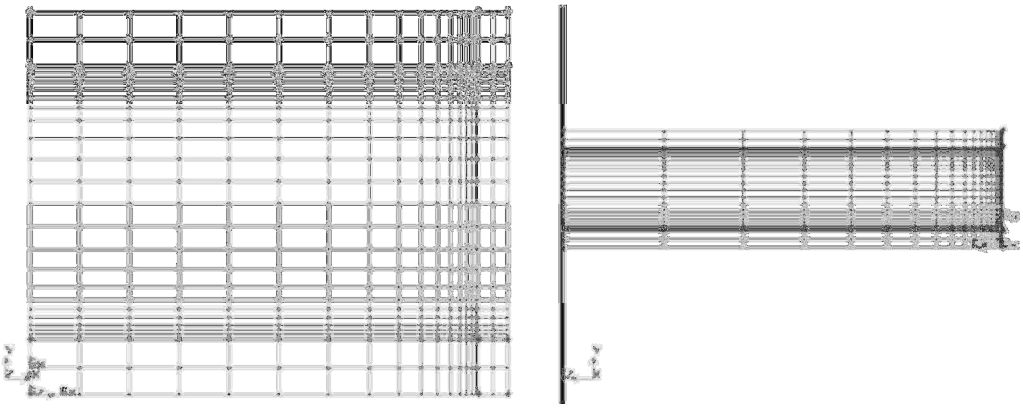

Figure 7.2 Mesh refinement near the boundaries and near areas of expected higher temperature gradients

After generating the mesh, the PPCFD program automatically generates Fluent® journal files to read the specified mesh, set the appropriate boundary conditions, model parameters, and material properties. The inlet velocity is read from a text file. The boundary conditions are fixed for all designs. The materials and boundary conditions are defined in the Fluent® journal files and are fixed for the microchannel. For the case study, the temperature distribution at the channel exit and along the channel is shown in Figure 7.3(a) and Figure 7.3(b) respectively. By using Fluent® for solving the flow field, we take into consideration the effect of entrance length. The accuracy for the case shown in Figure 3 is determined by monitoring the energy balance error of 0.00037.

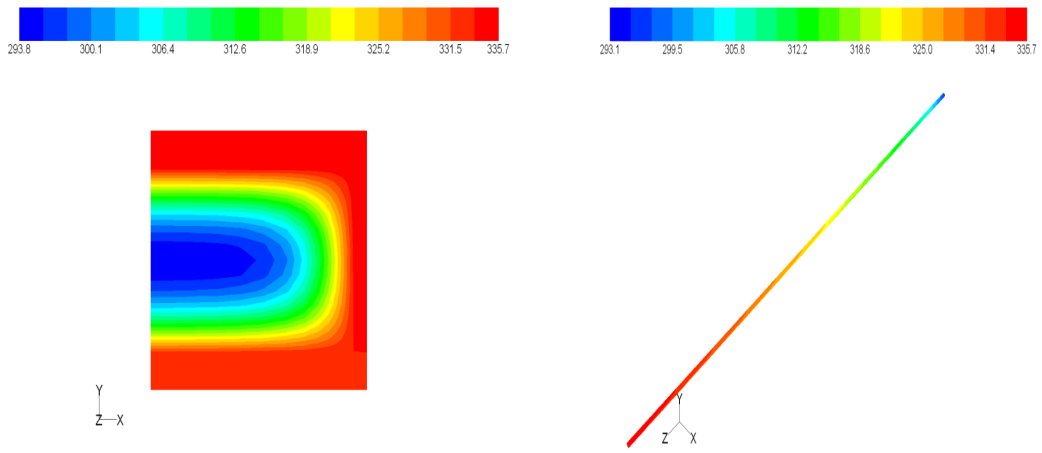

(a) **(b)**

Figure 7.3 Temperature contours (a) at channel exit, and (b) along the channel

7.2.3 Problem Definition

The goal is to find optimized designs that have least maximum temperature and minimum pressure drop. The different design variables that define the microchannel performance are shown in Figure 7.1(b). The six design variables are

defined in Table 7.1. The corresponding computational domain is shown in Figure 7.1(b). The maximum plate temperature and the channel pressure drop are obtained by solving the continuity and the momentum equations using a commercially available CFD tool. For different designs, the solutions are obtained for a fixed uniform heat flux at the top of the microchannel with variable coolant flow rate.

Table 7.1 Design Variables for Coldplate Optimization

Design Variable	**Lower Limit**	**Upper Limit**
Channel height, H_{ch}	H_o	$2.5\times H_o$
Channel width, W_{ch}	H_o	$75\times H_o$
Channel length, L_{ch}	$300\times H_o$	$80000\times H_o$
Side wall thickness, T_{side}	$0.1\times W_{ch}$	$0.5\times W_{ch}$
Top and bottom thickness, T_{top}, T_{bottom}	$0.1\times H_{ch}$	$0.5\times H_{ch}$
Coolant velocity, v [m/s]	0.2	12

In this approximation assisted optimization problem, individual metamodels are developed for each response and also for the fluid outlet temperature. The optimization problem can be summarized as shown in Eq. (7.1). The first objective is to minimize the maximum temperature at the top surface of the channel that is subjected to the heat flux. The second objective is to reduce the refrigerant pressure drop thus reducing the pumping power required.

$$\begin{aligned} &\text{minimize} \quad f_1(x) = T_{\max} \\ &\text{minimize} \quad f_2(x) = \Delta P \\ &\text{subject to:} \\ &\qquad 1kPa \le \Delta P \le 400\,kPa \\ &\qquad 2K \le \Delta T_f \le 14K \\ &\qquad T_{\max} \le 600K \end{aligned} \tag{7.1}$$

7.2.4 Online Approximation Assisted Optimization for Coldplate

Figure 7.4 shows the flowchart for coldplate online approximation assisted optimization approach. The stopping criterion is the maximum number of available simulations. The steps in OAMAO are as follows, as shown in Figure 7.4:

Step-1: Generate an initial set of design points using the maximum entropy design method and observe the corresponding responses for the maximum temperature on the microchannel surface (T_{max}) and the fluid pressure drop inside the microchannel (ΔP).

Step-2: Develop a metamodel for each objective; i.e., T_{max} and ΔP.

Step-3: Formulate a multiobjective optimization problem based on the metamodels and solve it using MOGA.

Step-4: From all Pareto points, select five points to improve the metamodel accuracy in the expected optimum region and to improve the diversity of the optimum designs according to OAAMO approach described in chapter 3. The two extreme points in the objective space are selected to improve the diversity. In addition, the closest point to the ideal point is selected in the objective space is selected as well. However, the points with minimum and maximum Kriging predicted variance are selected to improve the metamodels performance in the next iteration.

Step-5: Filter the new selected points to avoid sampling cluster in the design space.

Step-6: Evaluate the true response (i.e., run the simulation) for the newly chosen points and then go to Step-2.

Step-7: Repeat Step-2 to Step-6 until a limit on the number of function calls is achieved.

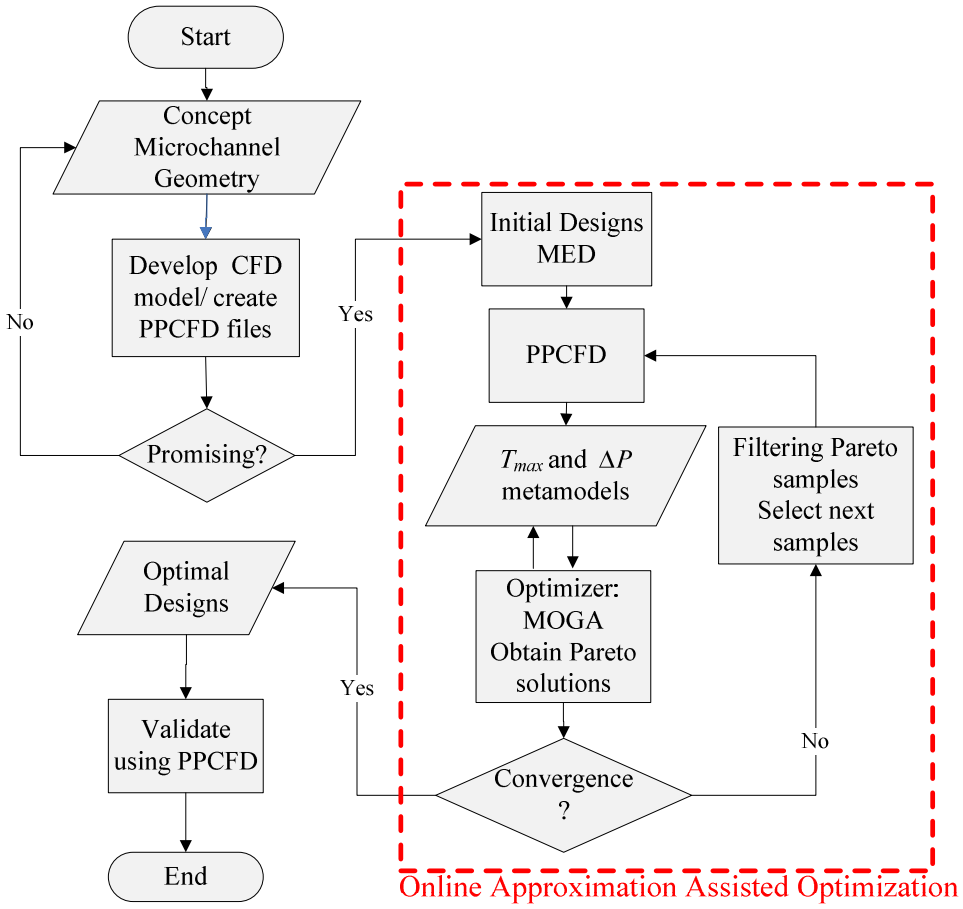

Figure 7.4 Coldplate online approximation assisted optimization flowchart

7.2.5 Results and Discussion

Two different metamodels were built for the two responses viz., T_{max} and coolant ΔP. The initial design comprising of 30 points is generated using the MED method and then OAAMO method developed in chapter 3 is used to sample 30 additional points. Kriging with logarithmic response (to avoid negative values during prediction) was used to develop the metamodel. For offline AAMO, 60 samples are generated using MED, a space filling sampling method.

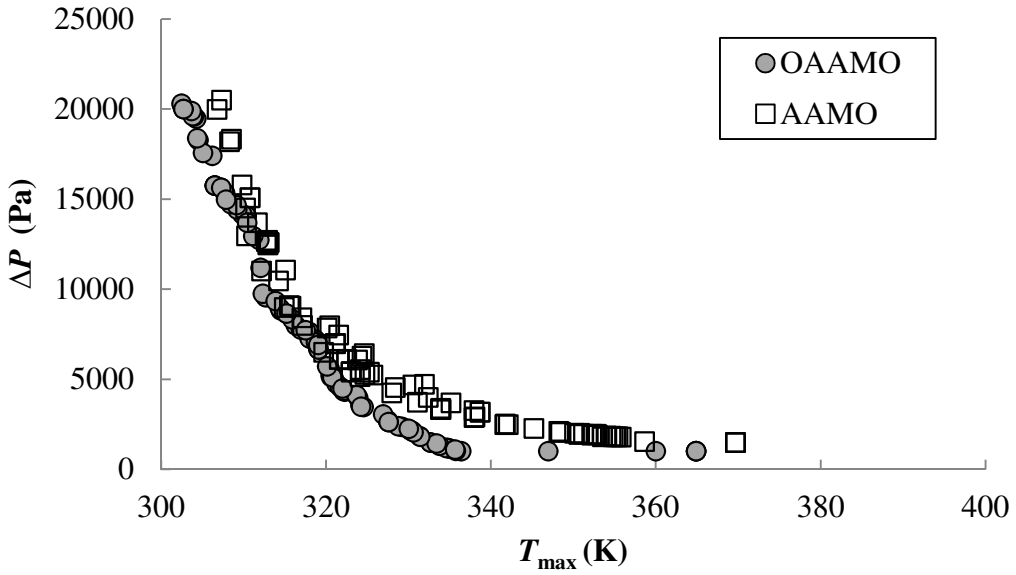

Figure 7.5 Comparison of OAAMO with AAMO optimum results for Coldplate optimization

As it can be seen from Figure 7.5, the performance of the OAAMO is better than offline AAMO. OAAMO can add more samples near the Pareto frontier. As a result Pareto obtained from OAAMO is better than offline AAMO as shown in Table 7.2 in terms of closeness. Generally speaking, having more sample points should improve the performance of both methods. However the error measures, for the Pareto points obtained using OAAMO are lower than those from offline AAMO given that the same number of sample points are used for both methods.

Table 7.2 Errors in optimum designs when using OAAMO vs. offline AAMO

	OAAMO		**Offline AAMO**	
	RError ***(ΔP %)***	***Error*** **(T_{max}, K)**	***RError*** ***(ΔP %)***	***Error*** **(T_{max}, K)**
Average	3.59	0.508	4.16	1.293
Max	15.80	1.828	16.31	3.684
Min	0.016	0.043	0.013	0.035
STD	4.3	0.365	5.24	0.612

7.2.6 Summary of Coldplate optimization

In this section, online approximation assisted multiobjective optimization method developed in chapter 3, OAAMO, is used to obtain optimum coldplate designs based on single phase liquid flow inside the channel. Kriging metamodels are built for maximum surface temperature and for the pressure drop inside the channel. These metamodels are used to predict the objectives and constraints within multi-objective genetic algorithm. Then the optimum solutions are filtered in order to select best samples to update the metamodels. The samples are selected in the expected optimum region with a space-filling constraint to prevent clustering of samples in the design space. This procedure is iterative in nature and is carried out until a predefined stopping criterion is met. This online optimization approach, OAAMO, predicted better optimum designs with high accuracy compared to offline approximation assisted optimization approach. The final results are verified using CFD simulations. The errors are small which indicates that the accuracy of the online approximation assisted optimization method is acceptable. The approximation technique resulted in a significant reduction in computational time compared to conventional optimization technique. Only 60 CFD simulations are required for building the metamodels, compared to several thousands of actual simulations required when conventional MOGA is used (5100 simulations). The approach proposed in this section is generic and can be applied for any heat exchanger or electronic cooling device optimization.

In the next exaction, another application for optimization Chevron plate heat exchanger is presented based on online approximation assisted multiobjective optimization.

7.3 Chevron Plate Heat Exchanger

This section presents a comparison between OAAMO and offline AAMO techniques to optimize chevron-type plate heat exchanger. The thermal-hydrodynamic characteristics of single phase turbulent flow in chevron-type plate heat exchangers with sinusoidal-shaped corrugations have been used in this section. The computational domain contains a corrugation channel and the simulations adopted the shear-stress transport (SST) κ-ω model as the turbulence model. Two different approximation assisted optimization approaches are tested. Offline approximation assisted optimization (AAMO), and online approximation assisted optimization (OAAMO) are compared to optimize plate heat exchanger design. For both approximation techniques (offline and online), design optimization is performed using multiobjective genetic algorithm based on metamodels that are built to represent the entire design space. In offline approximation, globally accurate metamodels are built which requires adding more samples. However in online approximation assisted optimization, samples are added just to improve the metamodels performance in the expected optimum region. Approximated optimum designs are validated using computationally expensive actual CFD simulations. Finally, a comparison between offline and online approximation assisted optimization is presented with guidelines to apply both approaches in the area of heat exchanger design optimization.

7.3.1 Related Work

Plate heat exchangers (PHXs) are widely used in the area of refrigeration, heat pumping, food industry and chemical processing. High thermal performance, ease of

maintenaunous, compactness and the ability to work with small temperature differences are the main advantages of using PHXs (Wang et al., 2007). Recently CFD models are being used to optimize different type of heat exchangers (Abdelaziz et al., 2010).

PHXs optimization studies can be found in the recent literature reflecting the increasing interest in the practical implementation of such systems (Kanaris et al., 2009; Han et al., 2011). Kanaris et al. (2009) searched the optimal design of PHXs with undulated surfaces using CFD techniques. An objective function that combines heat transfer together with friction losses accounting for the energy costs was employed in the optimization procedure using response surface methodology. However, the optimal designs of their study cannot be necessarily extrapolated to the cases of PHXs with sinusoidal-shaped corrugations. Recently AAMO technique was used to optimize single phase turbulent flow in chevron-type PHX with sinusoidal corrugations (Han et al., 2011). However, AAMO is computationally expensive as it requires building globally accurate metamodels.

The objective of this section is to present the method and results of a study on the optimal design of PHX using a multi-objective genetic algorithm based online approximation assisted multiobjective optimization method developed in chapter 3 (OAAMO) and compare the results with offline AAMO. The results are verified using CFD simulations. In the next section, the CFD model for chevron-type PHX is presented.

7.3.2 CFD Model

An essential step in AAMO is using a parallel parameterized CFD (PPCFD) approach (Abdelaziz et al., 2010) to automatically read the normalized design variables and then generate the corresponding Gambit® journal files. The PHX segment model is presented in Figure 7.6. Mesh refinement near the boundaries (boundary layer inflation) is applied. Also, a finer mesh is applied in locations where higher temperature gradients are expected, such as near the plate walls, as shown in Figure 7.7. More details about the model can be found in Han et al. (2011).

$$y^+ = \rho\sqrt{\tau_w/\rho_w}\, y/\mu \tag{7.2}$$

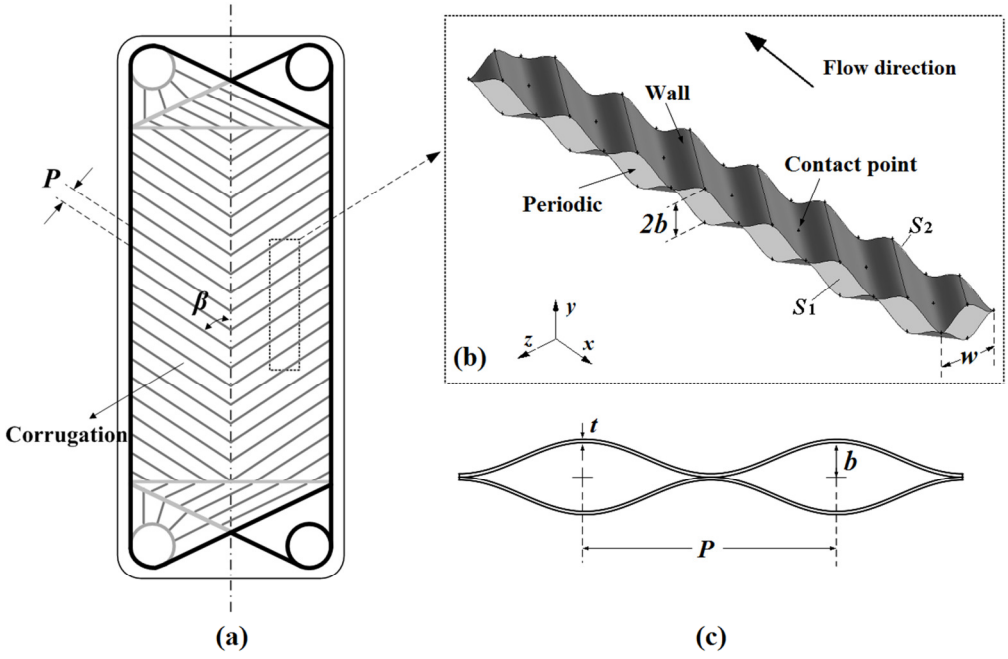

Figure 7.6 (a) Schematic diagram of corrugation plate; (b) Calculation domain; (c) Sinusoidal shape (Han et al., 2011)

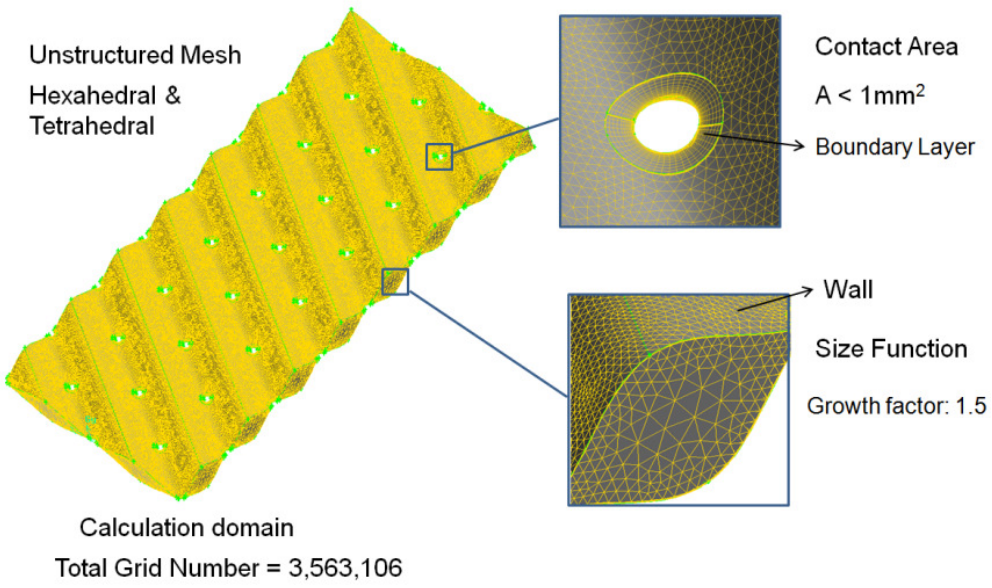

Figure 7.7 Mesh refinement near the boundaries

A small segment of the PHX is simulated to calculate both the pressure drop per unit length and the heat transfer coefficient. Steady state, 3-D model with pressure based solver and implicit scheme is used to solve the computational domain. In this case, the shear-stress transport (SST) κ-ω model is chosen as the turbulence model because of its robustness and the capability of combining both κ -ω model and κ-ε model, which makes it more accurate and reliable for a wide range of flow applications. It should be noted that in order to correctly utilize the SST κ -ω model, the mesh quality near the wall boundary must be sufficiently fine so that the dimensionless wall distance y^+ presented in Eq.(7.2) is of the order of 1 as imposed by the turbulent model (Kanaris et al. 2009; ANSYS FLUENT 12.0 Documentation, 2009).

The governing equations of continuity, momentum (Navier-Stokes) and energy are solved in Cartesian coordinates based on the assumptions as follows:

- Three-dimensional, incompressible and steady state flow
- Single phase flow, no gravity or any other body force involved
- Constant wall temperature with water as the working fluid
- No fouling of any kind exists in the computational domain
- The computational domain is located in the central part of the novel heat exchanger and the periodicity is established perpendicular to the flow direction
- Viscous dissipation is negligible in the energy equation

The PHX segment thermal and hydraulic performances are evaluated in terms of heat transfer coefficient (h) as given in Eq.(7.3) and pressure drop per unit length ($\Delta P/L$) where L is the segment length and ΔP is reported directly from CFD simulation as given in Eq. (7.4).

$$h = \frac{Q}{A \cdot LMTD}$$
$$Q = \dot{m} \cdot C_p \cdot (T_{out} - T_{in}) \tag{7.3}$$
$$LMTD = \frac{(T_{in} - T_w) - (T_{out} - T_w)}{ln\left[(T_{in} - T_w)/(T_{out} - T_w)\right]}$$

$$\Delta P = P_{in} - P_{out} \tag{7.4}$$

From the CFD simulation mass flow rate ($\dot{m}$) and outlet temperature (T_{out}) is calculated for a given inlet temperature (T_{in} = 295 K) and wall temperature (T_w = 300 K) and inlet design variables.

7.3.3 Problem Definition

The schematic of the PHX segment is shown in Figure 7.6. The goal is to find optimized designs that have maximum heat transfer coefficient h and minimum pressure drop per unit length $\Delta P/L$. The different design variables that define the PHX segment performance are shown in Figure 7.6. The four design variables are defined in Table 7.3. The corresponding computational domain is shown in Figure 7.7. The heat transfer coefficient and the PHX segment pressure drop are obtained by solving the continuity, the momentum, and the energy equations using a commercially available CFD tool such as Fluent®. For different designs, the solutions are obtained for a fixed wall temperature, T_w = 300 K, and constant coolant inlet temperature T_{in} = 295 K with variable coolant flow rate. Water is used in this study as the working fluid.

Table 7.3 Design variables for plate heat exchanger segment optimization

Design Variable	Lower limit	Upper limit
b [mm]	3.18	6.35
β	22°	68°
p [mm]	9.50	38.00
u [m/s]	0.10	1.20

Individual metamodels are developed for each response, i.e., for heat transfer coefficient h and pressure drop per unit length $\Delta P/L$. The optimization problem can be summarized as shown in Equation 7.5. The first objective is to maximize the heat transfer coefficient. The second objective is to reduce the pressure drop thus reducing the pumping power required.

$$
\begin{array}{lll}
\max & h & [\mathrm{W/m^2K}] \\
\min & \Delta P / L & [\mathrm{Pa/m}] \\
\text{subject to:} & & \\
& h \geq 5000 & \mathrm{W/m^2K} \\
& \Delta P / L \leq 100 & \mathrm{kPa/m}
\end{array}
\tag{7.5}
$$

7.3.4 Online Approximation Assisted Optimization

The same steps described in Figure 7.4 are applied here with building metamodels for heat transfer coefficient and pressure drop per unit length. For OAAMO, the stopping criterion is the maximum number of available simulations. The steps in OAAMO are as follows:

Step-1: Generate an initial set of design points using the maximum entropy design method and observe the corresponding responses for the heat transfer coefficient (h) and the fluid pressure drop per unit length inside the PHX segment ($\Delta P/L$).

Step-2: Develop a metamodel for each objective; i.e., h and $\Delta P/L$.

Step-3: Formulate a multiobjective optimization problem as given in Eq. (7.5) based on the metamodels and solve it using MOGA.

Step-4: From all Pareto points, select points to improve the metamodel accuracy in the expected optimum region and to improve the diversity of the optimum designs both in the design space and objective space base on OAAMO approach developed in chapter 3.

Step-5: Evaluate the true response (i.e., run the simulation) for the newly chosen points and then go to Step-2.

Step-6: Repeat Step-2 to Step-5 until a limit on the number of function calls is achieved.

7.3.5 Results and Discussion

Two different metamodels are built for the two responses viz., h and $\Delta P/L$. The initial design comprising of 50 points is generated using the MED method and then OAAMO method is used to sample additional 62 additional points in several runs as presented in Figure 7.8. In each run, metamodels are built then optimizer is run based on these metamodels and finally Pareto solutions are filtered to select the next samples to update the current metamodels. For offline AAMO, a set of 200 samples is generated before building the metamodels using MED method.

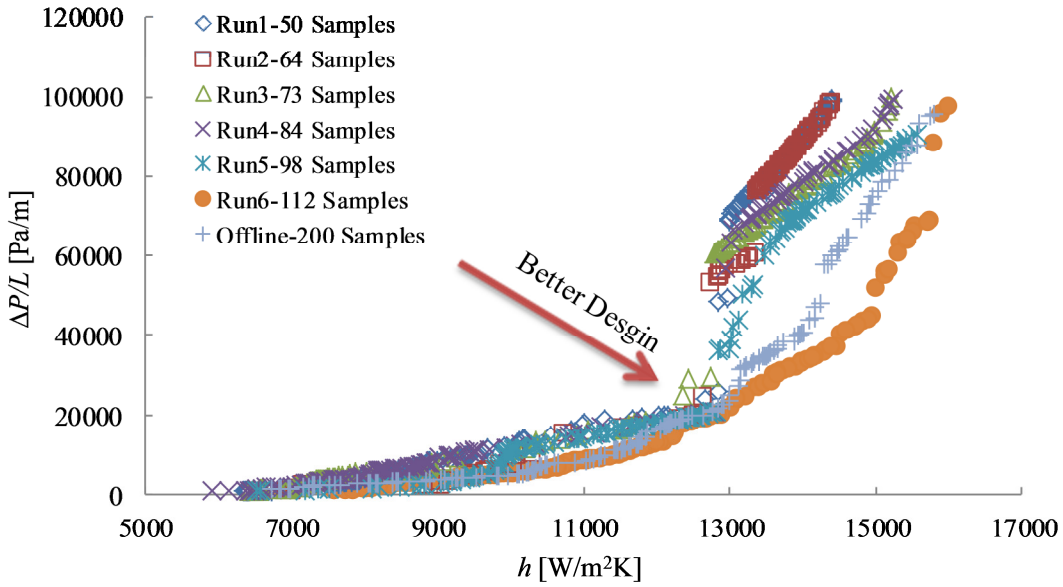

Figure 7.8 Comparison between online and offline approximation assisted optimization results

As it can be seen from Figure 7.8, the performance of the OAAMO is improved gradually by adding more samples in the expected optimum region. Compared with offline AAMO, OAAMO can add more samples near the Pareto frontier and can find better designs while reducing more than 40 % of the

computational cost. Consequently, Pareto obtained from OAAMO appears to be better than offline AAMO especially in the right upper corner as shown in Figure 7.8. Generally speaking, having more sample points in the excepted optimum region assistance to improve the performance of both methods. The relative error in the prediction is reported in Table 7.4. As it can be seen, OAAMO is performing much better in pressure drop prediction however offline AAMO is better in predicting heat transfer coefficient. The main advantage in using OAAMO as described earlier is the saving in the computational cost.

Table 7.4 Relative absolute error in Pareto set when using AAMO and OAAMO

	RError in h %		*RError in ΔP/L %*	
	AAMO	OAAMO	AAMO	OAAMO
Average	1.16	2.08	10.50	3.29
Maximum	6.12	4.56	41.82	6.43
Minimum	0.03	0.83	3.41	0.64
STD	1.31	1.15	7.89	2.10

It can be seen from the results that OAAMO is performing better while reducing significantly the computational cost, i.e., reducing the total number of CFD simulation required. These are the main advantages of using online approximation assisted optimization. However, offline approximation assisted optimization requires more samples to build a globally accurate metamodels which means more samples are wasted in the entire design space without affect the performance in the expected optimum region. Although the previous conclusion is true for a particular optimization problem, it is important as well to mention that offline approximation assisted optimization is more efficient if the globally accurate metamodels will be used later to optimize other products with different objectives based on the same

design space. In this case, no more CFD simulations will be needed. On the other hand, using online approximation assisted optimization with new objectives requires more runs as a result of changing the excepted optimum region.

In the next section, another example for rollbond plate heat exchanger optimization using simplified online approximation assisted is presented.

7.4 Rollbond Plate Heat Exchanger

As presented in the previous section, plate heat exchangers (PHXs) are the most widely used compact heat exchanger, due to its high thermal efficiency, and ease of manufacture. For application with low temperature lift heat pump, there is a need to improve the plate heat exchanger thermal and hydraulic performance. A modified rollbond PHX model is developed (Lee et al., 2012) to minimize the pumping power per unit length and to improve the heat transfer coefficient using an online approximation assisted optimization approach. The thermal-hydrodynamic characteristics of single phase turbulent flow in rollbond type plate heat exchangers with adapted wavy curve configuration have been used in this section. The computational domain contains a wavy curve configuration and the simulations adopted the shear-stress transport (SST) κ-ω model as the turbulence model. An online approximation assisted optimization approach is used to optimize the rollbond plate heat exchanger in order to maximize the heat transfer coefficient (h) and the pumping power per unit length ($Power/L$). Design optimization is performed using multiobjective genetic algorithm based on metamodels that are built to represent the entire design space. An online approximation assisted optimization approach based on space filling filter is used to add more samples to improve the metamodels

performance in the expected optimum region. Approximated optimum designs are validated using computationally expensive actual CFD simulations. The majority of the material presented in this section is presented in Lee et al. (2012).

7.4.1 CFD Model

A new heat exchanger is developed to improve the performance of PHX for the application of the low temperature lift heat pump. Two fluids are used: refrigerant and water. The refrigerant undergoes phase change, while the water undergoes temperature change only in single phase. By adapting a wavy curve configuration, the pressure drop on the single phase side is designed to decrease. In addition, heat transfer performance design enhancement is achieved by balancing the heat transfer coefficients of the two fluids, through regulating the flow area ratio between single phase flow and working fluid. The overall schematic of the novel heat exchanger is shown in Figure 7.9. Water flows over the outside of the plates, and refrigerant flows through the inside of the plates, perpendicular to the water flow, as shown with arrows in the figure. The refrigerant side inlet and outlet ports are connected to the header. Single phase side flow is designed to be a wavy curve by offsetting the refrigerant flow channel to single phase flow direction, thus reducing the pressure drop of water side. By adjusting the gap between the plates and the channel width or height, the flow area ratio of two fluids can be regulated. Design variables of the novel heat exchanger channel are defined as shown in Figure 7.10. A channel width (a), channel distance (b), plate width, plate length, channel number, summit width (a), channel height (h), plate gap (d), and thickness of plate (t) are defined in the novel heat exchanger.

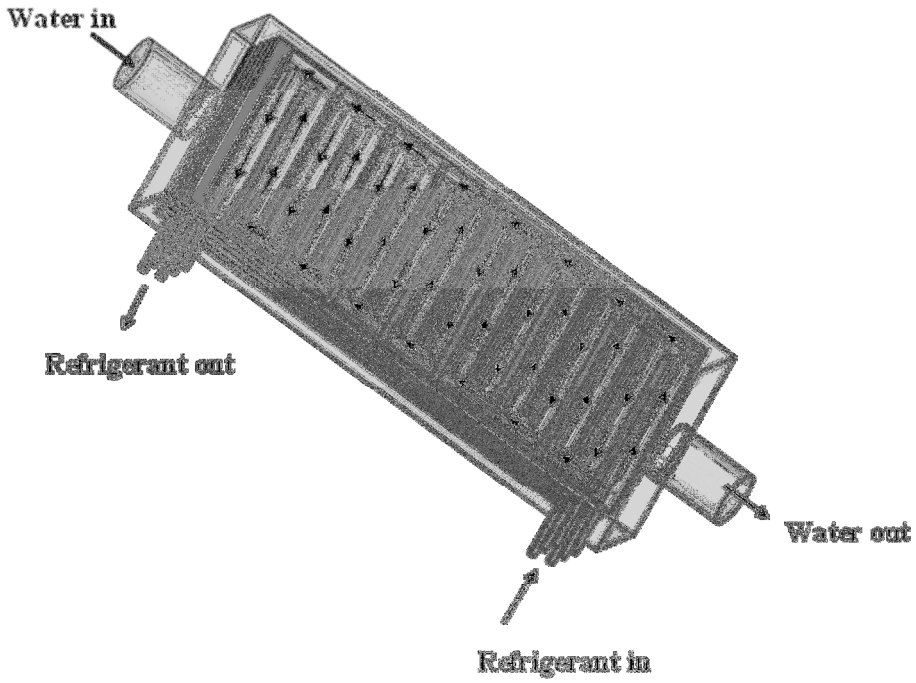

Figure 7.9 Schematic of novel heat exchanger

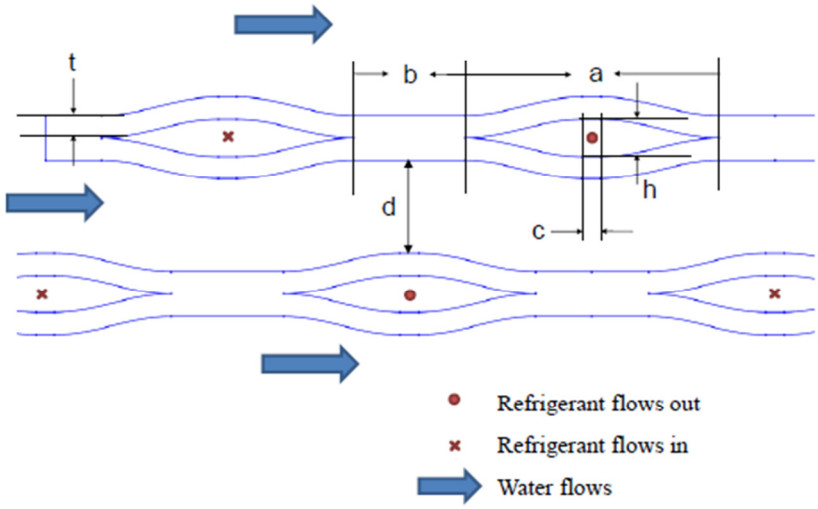

Figure 7.10 Parameters of novel heat exchanger channel

The calculation domain is presented in Figure 7.11, which simulates a section of the single phase flow side of the novel heat exchanger. The mesh of the plate and inner space are generated using Gambit®. An unstructured mesh system with a

tetrahedral type mesh is created for the inner space, and a structured mesh system with a hex type mesh is used for the wall space. To create a small viscous sub-layer, a boundary layer function is used with a 1.26 growth factor.

The governing equations of continuity, momentum (Navier-Stokes) and energy are solved in Cartesian coordinates based on the assumptions as follows:

- Three-dimensional, incompressible and steady state flow
- Single phase flow, no gravity or any other body force involved
- Constant wall temperature with water as the working fluid
- No fouling of any kind exists in the computational domain
- The computational domain is located in the central part of the novel heat exchanger and the periodicity is established perpendicular to the flow direction
- Viscous dissipation is negligible in the energy equation

The thermal and hydraulic performances of numerical modeling are evaluated in terms of heat transfer coefficient (h) and the pumping power ($Power/L$), which are calculated using Eq. (7.3) and Eq. (7.6) where $\dot{V}$ is the volume flow rate in (m^3/s), and $\Delta P / L$ is the pressure drop per unit length in (Pa/m). The shear-stress transport (SST) k- ω model is chosen as the turbulence model because of its robust and accurate formation of combining both the k- ω and k- ε models, which makes it more precise and reliable for a wider class of flows (ANSYS FLUENT 12.0 Documentation).

$$Power / L = \dot{V} \times \Delta P / L \tag{7.6}$$

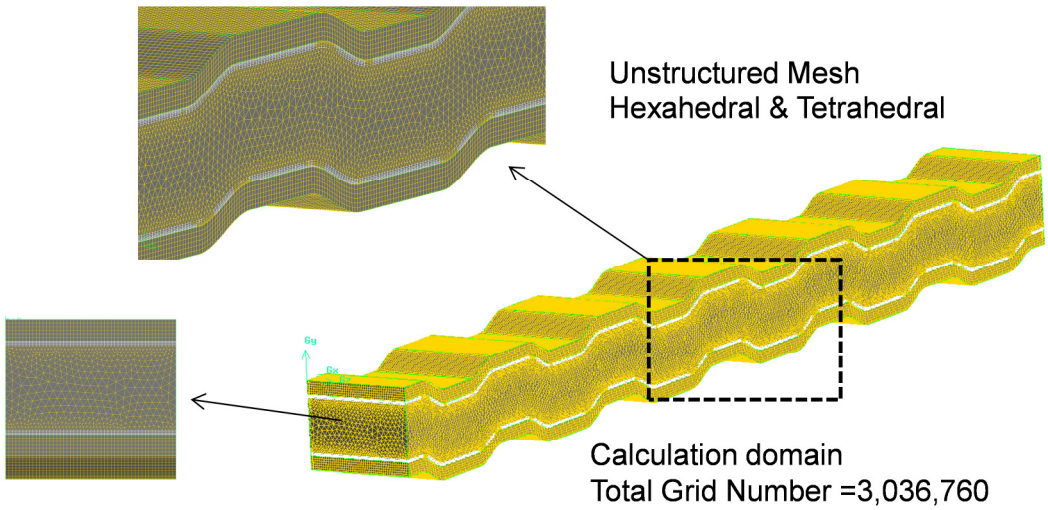

Figure 7.11 Computational domain and mesh refinement near the boundaries

Fig. 7.12 shows the contours of water temperature distribution in the rollbond heat exchanger segment for a certain operating conditions. Water flows along the X-axis from the left to right side. Water temperature decreases as the flow approaches near the wall. Fig. 7.13 shows velocity vectors by velocity magnitude. It can be found that high velocity developed near refrigerant channels. The wave shaped pattern enhanced the heat transfer between the wall and the fluid.

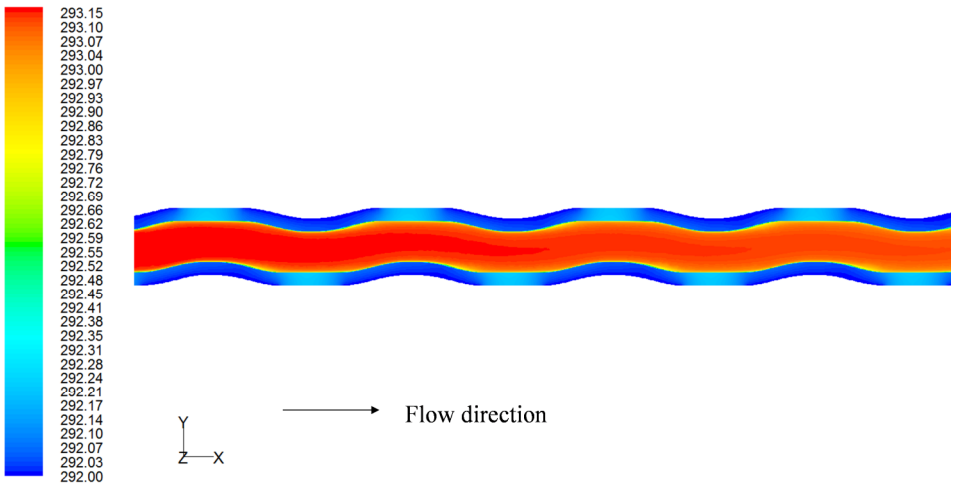

Figure 7.12 Temperature distribution in (K) for rollbond heat exchanger segment (Lee et al., 2012)

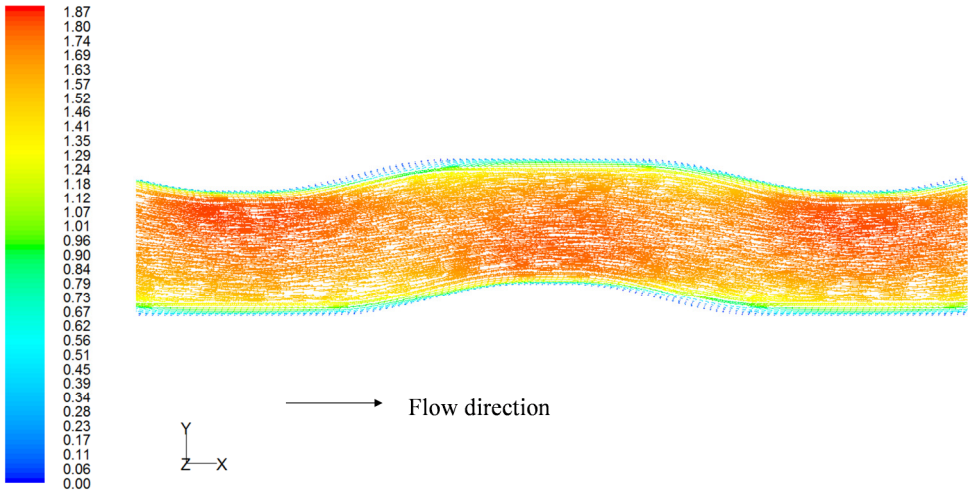

Figure 7.13 Velocity vectors in (m/s) inside the rollbond heat exchanger segment (Lee et al., 2012)

7.4.2 Problem Definition

For the rollbond heat exchanger optimization design, the objectives are to maximize the heat transfer coefficient (h) while minimizing the unit pump power per unit length ($Power/L$, along the HX flow direction) as given in Eq. (7.7). Because CFD simulation is conducted on a section of the heat exchanger, pumping power per unit length is used instead of pumping power. The final formulation of the optimization problem is given in Eq. (7.7).

$$\begin{aligned} &\max \quad h && [\mathrm{W/m^2K}] \\ &\min \quad Power/L && [\mathrm{W/m}] \\ &\text{subject to:} \\ &\qquad h \geq 8000 && \mathrm{W/m^2K} \\ &\qquad 2\,\mathrm{kPa/m} \leq \Delta P/L \leq 100 && \mathrm{kPa/m} \end{aligned} \tag{7.7}$$

The different design variables that define the rollbond segment performance are shown in Figure 7.10. The four design variables are defined in Table 7.5. The corresponding computational domain is shown in Figure 7.11. The heat transfer

coefficient and the segment pressure drop are obtained by solving the continuity, the momentum, and the energy equations using a commercially available CFD tool such as Fluent®. For different designs, the solutions are obtained for a fixed wall temperature, T_w = 291 K, and constant coolant inlet temperature T_{in} = 293K with variable coolant flow rate. Water is used in this study as the working fluid. Individual metamodels are developed for heat transfer coefficient h and pressure drop per unit length $\Delta P/L$.

Table 7.5 Normalized design variables for rollbond heat exchanger segment optimization

Normalized Design Variable	Lower limit	Upper limit
x_1, gap between the plates	0	1
x_2, channel height	0	1
x_3, channel width	0	1
x_4, summit width	0	1
x_5, water velocity	0	1

7.4.4 Online Approximation Assisted Optimization

Initially, MED sampling approach described in Chapter 2 is used to generate 150 designs. The responses of heat transfer coefficient, h, and the pumping pressure drop per unit length *Power/L* are obtained from these 150 numerical simulation runs, and then correlated into the metamodel using Kriging metamodel technique. After obtaining some intermediate optimum solutions calculated by the multiobjective genetic algorithm (MOGA), a simple online approximated assisted optimization approach based on space filling filter method is applied to filter some of the optimum solutions and select the next set of samples to improve the metamodels' performance in the excepted optimum region.

The metamodels have been built based on the 200 cases of CFD simulation with the aforementioned approach. These *h* and *Power/L* metamodels are then verified using a set of 20 random samples. The detailed validation of various building methods is shown in Table 7.6 using different correlation function and regression models in Kriging. It could be seen that the first order polynomial Gauss model has the best accuracy among these methods. The detailed comparisons of *h* and $\Delta P/L$ between the CFD and metamodel are shown in Table 7.6. The relative root mean squared error (*RRMSE*) between the CFD and current metamodel is 1.15% for the heat transfer coefficient and 4.24% for the pumping power per unit length, which is good enough for further optimization.

Table 7.6 Validation of different metamodel building methods

Correlation functions	Regression models	*RMSE*		*RRMSE* (%)	
		h (W/m^2K)	*Power/L* (W/m)	*h*	*Power/L*
Gauss	Poly0	138.85	0.03	1.38	5.29
	Poly1	120.58	0.03	1.15	4.24
	Poly2	105.46	0.05	1.02	10.49
Exponential	Poly0	142.04	0.07	1.38	9.51
	Poly1	105.32	0.06	1.09	12.41
	Poly2	112.05	0.07	1.26	29.91

7.4.5 Results and Discussion

The Pareto set solutions are obtained from three different runs of MOGA. Figure 7.14 shows the Pareto solutions as well as the DOE samples. It should be noted that the Pareto solutions are not obtained in the highlighted region A, because the constraints would have been violated.

The optimum designs selected from the Pareto solution set are shown in Table 7.7. Design variables in the optimum design are well distributed, except for summit

width (x_4) and channel width (x_3). A large summit width increased both h and *Power/L*. The effect of increased h is higher than that of an increased *Power/L*, so the optimum designs are developed at a relatively large summit width that ranged from 0.552 to 0.942. Furthermore, it can be seen that channel width (x_3) exhibited low value ranges in optimum designs. A small channel width creates more periodic wavy curves per unit length. This can increase the turbulence in the water flow, and eventually increase both h and *Power/L*. Therefore, the h increased faster than the *Power/L*, thus optimum designs were obtained in the regions of small channel width.

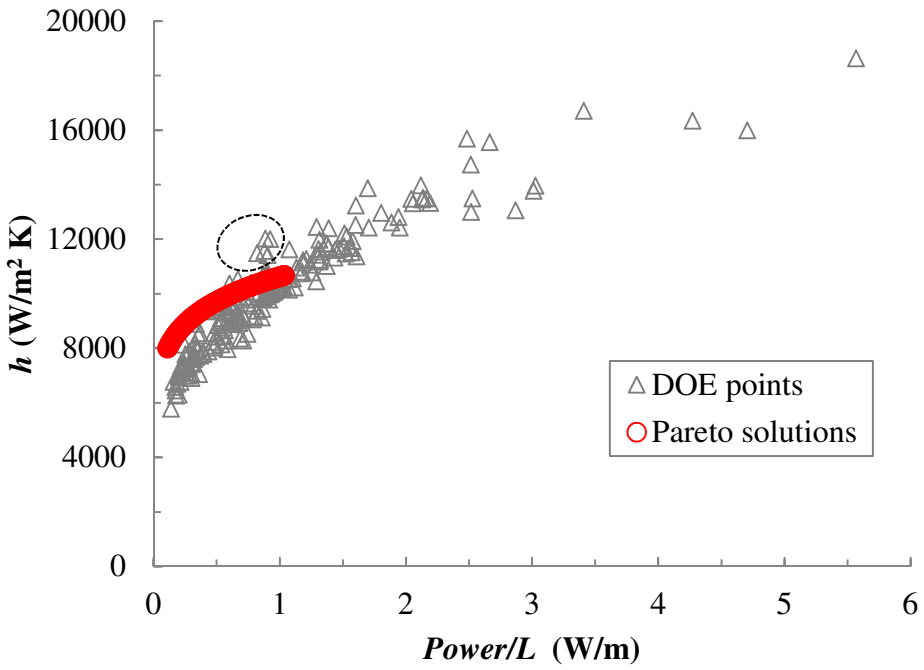

Figure 7.14 DOE points and optimum rollbond heat exchanger segment

Optimum designs in Table 7.7 are verified with the results obtained directly the from CFD simulation. The *RRMSE* between the approximated results and CFD simulation are 0.82% for the h and 16.15% for the *Power/L*. This indicates that the

optimum results obtained from approximated assisted optimization approach used in this study are acceptable, given the number of samples.

Table 7.7 Optimum designs selected from Pareto solution set

Optimum Designs	x_1	x_2	x_3	x_4	x_5	h (W/m^2K)	*Power/L* (W/m)	$\Delta P/L$ (kPa/m)
1	0.399	0.120	0.323	0.662	0.508	9958	0.696	8.87
2	0.728	0.021	0.474	0.943	0.674	10618	0.962	9.28
3	0.291	0.022	0.361	0.645	0.674	10204	0.787	9.64
4	0.020	0.173	0.296	0.934	0.000	9139	0.345	8.49
5	0.078	0.008	0.098	0.853	0.195	9937	0.492	9.71
6	0.001	0.278	0.390	0.920	0.000	9152	0.353	8.81
7	0.660	0.171	0.780	0.733	0.981	10826	1.193	10.00
8	0.509	0.106	0.249	0.709	0.527	10357	0.789	9.35
9	0.503	0.575	0.808	0.701	0.527	9965	0.812	9.65
10	0.260	0.024	0.169	0.885	0.250	9908	0.542	9.06
11	0.007	0.351	0.431	0.749	0.167	9321	0.432	9.20
12	0.006	0.376	0.711	0.771	0.190	8671	0.378	7.90
13	0.221	0.637	0.027	0.552	0.038	9842	0.460	9.50
14	0.000	0.014	0.320	0.918	0.000	8356	0.271	6.76

7.5 Summary

In this chapter, three examples are presented for coldplate as an example for electronic cooling devices and two different types of plate heat exchanger, i.e., chevron and rollbond plate heat exchangers. The advantages of using online approximation assisted optimization to optimize these different heat exchangers are discussed.

For coldplate example, two objectives are considered; minimizing the maximum temperature and minimizing the refrigerant pressure drop. OAAMO method developed in chapter 3 is used as the online approximation assisted optimization approach. OAAMO predicted better optimum designs with higher accuracy compared to offline approximation assisted optimization approach. The final

results are verified using CFD simulations. The errors are small which indicates that the accuracy of the online approximation assisted optimization method is acceptable. The approximation technique resulted in a significant reduction in computational time compared to conventional optimization technique. Only 60 CFD simulations are required for building the metamodels, compared to several thousands of actual simulations required when conventional MOGA is used (5100 simulations).

As for the chevron plate heat exchanger, Online and offline approximation assisted optimization approaches are used to obtain optimum plate heat exchanger designs based on single phase liquid. Kriging metamodels are built for both the heat transfer coefficient and for the pressure drop per unit length. These metamodels are used to predict the objectives and constraints within multiobjective genetic algorithm (MOGA). In online approximation assisted optimization, OAAMO method is used to find the optimum designs. OAAMO approach predicted better optimum designs with high accuracy compared to offline approximation assisted optimization approach. The final results are also verified using CFD simulations. The errors are small which indicates that the accuracy of the online approximation assisted optimization method is acceptable. The approximation technique resulted in a significant reduction in computational time compared to conventional optimization technique. Only 112 CFD simulations are required for building and updating the metamodels in online approximation assisted optimization compared with 200 samples required for offline approximation approach. Both offline and online approximation techniques are efficient when compared to several thousands of actual simulations required for conventional MOGA (~ 5100 simulations).

In rollbond plate heat exchanger, a simplified online approximation assisted multiobjective optimization approach is used. The water heat transfer coefficient and pumping power associated with the heat exchanger are optimized using the simplified online approximation assisted optimization approach. The plate gap, channel height, channel width, summit width, and fluid inlet velocity are defined as design variables, and 200 samples are selected using the maximum entropy design method to build a metamodel for obtaining the heat transfer coefficient, as well as the pumping power per unit length. The optimized designs are calculated using a multi-objective genetic algorithm, and are presented. Finally, the Pareto optimal designs are verified against the values that were directly obtained from CFD simulations. When the refrigerant side heat transfer coefficient is properly designed according to the water side heat transfer coefficient, overall heat transfer of the rollbond heat exchanger can be maximized. This can decrease the cost of the heat exchanger and increase the performance of a low temperature lift heat pump system.

In the next chapter, the conclusion of this dissertation is presented. The chapter highlights the contributions of the four research thrusts of this dissertation followed by the recommendations for future work.

Chapter 8: Conclusions

8.1 Introduction

This dissertation is focused on four research thrusts. These are: (i) A new online approximation assisted multiobjective optimization (OAAMO), (ii) a new approximation assisted multiobjective optimization with global and local metamodeling, (iii) a new framework for integrating OAAMO heat exchanger design problems with multiscale simulations (OAAMOMS), and (iv) a new header optimization model for a new generation of air-cooled heat exchangers. In addition, several heat exchanger types are optimized using the newly developed methods.

This chapter is organized as follows: Section 8.2 provides a summary of the four research thrusts including the different heat exchangers applications presented in the dissertation. This is followed by a statement of the main contributions in Section 8.3. Finally, the recommendations for the future work are provided in Section 8.4.

8.2 Summary

In Chapter 3, a new online approximation assisted multiobjective optimization approach called OAAMO is presented. Two main goals are considered while building this new approach: (a) improving both the metamodel performance for objectives and constraints in the expected optimum region and the accuracy of the predicted optimum solutions, and (b) improving the quality of the predicted optimum solutions by improving both the closeness to target solution and diversity of the optimum solutions obtained. In order to achieve these goals, selected points are chosen to update the metamodels iteratively. The proposed approach starts with initial samples and initial metamodels are built for all objectives and constraints. Then

MOGA is applied to the metamodel based optimization problem and a set of predicted optimum solutions are generated. Afterwards, five points are selected based on the criterion described in OAAMO in order to achieve the above mentioned goals. Finally, a space filling filter is used to avoid samples' clustering in the design space. OAAMO is tested and compared with an offline approach called AAMO. The results show that OAAMO outperforms AAMO in terms of accuracy of the predicted solutions. Also, OAAMO is compared with ParEGO, an online AAMO method from the literature. OAAMO performs better in terms of closeness and diversity for most of the problems with respect to ParEGO. In addition, OAAMO is applied to an engineering test problem and compared with an offline AAMO approach. The results of the engineering example show that OAAMO produced better optimum solutions in terms of both the accuracy and the quality (closeness to target optimum solutions and diversity).

In Chapter 4, a new and novel online approximation assisted multiobjective optimization approach using both global and local metamodeling is presented. The approach combines both metamodeling in the global and local optimum regions and random search in both regions to find the best optimum solutions. The approach starts with generating initial samples that are used to build global metamodels for objectives and constraints and then using these metamodels to predict the responses (objectives and constraints) for a large number of randomly generated points. Then, using non-dominating sorting, the most promising points (among the initial samples and the randomly evaluated samples) are selected. The actual simulation is run for a few new points selected based on spread in both design and objective spaces. Based

on these values, the "best" points are grouped in multiple clustered regions in the design space and then local metamodels of objectives/constraints are constructed in each region. These clusters are adaptively built and updated. All observed points are also used to iteratively update the global metamodels. In this way, the accuracy of the metamodels is gradually improved as the optimizer approaches the Pareto optimum frontier. One of the important advantages of the proposed approach is that: the most promising points are observed which means that there is no need to verify the final solutions separately and all the final solutions are feasible as well. Both numerical and engineering examples are tested using the proposed approach. A CFD coldplate design example is demonstrated with the proposed approach as well. It is found that a reasonable set of optimum design solutions are obtained with a few number of CFD simulations.

In Chapter 5, a new approach for online approximated assisted multiobjective optimization for problems with multiscale simulations such as heat exchanger design is presented. The approach aims at reducing the computational cost while improving the accuracy of the predict optimum solutions by combining an adaptive update of metamodels used to predict the performance in the segment level while running the optimizer for the entire heat exchanger based on a heat exchanger solver. For examples, the metamodels for air heat transfer coefficient and air pressure drop on the segment level are updated while the MOGA is run based on the entire heat exchanger solver for new generation of air-cooled heat exchangers. The accuracy of the results is comparable with an offline based multiscale simulation approach. The online multiscale multiobjective approximation assisted optimization approach saved more

than 60% of the computational time required to obtain similar results as the offline multiscale approximation techniques. The approach presented in this chapter is generic in nature and applicable to any similar heat exchanger optimization problem.

In Chapter 6, a 3D-CFD model is used and modified for headers used in the next generation of air-cooled heat exchangers based on mini and micro tubes. In order to reduce the mass flow rate misdistribution inside the header and to reduce the total header volume, NURBS are used to represent and manipulate the header shape. Then a systematic and generic approach for header optimization is developed using an OAAMO approach developed in Chapter 3 that enables to find more accurate optimum header designs while significantly reducing the computational cost. Finally, design guidelines for headers used in the new generation of air-cooled heat exchangers are provided. Based on the results obtained, there is a tradeoff between header area ratio and refrigerant mass flow rate's relative standard deviation. For instance, some of the optimum designs obtained have mass flow rate standard deviations of less than 2% while other designs had headers area ratio less than 2%. Selected designs are validated using CFD simulations. The error in the predicted total pressure drop is less than 6% and that for the mass flow rate relative standard deviation is less than 8%, thus verifying the acceptable accuracy of the metamodels. Finally, parametric studies are presented in this chapter to optimize 1-kW integrated heat exchanger and header module.

In Chapter 7, three examples are presented to optimize the different types of electronic cooling devices and heat exchangers. Coldplate is used as an example for electronic cooling devices and two different types of plate heat exchanger are used as

well, i.e., chevron and rollbond plate heat exchangers. The advantages of using online approximation assisted optimization to optimize these different heat exchangers are discussed at the end of this chapter. For the coldplate example, two objectives are considered: minimizing the maximum temperature and minimizing the refrigerant pressure drop. Six design variables are optimized: channel height, length, and width, thickness of the middle wall, top and bottom channel wall, in addition to the refrigerant inlet velocity. Comparing with offline based AAMO, OAAMO predicted better optimum designs with a higher accuracy. Finally, only 60 CFD simulations are required for building the metamodels, compared to several thousands (5100 simulations)of actual simulations required when a conventional MOGA is used.

As for the chevron plate heat exchanger, two objectives are considered: minimizing the pressure drop per unit length and maximizing the heat transfer coefficient. Four design variables are optimized: chevron angle, pitch, height and fluid velocity. Similarly, the OAAMO approach predicts better optimum designs with a high accuracy compared to an offline AAMO approach. The errors are small which indicates that the accuracy of the online approximation assisted optimization method is acceptable. Only 112 CFD simulations are required for building and updating the metamodels in online approximation assisted optimization compared with 200 samples required for offline approximation approach which means that OAAMO approach can save more than 40% of the computational cost while obtaining better optimum solutions.

In a rollbond plate heat exchanger, a simplified online approximation assisted multiobjective optimization approach is used to optimize the rollbond heat exchanger

design with two objectives: minimizing the pumping power per unit length and maximizing the heat transfer coefficient Five design variables are optimized: gap between the plates, channel height and width, summit width and water inlet velocity. The water heat transfer coefficient and pumping power associated with the heat exchanger are optimized using the simplified online approximation assisted optimization approach. Only 150 samples are selected using the maximum entropy design method to build a metamodel for obtaining the heat transfer coefficient, as well as the pumping power per unit length. Another 50 samples are added based on the simplified online approximation assisted optimization approach used in this chapter. The final optimum designs are validated using CFD simulations. Based on the results, it is observed that when the refrigerant side heat transfer coefficient is properly designed according to the water side heat transfer coefficient, overall heat transfer of the rollbond heat exchanger can be maximized. This can decrease the cost of the heat exchanger and increase the performance of a low temperature lift heat pump system.

8.3 Contributions

The main contributions of this dissertation are discussed in the following subsections.

8.2.1 Online Approximation Assisted Multiobjective Optimization

A new approach (OAAMO) is proposed which has some distinct characteristics as in the following: (i) A significant number of the previous AAO methods only uses a globally accurate meta-model to find optimum solutions. In the proposed approach, online AAO is used to improve the meta-models' performance in the expected optimum region. (ii) Some previous approaches try to approximate the optimum frontier using an expected improvement measure. However, OAAMO uses the information from the estimated optimum solutions directly and does not use any scalar measure. (iii) OAAMO aims at improving the spread, closeness, and accuracy of the solution points while avoiding clustering of the points.

8.2.2 Approximation Assisted Multiobjective Optimization with Combined and Local Metamodeling

A new online approximation assisted multiobjective optimization approach that combines global and local metamodeling is developed. The approach is developed collaboratively by the coauthors of the papers (Hu et al., 2012a; Hu et al., 2012b). The main idea for using global and local metamodeling to enhance the online approximation assisted multiobjective optimization is developed by me. In addition, the sampling selection criterion based on both design and objective spaces is proposed by me.

The approach has the following characteristics: (i) combining online metamodeling updating in both global and promising local optimum regions can reduce significantly the computational cost, (ii) selecting the clusters adaptively in the promising optimum regions based on "spread distance" of the non-dominated points which is calibrated in both the design variable and objective spaces, and (iii) creating the clusters around the current best design points which helps to significantly enhance the accuracy of the local metamodels.

8.2.3 Online Approximation Assisted Multiobjective Optimization for Problems with Multiscale Simulation (OAAMOMS)

A new framework is developed for applying OAAMO to problems with multiscale simulation such as heat exchanger design optimization. This framework combines an adaptive update of metamodels for air heat transfer coefficient and air pressure drop at the segment level with the entire heat exchanger simulation for a new generation of air-cooled heat exchangers.

8.2.4 Header Optimization for New Generation of Air Cooled Heat Exchanger using NURBS

A 3D-CFD model for a header is used in a new generation of air-cooled heat exchangers by adding NURBS to represent and manipulating the header shape in order to reduce the mass flow rate maldistribution inside the header. In addition, a systematic and generic approach for header optimization is developed using OAAMO that helps to find more accurate optimum header designs while significantly reducing the computational cost. Finally, design guidelines are provided for header optimization for a new generation of air-cooled heat exchangers. The results output

from this study can enhance the design of all header used in micro channels based tubes heat exchangers.

8.4 Future Research Directions

There are a number of directions for future research as discussed in the following.

1. ***Discrete Design Variables***

The approaches developed in this dissertation are developed with the assumption that all design variables are continues. This is not the case in many heat exchanger design optimization problems where there are several discrete design variables. An example for discrete design variables in heat exchanger problem includes the number of tubes, number of fins, and others. So, there is a need to consider discrete design variables as well under online approximation assisted multiobjective optimization framework in order to reduce the computational cost.

2. ***Large Number of Design Variables***

The approaches developed in this dissertation are developed for problems with the number of design variables of about 50, which is the limit for the Kriging metamodeling technique. This is not the case in some optimization problems where there are several hundreds or even thousands of design variables are used, as is the case in topology optimization. There is a need to consider problems with a large number of design variables combined with online approximation assisted multiobjective optimization framework.

Proper Orthogonal Decomposition (POD) method (Loéve, 1955) is a possible method that can be used to handle this problem. POD has been developed as an

alternative method of deriving a basis vector for high-order systems. POD has been widely used in CFD applications (Sirovich, 1987; Berkooz et al., 1993). Coupling POD with the methods in this dissertation should be explored particularly for problems with a large number of design variables.

3. Resource Allocation

In many optimization problems, the total number of available function calls is fixed and limited. Although the performance of any approximation assisted optimization technique depends on the relation between the design variables, there are several questions that should be addressed such as: a) how many samples should be used as initial designs? What is the relation between the number of design variables and the total number of samples in the initial designs? Is it better to generate the initial designs using space filling DOE method such as MED or LHS or to use an adaptive sampling technique such as SFCVT (Aute et al., 2008)?

4. Metamodeling Methods

It is important to investigate the use of non-Kriging based metamodels especially for problems with a large number of design variables. In addition, in the case of using Kriging, it is important to explore how to identify the best regression model and correlation function before applying the Kriging metamodeling technique. Poor choice of these can lead to an increase in the computational cost.

5. Heat Exchanger Applications

In chapter 5, OAAMOMS approach was applied only to a new generation of air-cooled heat exchangers. It is important to apply this approach to optimize different types of heat exchangers such as plate type, shell and tube, and spiral heat exchanger.

6. Combining Headers with Heat Exchanger Body

In chapter 6, OAAMO approach was applied only to optimize the header for the new generation of air-cooled heat exchangers. Then based on the results, a parametric study was used to find an integrated optimum 1 kW heat exchanger module. However, it should be more accurate to use multi-disciplinary optimization (MDO) approach to optimize the heat exchanger module and consider both the heat exchanger body and the headers as subsystems while defining the main objectives to minimize the heat exchanger volume and the refrigerant pressure drop as system objectives. That can result in more compact heat exchangers.

7. Flexible Heat Exchanger Walls

One of the assumptions for all CFD based models in this dissertation is that; the heat exchanger wall is rigid as stated in section 2.7. However, due to using thin wall thicknesses and sometimes high fluid pressures, it is important as well to consider using flexible walls instead of rigid walls as boundary conditions. That will lead to modify the computational model to consider fluid-structure interactions. In addition, using flexible walls will result in changing the dimensions of the model. Consequently, finding the robust optimum designs should consider uncertainties as well in both design variables and design parameters.

8. Heat Exchanger Design Under Uncertainty

In this dissertation, uncertainties in heat exchanger geometric parameters and design variables and flow conditions are not considered. However, using micro and mini channels in new generation of heat exchangers make manufacturing processes very challenging. As a result, large tolerances might exist compared with the original

design variables. In addition, uncertainties can result in fouling and even blockage resulting from the flow distribution and hence pressure drop. Accordingly, it is important to use robust optimization approaches to find optimum heat exchangers which are relatively insensitive to uncertainties.

Bibliography

1. Abdelaziz O., Aute, V., Azarm, S., and Radermacher, R., 2010, "Approximation Assisted Optimization for Novel Compact Heat Exchanger Designs," *HVAC&R Research*, Vol. 16, No. 5, pp. 707-728.
2. Abdelaziz O., 2009, "Development of Multi-Scale, Multi-Physics, Analysis Capability and its Application to Novel Heat Exchanger Design and Optimization," Ph.D., Mechanical Engineering, University of Maryland, College Park.
3. ANSYS FLUENT 12.0 Documentation, ANSYS Inc., 2009.
4. Armstrong, M., 1998, Basic Linear Geostatistics, *Springer*. New York, NY.
5. Aute, V. C., Radermacher, R. and Valiya Naduvath. M., 2004, "Constrained Multiobjective Optimization of an Air-Cooled Condenser," *in the Proceedings of the 10th International Refrigeration & Air-Conditioning Conference at Purdue*, Purdue, Indiana.
6. Aute V., Abdelaziz, O., Azarm, S., and Radermacher, R., 2008, "Cross-validation Based Single Response Adaptive Design of Experiments for Deterministic Computer Simulations," *12th AIAA/ISSMO Multidisciplinary Analysis and Optimization Conference*, AIAA-2008-6067, Victoria, British Columbia, Canada.
7. Aute, V., 2009, "Single and Multiresponse Adaptive Design of Experiments with Application to Design Optimization of Novel Heat Exchangers," Ph.D., Mechanical Engineering, University of Maryland, College Park.

8. Bakker, T. M. D., 2000, Design Optimization with Kriging Models, WBBM Report Series 47, Delft University Press.

9. Bejan, A., 1997, "Constructal theory network of conducting paths for cooling a heat generating volume," *International Journal of Heat Mass Transfer*, Vol. 40, pp.799-816.

10. Bejan, A., 2000, Shape and Structure, from Engineering to Nature, first ed., *Cambridge University Press*, UK.

11. Bejan, A., and Lorente, S., 2006, "Constructal theory of generation of configuration in nature and engineering," *Journal of Applied Physics*, Vol. 100, No.4, Article number. 041301.

12. Bergles, E., 2002, "ExHFT for fourth generation heat transfer technology," *Experimental Thermal and Fluid Science*, Vol. 26, pp. 335-344.

13. Berkooz, G., Holmes, P., and Lumley, J., 1993, "The Proper Orthogonal Decomposition in the Analysis of Turbulent Flows," *Annual Review of Fluid Mechanics*, Vol. 25, pp. 539–575.

14. Buche, D., Schraudolph, N. N. and Koumoutsakos, P., 2005, "Accelerating Evolutionary Algorithms with Gaussian Process Fitness Function Models," *Systems, Man, and Cybernetics, Part C: Applications and Reviews, IEEE Transactions*, Vol. 35, No. 2, pp. 183–194.

15. Cetegen, E., Dessiatoun, S., and Ohadi, M., 2009, "Multi Objective Optimization of a Force Fed Microchannel Heat Sink," *Proceedings of MNHMT2009 ASME 2009 2nd Micro/Nanoscale Heat & Mass Transfer International Conference*, Shanghai, China.

16. Charnes, A., Cooper, W., and Ferguson, R., 1955, "Optimal Estimation of executive Compensation by Linear Programming," *Management Science*, Vol. 1 No. 2, pp. 138-151.
17. Chong, S., Ooi, K., and Wong, T., 2002, "Optimization of Single and Double Layer Counter Flow Microchannel Heat Sinks," *Applied Thermal Engineering*, Vol. 22, pp. 1569-1585.
18. Coello, C., 2000, "Multiobjective Optimization of Trusses Using Genetic Algorithms," *Computers & Structures*, Vol.75, No.6, pp.647-660.
19. Coello, C. A., Veldhuizen D. A. and Lamont, G. B., 2002, Evolutionary Algorithms for Solving Multi-Objective Problems, Second edition, *Springer*, New York.
20. Coello, A. C., Pulido, G. T., and Lechuga, M. S., 2004, "Handling Multiple Objectives with Particle Swarm Optimization", *IEEE Transactions on Evolutionary Computation*, Vol. 8, No. 3, pp. 256-279.
21. Coello, C. A., Lamont, G. B., and Van Veldhuizen, D. A., 2007, Evolutionary Algorithms for Solving Multi-Objective Problems, *Springer*, New York.
22. Cohon, J. L., 1978, Multiobjective Programming and Planning, Mathematics in Science and Engineering, Vol. 140, *Academic Press.*
23. Cressie N. A. C., 1993, Statistics for Spatial Data, Wiley Series in Probability and Mathematical Statistics, *John Wiley& Sons*, Chichester, UK.

24. Currin, C., Mitchell, M., Morris, M., Ylvisaker, D., 1988, "A Bayesian Approach to the Design and Analysis of Computer Experiments", *Oak Ridge National Laboratory, Report ORNL-6498.*

25. Das, I., and Dennis, J. E., 1998, "Normal Boundary Intersection: A new method for generating Pareto surface in nonlinear multi-criteria optimization problems," *SIAM Journal of Optimization*, Vol. 8, No. 3, pp. 631-657.

26. Deb, K., 2001, Multi-Objective Optimization using Evolutionary Algorithms, *John Wiley & Sons*, Ltd, New York.

27. Deb, K., Pratap, A., Agarwal, S. and Meyarivan, T., 2002, "A fast and elitist multiobjective genetic algorithm: NSGA-II," *IEEE Transactions on Evolutionary Computation*, Vol. 6, No. 2, pp. 182–197.

28. De Losier, R., Subramanian, S., Ponyavin, V., Chen, Y., Hechanova, E. and Peterson, F., 2007, "The parametric study of an innovative offset strip-fin heat exchanger", *ASME Journal of Heat Transfer*, Vol. 129, No. 10, pp. 1453-1458.

29. Dybvig R. K., 2003, The Scheme Programming Language, third ed., *MIT Press*, Cambridge, Mass., USA,

30. Emmerich, M., Giannakoglou, K. and Naujoks, B., 2006, "Single and multiobjective evolutionary optimization assisted by Gaussian random fields metamodels," *IEEE Transactions on Evolutionary Computation*, Vol. 10,No. 4, pp. 421–439.

31. Fang H., Rais Rohani, M., and Horstemeyer, M., 2004, "Multiobjective Crashworthiness Optimization with Radial Basis Functions," *10th*

AIAA/ISSMO Multidisciplinary Analysis and Optimization Conference, Albany, NY.

32. Fang H., Rais Rohani, M. and Horstemeyer, M., 2005, "A Comparative Study of Metamodeling Methods for Multiobjective Crashworthiness Optimization," *Computers & Structures*, Vol. 83(25–26), pp. 2121–2136.
33. Farina M., 2001, "A Minimal Cost Hybrid Strategy for Pareto Optimal Front Approximation," *Evolutionary Optimization*, Vol.3, No. 1, pp. 41-52.
34. Farina M., 2002, "A Neural Network Based Generalized Response Surface Multiobjective Evolutionary Algorithm," *Proceedings of IEEE Congress on Evolutionary Computation*, Vol. 1, pp.956-961.
35. Fluent (2007) 'User's Guide', Version 6.3
36. Foli, K., Okabe, T., Olhofer, M., Jin, Y., and Sendhoff, B., 2006, "Optimization of Micro Heat Exchanger: CFD, Analytical Approach and Multi-Objective Evolutionary Algorithms," *International Journal of Heat and Mass Transfer*, Vol. 49, pp. 1090–1099.
37. Fonseca, C. M. and Fleming, P. J., 1993, "Genetic Algorithms for Multiobjective Optimization: Formulation, discussion and generalization," in *Proceedings of the Fifth International Conference on Genetic Algorithms*, pp. 416-423.
38. Fonseca, L., Barbosa, H. and Lemonge, A, 2010, "On Similarity-Based Surrogate Models for Expensive Single-and Multi-Objective Evolutionary Optimization," *Computational Intelligence in Expensive Optimization Problems*, pp. 219–248.

39. Forrester, A., Sobester, A. and Keane, A., 2008, Engineering Design via Surrogate Modelling: A Practical Guide, *John Wiley & Sons,* Ltd, New York.

40. Galeazzo, F., Miura, R., Gut, J., and Tadini, C., 2006, "Experimental and numerical heat transfer in a plate heat exchanger," *Chemical Engineering Science*, Vol. 61, pp.7133-7138.

41. Georgopolou, C., and Giannakoglou, K., 2009, "A Multi-Objective Metamodel-Assisted Memetic Algorithm with Strength-Based Local Refinement," *Engineering Optimization*, Vo. 41, No. 10, pp. 909-923.

42. Goldberg. D. E., 1989, "Genetic Algorithms in Search, Optimization and Machine Learning", *Addison-Wesley Pub. Co*., ISBN: 0201157675.

43. Gopinath, D., Joshi, Y., and Azarm, S., 2005, "An Integrated Methodology for Multiobjective Optimal Component Placement and Heat Sink Sizing," *IEEE Transactions On Components And Packaging Technologies*, Vol. 28, No. 4, pp. 869-876.

44. Habib, M., Ben-Mansour, R., Said, S., Al-Bagawi, J., and Al-Mansour K., 2008, "Correlations of flow distribution parameters in an air cooled heat exchanger", *International Journal of Numerical Methods in Fluids*, Vol. 56, pp.143-165.

45. Haftka, R.T., 1991, "Combining Global and Local Approximations," (Technical Note), *AIAA Journal*, Vol.29, No.9, pp. 1523-1525.

46. Hacker, K., 2002, "Efficient Global Optimization Using Hybrid Genetic Algorithms," *9th AIAA/ISSMO Symposium on Multidisciplinary Analysis and Optimization*, Atlanta, Georgia, September 4-6, pp. 5429-5440.

47. Haimes, Y. Y., Lasdon, L. S. and Wismer, D. A., 1971, "On a bicriterion formulation of the problems of integrated system identification and system optimization," *IEEE Transactions on Systems, Man, and Cybernetics*, Vol. 1, No. 3, pp. 296-297.

48. Han, W., Saleh, K., Aute, V., Ding G., Hwang Y., and Radermacher, R., 2011, "Numerical Simulation and Optimization of Single Phase Turbulent Flow in Chevron-type Plate Heat Exchanger with Sinusoidal Corrugations", *HVAC & R Research*, Vol. 17, No. 2, p.186-197.

49. Hastie, T., Tibshirani, R. and Friedman, J., 2001, The Element of Statistical Learning, *Springer-Verlag*, New York.

50. Horn, J., Nafploitis, N. and Goldberg, D., 1994, "A niched Pareto genetic algorithm for multi-objective optimization," in *Proceedings of the First IEEE Conference on Evolutionary Computation*, pp. 82-87.

51. Hosder, S., Schetz, J.A., Mason, W.H., Grossman, B., and Haftka, R.T., 2010, "Computational-Fluid-Dynamics-Based Clean-Wing Aerodynamic Noise Model for Design," *Journal of Aircraft*, Vol. 47, No. 3, pp. 754–762.

52. Hong, Y. S, Lee, H., and Tahk, M. J., 2003, "Acceleration of the Convergence Speed of Evolutionary Algorithms Using Multilayer Neural Networks," *Engineering Optimization*, Vol.35, No.1, pp. 91-102.

53. Hu W., Saleh, K., and Azarm, S., 2012a, Approximation Assisted Optimization with Combined Global and Local Metamodeling, ASME 2012 International Design Engineering Technical Conference, IDETC 2012, August 12-12, 2012, Chicago, IL, USA.

54. Hu W., Saleh, K., Azarm, S., and Mosier, G., 2012b, "Approximation Assisted Optimization with Combined Global and Local Metamodeling," *Manuscript Submitted to Journal of Mechanical Design*, June 5, 2012.

55. Huang, D., Allen, T. T., Notz, W. I., and Zeng, N., 2006, "Global Optimization of Stochastic Black-Box Systems via Sequential Kriging Metamodels," *Journal of Global Optimization*, Vol. 34, No.3, pp. 441-466.

56. Hwang, Y., Jin, D., and Radermacher, R., 2007, "Refrigerant distribution in minichannel evaporator manifolds," *HVAC&R Research*, Vol.13, No.4, pp. 543-555.

57. Jeong S., Obayashi S., 2005, "Efficient Global Optimization (EGO) for Multi-Objective Problem and Data Mining," *IEEE Congress on Evolutionary Computation, IEEE, Piscataway*, NJ, Vol.3, pp. 2138-2145.

58. Jiao, A., and Baek, S., 2005, "Effects of distributor configuration on flow maldistribution in plate-fin heat exchangers", *Heat Transfer Engineering*, Vol. 26, pp.19-25.

59. Jiao, A., Zhang, R., and Jeong, S., 2003, "Experimental investigation of header configuration on flow maldistribution in plate-fin heat exchanger". *Applied Thermal Engineering*, Vol. 23, pp. 1235-1246.

60. Jiang, H. B., Aute, V. and Radermacher, R., 2006, "CoilDesigner: a general-purpose simulation and design tool for air-to-refrigerant heat exchangers", *International Journal of Refrigeration*, Vol.29, No.4, pp. 601-610.

61. Jin Y., Olhofer, M., and Sendhoff, B., 2001, "Managing Approximate Models in Evolutionary Aerodynamic Design Optimization," *Proceedings of IEEE Congress on Evolutionary Computation*, Vol.1, pp.592-599.

62. Jin Y., Olhofer, M., and Sendhoff, B., 2002, "A Framework for Evolutionary Optimization with Approximate Fitness Functions," *IEEE Transactions on Evolutionary Computation*, Vol.6, No.5, pp.48-494.

63. Jin Y., 2005, "A Comprehensive Survey of Fitness Approximation in Evolutionary Computation," *Soft Computing*, Vol. 9, No. 1, pp. 3-12.

64. Jing W., Jianbing, W., Liuyang, G., Suili, W., and Dayong, H., 2005, "CFD optimization application on airside plate fins of condenser coil of gravity-assisted heat pipe," *translated by San Francisco, CA, United states: American Society of Mechanical Engineers*, pp. 79-785.

65. Jones, D. R., Schonlau, M., and Welch, W. J., 1998, "Efficient Global Optimization of Expensive Black-Box Functions," *Journal of Global Optimization*, Vol. 13, pp. 455-492.

66. Jones D. R., 2001, "A Taxonomy of Global Optimization Methods Based on Response Surfaces," *Journal of Global Optimization*, Vol. 21, pp. 345-383.

67. Kanaris, A.G., Mouza ., A.A., and Paras. S.V., 2009, "Optimal design of a plate heat exchanger with undulated surfaces," *International Journal of Thermal Sciences*, Vol. 48, pp. 1184-1195.

68. Kandlikar, S. G., Garimella, S., Li, D., Colin, S., and King, M. R., 2006, Heat Transfer and Fluid Flow in Minichannels and Microchannels, ISBN: 0-0804-4527-6, first ed., *ELSEVIER*, Kidlington, Oxford, UK.

69. Karakasis, M.K., Giotis, A. and Giannakoglou, K. C., 2001, "Efficient Genetic Optimization using Inexact Information and Sensitivity Analysis. Application in Shape Optimization Problems," *ECCOMAS Computational Dynamics Conference*, Vol. 43, Swansea, Wales, UK.

70. Kays, W. M., and London, A. L., 1998, Compact heat exchangers, Third ed., *Krieger Publishing Company*, Malabar, Florida, USA.

71. Keane, A.J., 2006, "Statistical Improvement Criteria for use in Multiobjective Design Optimization," *AIAA Journal*, Vol.44, No.4, pp. 879-891.

72. Keeny, R. L., and Raiffa, H., 1976, Decisions with Multiple Objectives: Preferences and Value Tradeoffs, New York Wiley.

73. Knowles, J., 2005, "Multiobjective Optimization on a Budget of 250 Evaluations," *Lecture Notes in Computer Science, Evolutionary Multi-Criterion Optimization*, Vol. 3410, pp. 176-190.

74. Knowles, J., 2006, "ParEGO: A Hybrid Algorithm with On-line Landscape Approximation for Expensive Multiobjective Optimization Problems," *IEEE Transactions on Evolutionary Computation*, Vol.10, No.1, pp. 50-66.

75. Koch P. N., Wujek, B. A., Golovidov, O., and Simpson. T. W., 2002, "Facilitating Probabilistic Multidisciplinary Design Optimization Using Kriging Approximation Models," *Proceedings of the 9th AIAA/ISSMO Symposium on Multidisciplinary Analysis and Optimization*, Atlanta, Georgia.

76. Koehler, J. R. and Owen, A. B., 1996, "Computer Experiments," *Handbook of Statistics*, *Elsevier Science*, New York, pp. 261–308.

77. Kulkarni, T., Bullard, C., and Cho, K., 2004, "Header design tradeoffs in micro- channel evaporators", *Applied Thermal Engineering*, Vol.24, pp. 759-776.

78. Kuppan, K., 2000, Heat Exchanger Design Handbook, *Marcel Dekker*, New York, NY.

79. Kurpati, A., Azarm, S., Wu, J., 2002, "Constraint Handling Improvements for Multi-Objective Genetic Algorithms," *Structural and Multidisciplinary Optimization,* Vol.23, No.3, pp. 204-213.

80. Lee, H., Saleh, K., Hwang Y., and Radermacher, R., 2012, "Optimization of Novel Heat Exchanger Design for the Application of Low Temperature Lift Heat Pump," *Energy Journal*, Vol.42, pp.204-212.

81. Lee K. S., Kim W. S., and Si, J. M., 2001, "Optimal shape and arrangement of staggered pins in the channel of a plate heat exchanger," *International Journal of Heat and Mass Transfer*, Vol. 44, No. 17, pp. 3223-3231.

82. Li, M., Li, G., and Azarm, S., 2008, "A Kriging Metamodel Assisted Multi-Objective Genetic Algorithm for Design Optimization," *Journal of Mechanical Design*, Vol. 130, No.3, pp.031401-1-031401-10.

83. Li, Z., Davidson, H., and Mantell, C., 2006, "Numerical simulation of flow field and heat transfer of streamlined cylinders in cross flow", *ASME Journal of Heat Transfer*, Vol. 128, No. 6, pp. 564-570.

84. Lian Y., and Liou, M., 2004, "Multiobjective Optimization Using Coupled Response Surface Model and Evolutionary Algorithm," *Proceedings of the 10th AIAA/ISSMO Multidisciplinary Analysis and Optimization Conference,* Albany, NY.

85. Lindley, D. V., 1956, "On a measure of the information provided by an experiment," in *The Annals of Mathematical Statistics*, Vol. 27, pp. 986-1005.

86. Liu, D., and Garimella S., 2005, Analysis and Optimization of the Thermal Performance of Microchannel Heat Sinks, *International Journal of Numerical Methods for Heat and Fluid Flow*, Vol. 15, pp. 7-26.

87. Loéve, M., 1955, Probability Theory, *Van Nostrand*, New York.

88. Lophaven, S. N., Nielsen, H. B., and Søndergaard, J., 2002, "Aspects of the Matlab Toolbox DACE," *IMM-TR2002-13*, Technical University of Denmark, DK.

89. Luo, L. and Tondeur, D., 2005, "Optimal distribution of viscous dissipation in a multi-scale branched fluid distributor," *International Journal of Thermal Science*, Vol.44, pp. 1131-1141.

90. Markine, V.L. and Toropov, V. V., 2002, "Use Of High and Low Fidelity Models in Approximations for Design Optimization," *9th AIAA/ISSMO Symposium on Multidisciplinary Analysis and Optimization* Atlanta, Georgia, September 4-6, pp. 5651-5651.

91. Martin, J. D., and Simpson, T. W., 2005, “Use of Kriging Models to Approximate Deterministic Computer Models,” *AIAA Journal*, Vol. 43, No. 4, pp. 853-863.

92. MATLAB, 2008, “MATLAB and Simulink for Technical Computing,” Mathworks, Version 2007a.

93. McKay, M. D., Beckman, R. J., and Conover, W. J., 1979, "A Comparison of Three Methods for Selecting Values of Input Variables in the Analysis of Response from a Computer Code," *Technometrics*, Vol. 21, No. 2, pp. 239-245.

94. Myers, R. H., and Montgomery, D. C., 2002, Response Surface Methodology: Process and Product Optimization Using Designed Experiments, *John Wiley & Sons*, New York. NY, USA.

95. Nain P., and Deb, K., 2003, “Computationally Effective Search and Optimization Procedure Using Coarse to Fine Approximations,” *Proceedings of the Congress on Evolutionary Computation (CEC-2003)*, Canberra, Australia, pp. 2081-2088.

96. Nair P. B., and Keane, A. J., 1998, “Combining Approximation Concepts with Genetic Algorithm-based Structural Optimization Procedures,” *Proceedings of the 39th AIAA/ASME/ASCE/AHS/ASC Structures, Structural Dynamics, and Materials Conference and Exhibit, and AIAA/ASME/AHS Adaptive Structures Forum*, Long Beach, CA.

97. Nakayama, H., Arakawa, M. and Washino, K., 2003, "Using Support Vector Machines in Optimization for Black-box Objective Functions," *Proceedings of the International Joint Conference on Neural Networks*, 2, pp. 1617-1622.

98. Nam, D., and Park, C. H., 2000, "Multiobjective Simulated Annealing: A Comparative Study to Evolutionary Algorithms," *International Journal of Fuzzy Systems*, Vol. 2, No. 2, pp. 87-97.

99. Obayashi, Sh., Jeong, S., Chiba K., 2005, "Multi-objective Design Optimization Exploration for Aerodynamic Configuration," *AIAA Journal* - 2005-4666.

100. Otto, J. C., Landman, D. and Patera, A. T., 1996, "A Surrogate Approach to the Experimental Optimization of Multi-element Airfoils," *Proceedings of the 6th AIAA/NASA/ISSMO Symposium on Multidisciplinary Analysis and Optimization*, Bellevue Wa, September 4–6, AIAA 96-4138 CP.

101. Oyama, A., Obayashi, Sh. and Nakahashi, K., 2001, "Real-coded adaptive range genetic algorithm applied to transonic wing optimization," *Journal of Applied Computing*, Vol. 1, No. 3, pp.179–187.

102. Papadrakakis, M., Lagaros, N. D., and Tsompanakis, Y., 1999, "Optimization of Large-Scale 3D Trusses Using Evolution Strategies and Neural Networks," *International Journal of Space Structures*, Vol.14, Part 3, pp.211-223.

103. Park K. and Moon, S. , 2005, "Optimal design of heat exchangers using the progressive quadratic response surface model", *International Journal of Heat and Mass Transfer*, Vol. 48, No.11, pp. 2126-2139.

104. Park K., Oh, P. K., and Lim, H. J., 2006, "The application of the CFD and Kriging method to an optimization of heat sink", *International Journal of Heat and Mass Transfer*, Vol. 49, No. 19-20, pp. 3439-3447.

105. Picheny, V., Ginsbourger, D., Roustant, O., and Haftka, R., 2010, "Adaptive Designs Of Experiments For Accurate Approximation Of A Target Region," *Journal of Mechanical Design*, Vol. 132, No.7, pp. 071008-1 to 071008-9.

106. Piegl L., and Tiller W., 1997, The NURBS Book, ISBN 3-540-61545-8, 2nd ed., *Springer-Verlag Berlin Hidelberg*, New York, USA.

107. Pilat, M., Neruda, R., 2011, "Improving Many-Objective Optimizers with Aggregate Metamodels," *Hybrid Intelligent Systems (HIS), 11th International Conference*, pp. 555–560.

108. Pilat, M. and Neruda, R., 2012, "Local Metamodels for ASM-MOMA," *Bio-Inspired Computing And Applications, Lecture Notes in Computer Science*, 6840, pp. 79-84.

109. Pineda, L., Fregly, B., Haftka R., Queipo, N., 2010, "Estimating training data boundaries in surrogate-based modeling," *Structural and Multidisciplinary Optimization*, Vol.42, No.6, pp. 811–821.

110. Ponweiser, W., Wagner, T., Biermann, D., and Vincze, M., 2008, "Multiobjective optimization on a limited budget of evaluations using model assisted S-Metric selection," *Lecture Notes in Computer Science, Parallel Problem Solving From Nature*, Vol. 5199, pp. 784–794.

111. Praveen, C. and Duvigneau, R., 2009, "Low Cost PSO Using Metamodels and Inexact Pre-Evaluation: Application To Aerodynamic Shape Design,"

Computer Methods in Applied Mechanics and Engineering, Vol. 198(9-12), pp. 1087–1096.

112. Ratle, A., 1998, "Accelerating the Convergence of Evolutionary Algorithms by Fitness Landscape Approximation," *Parallel Problem Solving from Nature—PPSN*, 1498, pp. 87-96.

113. Romero-Méndez, R., Sen, M., Yang, T. and McClain, R., 2000, "Effect of fin spacing on convection in a plate fin and tube heat exchanger", *International Journal of Heat and Mass Transfer*, Vol. 43, No. 1, pp. 39-51.

114. Sacks, J., Welch, W. J., Mitchell, T. J., and Wynn, H. P., 1989, "Design and Analysis of Computer Experiments," *Statistical Science*, Vol.4, No.4, pp. 409–435.

115. Sakata, S., Ashida, F., Tanaka, H., 2011, "Kriging-Based Convex Subspace Single Linkage Method with Path-Based Clustering Technique for Approximation-Based Global Optimization" *Structural and Multidisciplinary Optimization*, Vol.44,No.3, pp. 393-408.

116. Saleh, K., Abdelaziz, O., Aute, V., Radermacher, R., and Azarm, S., 2010a, "Microchannel Approximation Assisted Design Optimization and CFD Verification", *13th International Refrigeration and Air-Conditioning Conference at Purdue*, IN, USA, p.2312.

117. Saleh, K., Aute, V., Azarm, S., and Radermacher, R., 2010b, "Online Approximation Assisted Multiobjective Optimization with Space Filling, Variance and Pareto Measures," *13th AIAA/ISSMO Multidisciplinary Analysis and Optimization Conference, AIAA-2010*, Fort Worth, Texas, USA.

118. Saleh, K., Radermacher, R., Aute, V., and Azarm, S., 2011a, "Online Approximation Assisted Optimization of a Novel Air-Cooled Heat Exchanger",*10th IEA Heat Pump Conference 2011*, Tokyo, Japan, Paper No. 00272.

119. Saleh, K., Aute, V., Radermacher, R., and Azarm, S., 2011b, "Online Approximation Assisted Optimization and CFD verification of Microchannel Designs," *Thermal &Fluid Analysis Workshop (TFAWS),* Newport News, VA, USA, Paper No.TFAWS2011-AT-007.

120. Saleh, K., Abdelaziz, O., Aute, V., Radermacher, R., and Azarm, S., 2012a, "Approximation Assisted Optimization of Headers for New Generation of Air-Cooled Heat Exchangers," *Applied Thermal Engineering* (2012) http://dx.doi.org/10.1016/j.applthermaleng.2012.06.007 accepted

121. Saleh, K., Abdelaziz, O., Aute, V., Radermacher, R., and Azarm, S., 2012b, "New Generation of Air Cooled Heat Exchanger 1 kW Module Design Optimization," *14th International Refrigeration and Air-Conditioning Conference at Purdue*, IN, USA, Paper No. 2178

122. Saleh, K., Aute, V., Radermacher, R., and Azarm, S., 2012c, "Plate Heat Exchanger Optimization Using Different Approximation Assisted Multiobjective Optimization Techniques," *14th International Refrigeration and Air-Conditioning Conference at Purdue*, IN, USA, Paper No. 2188.

123. Saleh, K., Aute, V., Azarm, S., and Radermacher, R., 2012d, "Online Approximation Assisted Multiobjective Optimization (OAAMO) with Space

Filling, Variance and Pareto Measures," *Manuscript Submitted to Structural and Multidisciplinary Optimization Journal*, June 2012.

124. Sasaki, D., Obayashi, Sh. and Nakahashi, K., 2002, "Navier-Stokes optimization of supersonic wings with four objectives using evolutionary algorithm," *Journal of Aircraft*, Vol. 39, No. 4, pp. 621–629.

125. Sasena, M., Papalambros, P., and Goovaerts, P., 2002, "Exploration of Metamodeling Sampling Criteria for Constrained Global Optimization" *Engineering Optimization*, Vol.34, pp. 263-278.

126. Schaffler, S., Schultz, R., Weinzierl, K., 2002, "Stochastic Method for the Solution of unconstrained vector optimization problems", *Journal of Optimization Theory and Applications*, Vol. 114, No. 1, pp. 209-222.

127. Seber, G., 1984, Multivariate Observations, *John Wiley & Sons*, Hoboken, New Jersey.

128. Serafini, P., 1992, "Simulated Annealing for Multiple Objective Optimization Problems," *Proceedings of the 10th International Conference on Multiple Criteria Decision Making*, Taipei, pp. 87-96.

129. Shah, R. K., and London, A. L., 1978, Laminar flow forced convection in ducts, a supplement to Advances in Heat Transfer, *Academic*, New York, USA.

130. Shah, R. K., and Sekulić, D.P., 1998, Heat Exchangers, in Handbook of Heat Transfer, 3rd edition, ed. W. M. Rohseow, J.P. Hartnett, and Y.I. Cho, *McGraw-Hill, New York*, NY, chapter 17.

131. Shah, R. K., and Sekulić, D.P., 2003, Fundamentals of heat exchanger design, *John Wiley & Sons*, Hoboken, NJ, USA.

132. Shah, R. K., 2006, "Advances in science and technology of compact heat exchangers," *Heat Transfer Engineering*, Vol. 27, No. 5, pp. 3-22.

133. Shan, S. and Wang G., 2005, "An Efficient Pareto Set Identification Approach for Multiobjective Optimization on Black-Box Functions," *Journal of Mechanical Design*, Vol. 127, No.5, pp. 866-874.

134. Shewry M. C., and Wynn, H. P., 1987, "Maximum Entropy Sampling," *Journal of Applied Statistics*, Vol. 14, pp. 165-170.

135. Shukla, P. K., Deb, K., and Tiwari, S., 2005, "Comparing Classical Generating Methods with Evolutionary Multi-Objective Optimization Methods", EMO 2005

136. Simpson T. W., Peplinski, J. D. , Koch, P. N., and Allen, J. K. , 2001, "Metamodels for computer-based engineering design: Survey and recommendations", *Engineering with Computers*, Vol. 17, No. 2, pp. 129-150.

137. Singh, V., Aute V., and Radermacher R., 2008, "Numerical Approach for Modeling Air-to-Refrigerant Fin and Tube Heat Exchanger with Tube to Tube Heat Transfer,", *International Journal of Refrigeration*, Vol. 31, No. 8, pp. 1414-1425.

138. Sirovich, L., 1987, "Turbulence and the Dynamics of Coherent Structures. Part 1: Coherent Structures," Quarterly of Applied Mathematics, Vol. 45, No. 3, pp. 561–571.

139. Sobhan, C., and Garimella, S., 2001, A Comparative Analysis of Studies on Heat Transfer and Fluid Flow in Microchannels, *Nanoscale and Microscale Thermophysical Eng*ineering, Vol. 5, pp. 293-311.

140. Sobieski, I.P., Manning, V.M. and Kroo, I. M., 1998, "Response Surface Estimation and Refinement in Collaborative Optimization," *Proceedings of the 6th AIAA/NASA/ISSMO Symposium on Multidisciplinary Analysis and Optimization*, St. Louis, MS, AIAA-98-4753, pp. 359-370.

141. Srinivas, N, and Deb, K., 1994, "Multiobjective Optimization Using Nondominated Sorting in Genetic Algorithms," *Evolutionary Computation*, Vol. 2, No. 3, pp. 221-248.

142. Su, R., Gui, L., Fan, Z., 2011, "Multi-Objective Optimization For Bus Body With Strength And Rollover Safety Constraints Based On Surrogate Models," *Structural and Multidisciplinary Optimization*, Vol. 44, No.3, pp. 431-441.

143. Sukhatme, S. P., and Devotta, S., 1988, "Classification of Heat Transfer Equipment", in *Heat transfer Equipment Design*, ed. R.K. Shah, E.C. Subbarao and R.A. Mashelkar, Hemisphere, New York, NY.

144. Sunden, B., 2007, "Computational fluid dynamics in research and design of heat exchangers", *Heat Transfer Engineering*, Vol. 28, No. 11, pp. 898-910.

145. Tondeur, D., and Luo, L., 2004, "Design and scaling laws of ramified fluid distributors by the constructal approach," *Chemical Engineering Science*, Vol. 59, pp.1799-1813.

146. Tuckerman, D., and Pease, R., 1981, "High Performance Heat Sinking for VLSI," *IEEE Electron Device Letters*, vol. EDL-2, pp. 126-129.

147. Turner, C.J., Campbell, M.I., and Crawford, R. H., 2003, "Generic Sequential Sampling for Metamodeling Approximations" *ASME Design Engineering Technical Conferences*, Paper No. DETC2003/CIE-48230, Chicago, IL, USA.

148. Van Doormaal, J. P., and Raithby, G. D., 1984, "Enhancement of the SIMPLE method for predicting incompressible fluid flows," *Numerical Heat Transfer*, Vol. 7, No. 2, pp. 147-163.

149. Viana, F.A.C., Haftka, R.T. and Steffen,V., 2009, "Multiple Surrogates: How Cross-Validation Errors Can Help Us to Obtain the Best Predictor," *Structural and Multidisciplinary Optimization,* Vol. 39, No. 4, pp. 439-457.

150. Voutchkov, I. and Keane, A., 2010, Multi-objective Optimization Using Surrogates, Computational Intelligence in Optimization, *Springer-Verlag, Berlin* Heidelberg, pp. 155-175.

151. Walker, G., 1990, Industrial Heat Exchanger: A Basic Guide, 2nd edition, Hemisphere, New York, NY.

152. Wang, G. and Simpson, T., 2004, "Fuzzy clustering based hierarchical metamodeling for design space reduction and optimization", *Engineering Optimization*, Vol.36, No.3, pp. 313-335.

153. Wang, G. G., and Shan, S., 2004, "An Efficient Pareto Set Identification Approach for Multi-Objective Optimization on Black-Box Functions" *ASME*

International Design Engineering Technical Conferences, Paper No. DETC2004-57194, Salt Lake City, Utah, USA.

154. Wang, J.F., Periaux, J., and Sefrioui, M, 2002, "Parallel evolutionary algorithms for optimization problems in aerospace Engineering," *Journal of Computational and Applied Mathematics*, Vol.149, pp. 155–169.

155. Wang, G. G., and Shan, S., 2007, "Review of Metamodeling Techniques in Support of Engineering Design Optimization", *Journal of Mechanical Design*, Vol. 129, No. 4, pp. 369-463.

156. Wang, L., Sunden, B., Manglik, R. M., 2007, Plate Heat Exchangers: Design, Applications and Performance, *WIT press, Billercia*, MA 01821, USA

157. Wen, J., and Li, Y., 2004, "Study of flow distribution and its improvement on the header of plate-fin heat exchanger", *Cryogenics*, Vol. 44, pp. 823-831.

158. Wen, J., Li, Y., Wang, S., and Zhou, A., 2007, "Experimental investigation of header configuration improvement in plate-fin heat exchanger", *Applied Thermal Engineering*, Vol. 27, pp.1761-1770.

159. Wilson, B., Cappelleri, D., Frecker, M., and Simpson, T. W., 2001, "Efficient Pareto Frontier Exploration Using Surrogate Approximations," *Optimization and Engineering*, Vol.2, pp. 31-50.

160. Wu, J., and Azarm, S., 2001, "Metrics for Quality Assessment of a Multiobjective Design Optimization Solution Set," *Journal of Mechanical Design*, Vol.123, pp. 18-25.

161. Wu, M. and Tao, Q. , 2007, "Investigation on laminar convection heat transfer in fin-and-tube heat exchanger in aligned arrangement with

longitudinal vortex generator from the viewpoint of field synergy principle", *Applied Thermal Engineering*, Vol. 27, pp. 2609-2617.

162. Zhang, Z., and Li, Y., 2003, "CFD simulation on inlet configuration of plate-fin heat exchangers", *Cryogenics*, Vol. 43, pp.673-678.

163. Zitzler, E., and Thiele, L., 1998, "Multiobjective optimization using evolutionary algorithms—A comparative case study," *in Parallel Problem Solving From Nature*, V, A. E. Eiben, T. Bäck, M. Schoenauer, and H.-P. Schwefel, Eds. Berlin, Germany: Springer-Verlag, pp.292–301.